THESIS
2
2008

LIBRARY
Michigan State
University

This is to certify that the
dissertation entitled

ADVANCEMENT OF BIOBASED PRODUCTS THROUGH DESIGN, SYNTHESIS AND ENGINEERING OF BIOPOLYESTERS

presented by

CHISA KANDYDA BROOKES

has been accepted towards fulfillment
of the requirements for the

DOCTORAL degree in CHEMICAL ENGINEERING

Ramani Narayan
Major Professor's Signature

Nov 27, 2007
Date

MSU is an affirmative-action, equal-opportunity employer

PLACE IN RETURN BOX to remove this checkout from your record.
TO AVOID FINES return on or before date due.
MAY BE RECALLED with earlier due date if requested.

DATE DUE	DATE DUE	DATE DUE

6/07 p:/CIRC/DateDue.indd-p.1

ADVANCEMENT OF BIOBASED PRODUCTS THROUGH DESIGN, SYNTHESIS AND ENGINEERING OF BIOPOLYESTERS

By

CHISA KANDYDA BROOKES

A DISSERTATION

Submitted to
Michigan State University
in partial fulfillment of the requirements
for the degree of

DOCTOR OF PHILOSOPHY

Department of Chemical Engineering and Materials Science

2007

ABSTRACT

ADVANCEMENT OF BIOBASED PRODUCTS THROUGH DESIGN, SYNTHESIS AND ENGINEERING OF BIOPOLYESTERS

By

Chisa Kandyda Brookes

As crude oil approaches $100/barrel, the need for sustainable products continues to grow. While development of biobased products is necessary and crucial to sustainability, integration of biobased materials into biodegradable synthetic-based materials is another viable route to advancing biobased, biodegradable products. In this work, glycerol, cellulose acetate (CA) and a glycerol-based pre-polymer are the materials selected to incorporate biocontent into the synthetic monomer, dimethyl terephthalate (DMT), and the biodegradable synthetic polymer poly(butylene adipate-co-terephthalate) (PBAT or Ecoflex). Synthesis, via transesterification of glycerol with DMT, and reactive extrusion are the processing methods employed. Synthesis products were characterized by hydroxyl values, molecular weights and thermal properties. Molecular weight and thermal analysis results were also used for the characterization of extrusion products. In addition, extrusion products were characterized using dynamic mechanical analysis and microscopy. The results reveal that there is some interaction between CA and PBAT, and the two can form a compatible blend allowing for the addition of biocontent. Plasticization and catalytic effects of these blends were studied. Incorporation of biocontent via transesterification produced a novel bio pre-polymer that was a transparent solid. Results indicated that using a dibutyltin (IV) oxide catalyst at 0.1 wt.% of DMT yielded optimal performance. Blends of glycerol-based materials and PBAT confirmed the reactivity of the new material with PBAT based on residual catalyst.

This one is for my island,
St. Croix USVI

ACKNOWLEDGEMENTS

Glory goes to God for completing another phase of His work within me. Only He truly understands the experiences I've had throughout this process. Thanks to Dr. Narayan for taking me on as a student when he had no plans of accepting any students. I'd also like to thank Dr. Narayan for the freedom with which he allowed me to think and work. I am even more confident in my abilities, largely because of the latitude given me by Dr. Narayan. Thanks to Dr. Dale, Dr. Jayaraman and Dr. Selke for sitting on my committee and providing good discussion around my work. Thanks to the BMRG (formerly SINAS) group for the experiences we've shared. Special thanks to Sloan, Royal/Dutch Shell, GEM, MSU Graduate School and MSU College of Engineering for their financial support during this process. Thanks to the Edwards family for being my closest friends in MI. I'll miss leaving MI *only* because of you guys. Thanks to my family and close loved ones (my confidante Ohm and best friend La'Vern), because of whom I never lacked support. I truly enjoyed my red carpet treatment during this unique journey. There is no better family or loved ones in the world for me; I am sure of it! I will forever thank my parents, Edred and Inez Brookes, for believing in me and in my ability to do great things. Mom and Dad you are indispensable! Thanks to my brother and sister-in-law, Nigel and Elaine Brookes, my sister and brother-in-law, Patrice and Kevin Hyatt, and my sisters Bethlyn and Kim Brookes. You guys are always straight with me, never failing to be there when I need you; you are all priceless. I love you. Unlimited thanks goes to all who have played a role in making me stronger and wiser. Finally, thank God I am done!

Table of Contents

List of Tables vi

List of Figures viii

Chapter 1 1
1.1 Motivation 1
1.2 Goals and Objectives 3

Chapter 2 5
2.1 Literature Review 5
2.2 Theory of Polymer Mixtures 14
2.3 Polyester Synthesis 33

Chapter 3 45
3.1 Materials 45
3.2 Processing and Characterization Methods 53

Chapter 4 62
4.1 Overview 62
4.2 Materials & Methods 65
4.3 Results and Discussion 66
4.4 Summary 95

Chapter 5 98
5.1 Overview 98
5.2 Materials and Methods 100
5.3 Results and Discussion 100
5.4 Summary 115

Chapter 6 117
6.1 Overview 117
6.2 Materials & Methods 117
6.3 Results and Discussion 119
6.4 Summary 127

Chapter 7 128
7.1 Conclusions 128
7.2 Recommendations for Future Work 131

References 133

List of Tables

Table 1: Eastman Cellulose Acetate Properties.....47

Table 2: BASF PBAT (also known as Ecoflex) Properties.....49

Table 3: Properties of Glycerol.....50

Table 4: Calculated solubilities compared to literature using Hoy parameters...64

Table 5: Extruded Blends of CA and PBAT without modification.....67

Table 6: Preliminary CAPBAT degradation values as retrieved by TGA.....68

Table 7: Summary of DSC thermal properties for preliminary CAPBAT blends.....71

Table 8: Molecular weight data for "unplasticized" and plasticized CA-PBAT samples showing actual and theoretical Mnmix and Mwmix values and their % difference values.....74

Table 9: Degradation temperatures for "unplasticized" and plasticized blends.....75

Table 10: DSC results for "unplasticized" and plasticized blends with varying plasticized blend compositions; * indicates values from DMA.....78

Table 11: GPC average molecular weight data of uncatalyzed and catalyzed blends.....85

Table 12: TGA degradation temperatures of uncatalyzed and catalyzed blends.....86

Table 13: DSC transitions for uncatalyzed and catalyzed blends; * indicates values from DMA.....89

Table 14: Comparison of percent conversion and Xn based on hydroxyl values versus methanol formation.....104

Table 15: Comparison of percent conversion and Xn based on hydroxyl values versus methanol formation after adjustments for trapped methanol.....108

Table 16: GPC Molecular weights and polydispersity index for all reactions.....110

Table 17: TGA degradation temperature values for both catalyst sets 111

Table 18: DSC glass transition temperatures of all reaction samples 114

Table 19: Summary of Runs for GDMT-PBAT blends 119

Table 20: TGA degradation temperature for GDMT-PBAT samples 120

Table 21: DSC thermal transitions for blends of GDMT-PBAT; * indicates values obtained from DMA.....122

List of Figures

Figure 1: Cellulose as polymer of β-D-glucose.....6

Figure 2: Portion of a Cellulose Diacetate Chain.....7

Figure 3: Graphical depiction of Equation 9 in regards to the Property of a Polymer Blend.....21

Figure 4: Free Energy of Mixing for Polymers A & B with the same molecular weight.....25

Figure 5: Phase and Transition Behaviors in Polymer Blends.....27

Figure 6: Phase Diagrams for Polymer Mixtures showing the binodal (solid) and spinodal (dashed) curves along with critical points.....29

Figure 7: Esterification reactions using Maleic Acid and Maleic Anhydride as examples and Transesterification reaction using Dimethyl terephthalate.....41

Figure 8: Structure of BASF Poly(butylene adipate-co-terephthalate).....48

Figure 9: Biodegradation of Cellulose Compared to that of PBAT.....48

Figure 10: Structure of Glycerol.....49

Figure 11: Biodiesel production chemical reaction showing Glycerol as a by-product.....50

Figure 12: Important External Plasticizers for Cellulose Acetate.....64

Figure 13: Weight loss and derivative weight loss (represented by two maximas) curve of CAPBAT sample to illustrate the two component blend of CA and PBAT.....69

Figure 14: Weight loss curves of preliminary CAPBAT samples.....70

Figure 15: DSC crystallization temperatures of preliminary CAPBAT blends.....72

Figure 16: Chromatogram of samples affected by varying contents of plasticizer and cellulose acetate: CP37 (0% plasticizer, CTP37 (9% plasticizer), CTP55 (15% plasticizer).....74

Figure 17: TGA weight loss curves for "unplasticized" and plasticized samples.....76

Figure 18: TGA derivative weight loss curves comparing plasticized compositions.....77

Figure 19: DMA storage modulus of "unplasticized" and plasticized blends along with varying compositions of plasticized blends.....80

Figure 20: DMA loss modulus of "unplasticized" and plasticized blends along with varying compositions of plasticized blends.....81

Figure 21: DMA tan delta of "unplasticized" and plasticized blends along with varying compositions of plasticized blends.....82

Figure 22: ESEM images of CP37, CTP37 and CTP55 by column from left to right, at 1000x, 2000x, 5000x by row from top to bottom. Values displayed at the bottom represent particle sizes for each sample.....84

Figure 23: GPC chromatogram of uncatalyzed and catalyzed blends.....86

Figure 24: TGA weight loss curve of uncatalyzed and catalyzed blends.....87

Figure 25: TGA derivative weight loss curve comparing compositions of catalyzed blends.....88

Figure 26: DMA storage modulus curves for uncatalyzed and catalyzed blends.....91

Figure 27: DMA loss modulus curves for uncatalyzed and catalyzed blends....92

Figure 28: DMA tan delta curves for uncatalyzed and catalyzed blends.....93

Figure 29: ESEM images of CTP37, CTPD37, CTP55 and CTPD55 by column from left to right, at 1000x, 2000x, 5000x by row from top to bottom. Values displayed at the bottom represent particle sizes for each sample.....95

Figure 30: Degree of polymerization and gel point for a 1:1 and 2:3 mixture of glycerol:dimethyl terephthalate.....99

Figure 31: a. Reaction conditions b. Reaction Matrix.....101

Figure 32: Conversion over time based on recorded methanol collection.....102

Figure 33: Degree of polymerization as calculated by Carothers' Theory for the theoretical curve and by experimental data for all other curves.....103

Figure 34: TGA derivative weight loss curve for NC samples showing % trapped methanol in the samples.....106

Figure 35: TGA derivative weight loss curve for DBTO samples showing % trapped methanol in the samples.....107

Figure 36: Catalyst perfomance based on MEOH for different types of catalysts at different concentrations.....108

Figure 37: Catalyst perfomance based on hydroxyl # for different types of catalysts at different concentrations.....109

Figure 38: Chromatogram for all reactions with different catalysts and different catalyst amounts.....110

Figure 39: Sodium Carbonate percent and derivative weight loss curves based on different catalyst amounts.....112

Figure 40: Dibutyltin oxide percent and derivative weight loss curves based on different catalyst amounts.....113

Figure 41: DSC glass transition temperature results for reaction products with varying amounts of a. Sodium Carbonate and b. Dibutyltin oxide.....114

Figure 42: TGA weight loss curve for GDMT-PBAT samples.....121

Figure 43: DSC crystallization transition for blends of GDMT-PBAT.....124

Figure 44: Storage modulus of GDMT-PBAT blends.....125

Figure 45: DMA tan dela curve for GDMT-PBAT blends.....126

Chapter 1

Introduction

1.1 Motivation

Sustainability is no longer just a "buzz" word or a vision of the future. Critical events, with the 2006 State of the Union Address being one, have contributed to moving sustainability from abstract to more of a growing reality. Instabilities in areas of the world where oil is present have been a driving force for the increasing oil prices over the past few years. This dwindling access to foreign oil is what has motivated government and industry to support the advancement of bio-based research [1], aiding in reducing our reliance on these sources of energy and raw materials. Bio-based research has managed to take center-stage, being the topic of discussion for major political debates reviewed in articles of respected trade journals. One example is a Government and Policy article by Jeff Johnson in Chemical and Engineering News' first issue of the year 2007 titled "Ethanol—Is it Worth it?"[2]. While the article highlights pro and con positions on the viability of corn as a source of fuel, using views from leading researchers like Dale and Pimental, it manages to end with the fact that the discussion on corn-based fuel is "likely" to be the start of a bio-fuels market, and not its end [2].

Not only is it a start for the bio-fuels market, but it is a start for the bio-based plastics market as well. Starch has been the primary feedstock [3], and one of the most successful and promising naturally occurring materials in the bio-

based industry. Researchers at Michigan State University (MSU) along with KTM Industries have developed a one step, reactive extrusion process using water as a plasticizer and blowing agent for starch, to manufacture bio-based (non-toxic), biodegradable foam for packaging [4]. More recently from a USDA News release, electro-active biopolymers made from cornstarch have been developed for potential use in charging lithium batteries [5].

Besides political drivers there are other fundamental motivations for "green" development. Environmental and social drivers, while less accepted, an important the motivation for advancement of biobased materials. The Kyoto Protocol [6], a world attempt to address concerns about the environment, has committed countries to decreasing greenhouse gases that contribute to climate change within the environment. This world effort to protect the environment has also led to the development of biomaterials research. In a paper published by the Journal of Industrial Ecology, Duncan mentions the enactment of Title III of the Agricultural Risk Protection Act (Public Law 106-224), the Biomass Research and Development Act of 2000 [7]. This act is in place to increase coordination across departments in the federal government in relation to biomass research and development [7]. This effort supports the conversion of biomass into bio-based products. Growth of a biobased industry can then affect the socio-economic conditions of farmers, and aid in the development of rural areas.

Amidst all the motivators for and excitement around bio-based products, there exists the need for a certain quality of products—those that excel in performance while being economically feasible, as is characteristic of synthetic

polymers. Narayan fairly describes the several benefits of oil-based polymeric materials after which he rightly identifies that "it is these very attributes of strength and indestructibility that cause problems when these materials enter the waste stream" [8]. Thus, in addition to performance and economics, the type of product for which there is a need is one that is not only bio-based, but one that also has the ability to be bio-degraded after its intended use. Narayan's ideas identify with the overall goal of this study in that he recognizes that there is great value, as well as large areas of improvement, for existing products as shown in the LCA of polyethylene and starch foams [9]. The successful integration of bio-based products to the market requires support of continuous improvement on new and existing products.

1.2 Goals and Objectives

The intent of this research is to incorporate the biobased materials, glycerol and cellulose acetate, into a synthetic based monomer and polymer, dimethyl terephthalate (DMT) and biodegradable poly(butylene adipate-co-terephthalate) (PBAT). Incorporating biocontent in this fashion will advance bioproduct development and broaden the utility of biomaterials. Biobased content will be incorporated using two routes, synthesis and reactive extrusion. Three objectives were set to achieve the goals of this research.

1. Investigate effects of composition, plasticizer and catalyst on reactive extruded blends of CA and PBAT

2. Determine catalyst performance in the synthesis of glycerol-based biopolyester (GDMT)
3. Study residual catalyst performance on blends of GDMT with PBAT

The benefit from each of these objectives is the infusion of bio-based materials into synthetic base products for the development of new-age products to address current problems. This research is timely in that the growing demand for biodiesel has brought along tremendous potential opportunities for these new glycerol-based esters, since glycerol is a waste of biodiesel production.

Chapter 2

Background

The aim of this chapter is to summarize the literature related to the overarching goals of this study and discuss the theory behind polymer blends and polyester synthesis with a brief overview of the chemistry related to polyester synthesis.

2.1 Literature Review

An overview of CA's origin and production is given, followed by a discussion of various CA blends documented in the literature. Cellulose acetate and its blends are the main focus of this literature review with minimal discussion of PBAT, given the small amount of work published regarding this relatively new polymer. The CA blends discussion centers on three categories, which include (1) miscible and immiscible blends, (2) effects of external and internal plasticizers on blends, and (3) biodegradation of blends.

2.1.1 Cellulose Acetate Background

Cellulose acetate (CA) is a derivative of the natural polysaccharide cellulose. Cellulose, whose structure is shown in Figure 1, is mainly found in plant cell walls and is the most abundant carbohydrate found in plants, followed by starch [11]. While cellulose has been an important starting material in plastics for some time, cellulose-based plastics have lost much of their market to cheaper

plastics like polyethylene and polypropylene [12]. As oil resources have continued to decrease with increasing

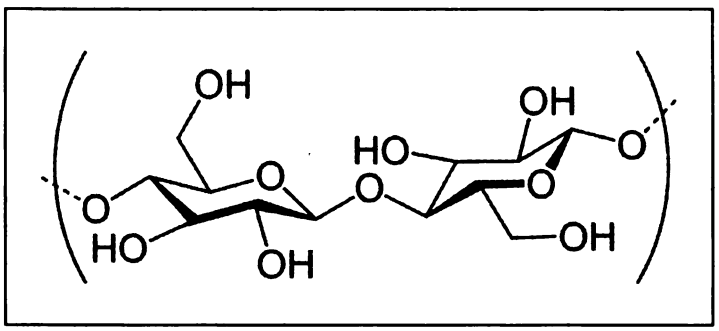

Figure 1. Cellulose as polymer of β-D-glucose [10]

potential to become extremely expensive, cellulose has once again gained interest as a renewable, abundant alternative raw material source for plastics.

One major class of cellulose derivatives is cellulose esters. Esterification of cellulose can be achieved with acids, with anhydrides, or with acid chlorides [13]. The most widely used method to convert cellulose to cellulose esters is via anhydrides [11]. To get to cellulose acetate (the material of interest in this study), cellulose goes through esterification to a cellulose triester via acetic anhydride. Esterification is then followed by hydrolysis with water or a diluted acetic acid solution to regain some of the OH-groups that were esterified. Separation then occurs via filtration, precipitation, washing, dewatering, drying and screening, yielding cellulose acetate of a certain degree of substitution (DS) [12]. Performing hydrolysis with a water-acid mix that incorporates the acid of

choice (ex. propionic anhydride or butyric anhydride) produces other cellulose acetate derivatives like cellulose acetate butyrate or cellulose acetate propionate.

The structure of CA, as shown in Figure 2, discloses important characteristics about its properties. Cellulose acetate has varying degrees of substitution from zero to three. The degree of substitution is based on the average number of acetyl groups that replace the OH-groups on an anyhdroglucose unit [11]. The degree of substitution is

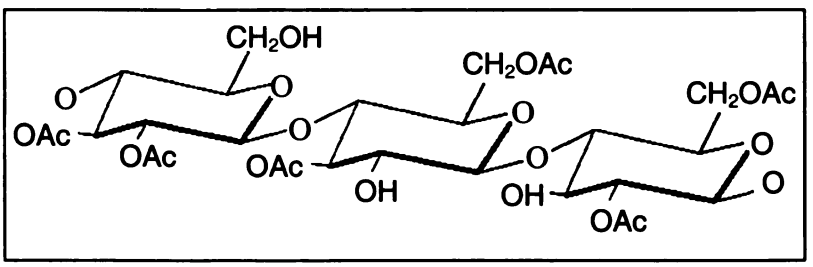

Figure 2. Portion of a Cellulose Diacetate Chain [14]

often measured by the % acetyl content. The acetyl content or degree of substitution often dictates the solubility characteristics of cellulose acetate [13]. With increasing acetyl content, the permeability rate increases while the tensile strength and elongation characteristics of cellulose acetate decrease[13]. This is because the strong hydrogen bonding originally occurring in cellulose is disrupted, and with the greater acetyl content the chains are not likely to have as strong an interaction (hydrogen bonding and van der Waals forces) as in cellulose. For situations in which the other acids or anhydrides are used to produce cellulose acetate derivatives such as cellulose acetate propionate and

cellulose acetate butyrate, the changes to the overall structure of cellulose acetate causes even more reduction in tensile and thermal properties as compared to cellulose acetate.

2.1.2 Cellulose Acetate Blends

Cellulose acetate blends provide a mechanism to achieve certain desired characteristics. K. J. Edgar and others did a review of the literature on blends of cellulose esters with other polymers [15]. Many of their findings for cellulose ester blends are included within this literature search.

Miscible and Immiscible Blends

Much of the work reviewed by Edgar and others regarding cellulose acetate blends, as well as additional studies, has been done with cellulose acetate propionate and cellulose acetate butyrate, probably due to easier processing as compared to cellulose acetate. Nonetheless, work done by Schauber et al. and Light et al. showed blends of CAP and CAB, respectively, capable of forming miscible and immiscible blends with certain copolymers [15, 16, 17]. Specifically, Schauber's composition, which yielded a miscible blend of CAP and a copolymer of propylene and carbon monoxide, decreased the toughness when compared to CAP alone. On the other hand, Light's composition which yielded miscible blends of CAB and copolymers of methyl and butyl acrylate, increased toughness as compared to CAB alone. Both Schauber's and Light's immiscible blend compositions of CAP and CAB with their

respective copolymers yielded significant improvement in toughness as compared to CAP or CAB alone [15, 16, 17]. Nabar et al. attempted to blend CA and polyethylene terephthalate in order to improve the crystallization rate of PET for better moldability, but the blend was immiscible and hard to process [18]. The difficulty of processing was attributed to the low processing temperatures used to avoid CA degradation.

External Plasticizers for CA and its Blends

Due to the high processing temperature of cellulose esters, plasticizers often must be added to lower the processing temperature [11]. In 1995, Ghiya and others processed CA with triethyl citrate and acetyl triethyl citrate and reported the miscibility of these plasticizers with CA along with the effects on strength and elongation [19]. The addition of these citrate esters increased the biodegradation rate of CA. More recently, Mohanty and others used triethylcitrate (TEC) as a plasticizer for cellulose acetate biocomposite applications, and studied the processing methods of (1) compression molding, (2) extrusion followed by compression molding and, finally, (3) extrusion followed by injection molding [20]. They concluded that high shear in extrusion and injection molding processes caused better mixing or may have enhanced crosslinking, resulting in increased tensile properties. They propose that 30% plasticizer is a "suitable balance for biocomposite materials" [20]. Wibowo et al [21] and Park et al [22] also used TEC as a plasticizer in a blend of CA with layered silicate nanocomposites, showing increased tensile and flexural strength

in both. Rosa's addition of polyethylene glycol to a CA/polycaprolactone blend resulted in increased elongation for CA/PCL blends, and for blends with more than 60% CA increased tensile strength [23].

Internal Plasticizers for CA and its Blends

Others have also attempted to get the plasticizing effect without actually using a liquid plasticizer. Nie and Narayan grafted styrene maleic anhydride (SMA) to cellulose acetate with the help of the common plasticizer diethyl phthalate and they reported that an increase in the maleic anhydride content of SMA helped to increase the grafting of the SMA to CA, thus reducing the immiscibility between the two, resulting in improved dimensional stability for the blend [24]. Light and others as well as Lee et al. attempted to get a plasticizing effect from CAB and CAP by using other polymers via polymeric plasticization [15, 17, 25]. In Light's case, there was an improvement in the impact strength and softening temperature for both CAB and CAP as compared to other normally plasticized cellulose esters when grafted polymers were blended with CAB and CAP [15, 17]. For Lee and others, the addition of biodegradable polyestercarbonates (PEC) did not improve the tensile strength [15, 25]. Crystallization of PEC from the blend above 40% composition was said to be the cause of poor tensile properties. However, below 40%, PEC proved to enhance the elongation and the melt flow of the blend. Edgar highlights that this work supports the idea of biodegradable polymeric plasticizers [15].

Biodegradable Blends of Cellulose Acetate

In addition to improving properties, CA blends have also been formulated to biodegrade. While Maheras and others have blended CA and starch acetate for cost purposes [15, 26], cellulose and starch blends are also attractive because of the biodegradation potential of each [27]. Starch is cheaper than cellulose. Also, like cellulose, it is very abundant and it comes from renewable resources. While starch acetate does decrease the tensile properties, and is not miscible at a 25% composition with cellulose acetate, it remains as a good addition in the mixture to help reduce cost and enhance biodegradation [26]. Biodegradation of cellulose acetate is strongly dependent on the degree of substitution of the cellulose acetate. As the degree of substitution (DS) increases, the biodegradation, in terms of CO_2 and CH_4 formation, decreases [15]. Cellulose acetate with a DS of 2.5 is proven to be biodegradable by exposing the residues of the acetyls on cellulose acetate to cellulose enzymes [27]. Guruprasad and Shashidhara have confirmed more recently the degradation of a 90/10, CA/starch blend. Weight loss was over 35% in three months, with a little over half of the weight loss due to starch [28].

Other researchers focused specifically on biodegradable blends with internal plasticizers for CA. In a series of publications, Teramoto and Nishio attempted to use polylactic acid (PLA) as an internal plasticizer for CA with a DS of 2.15 [29,30,31]. This form of PLA acted as an internal plasticizer and did reduce the T_g of the blend. It is important to mention that to get this plasticization of CA required an extensive 3-stage batch process to graft PLA onto CA for

composition-controlled grafting. Braganca and Rosa also used an internal plasticizer [32]. In their CA/PCL blends they noted the poor access to CA hydroxyl groups as compared to the hydroxyl groups on CAB. Only one blend of PCL/CA (20/80) showed some compatibility and increased tensile strength. With this increase in tensile strength came a 99% drop in elongation at yield as compared to PCL alone. Prior to Teramoto's work, Yoshioka, and Shiraishi had studied the plasticization of CA for several years [33,34,35]. They attempted to graft caprolactone and lactide onto CA using a stannous octoate selective catalyst and moderate temperatures. With just the right reaction conditions, they were able to add strength as well as elasticity to CA. They noted that the lactide component grafted to CA more readily than did the caprolactone, which resulted in brittle blends after short times (from lactide) and more flexible blends after longer times (from caprolactone) [33].

Their studies continued and led to the grafting of varying molar substitution combinations of caprolactone and poly(lactic acid) (PLA) CA [34]. This eliminated the lactide intermediate sensitive to moisture and resulted in better moldability of CA, attributed to preferential grafting of the more flexible caprolactone. Yoshioka, Shirashi and others also undertook grafting of dibasic anhydrides and mono epoxides to CA [35]. In this work sodium carbonate was used as an esterification catalyst that aided in increasing the grafting of oligomers to CA. Maleic anhydride and phenyl glycidyl ether proved to be the best pair due to the high reactivity of each in their respective classes. This pair

also took longer to biodegrade than succinic anhydride and glycidyl methacrylate, but biodegraded nonetheless.

Building from the successful plasticization and biodegradation of CA via maleic anhydride and epoxides, Lee and Shiraishi studied plasticization of CA using maleic anhydride, glycerol and citrate esters [36]. While the maleic anhydride glycerol mixtures with CA via a kneading process exhibited brittleness, addition of a small amount of citrate ester effectively plasticized CA, reducing the T_g of CA by 80-100 °C. Lee and Shiraishi claim the mechanical properties obtained were "comparable to those of general synthetic polymers or commercially plasticized cellulose acetate". These results are in line with Suvorova and Demchick's finding that ester plasticizers with shorter chains and polar groups mix well with CA [37].

2.1.3 Poly(butylene adipate-co-terephthalate) (PBAT) Blends

Blend literature on PBAT is not as extensive as CA blend literature. Over the past few years there have been some studies on the polymer blends of PBAT. Someya et al. have looked at adding nanocomposites to blends of PBAT with montmorillonite clay. The addition of the clay to PBAT was reported to slow the crystallization of PBAT [38]. Nabar et al. utilized PBAT as a functional aid to improve the properties of starch foams [39]. His later work included an extensive study on the maleation of PBAT for use as a compatibilizer in starch foams [40]. Results showed improved resilience and hydrophobic properties of starch foams. Most recently a study of PBAT-PLA blends reported significant increases in

elongation and toughness of PLA with the addition of 5 – 20% PBAT, but at the expense of tensile strength and modulus [41].

2.2 Theory of Polymer Mixtures

This segment focuses on the thermodynamics of polymer mixtures. It begins by covering the mixing of regular solutions and continues with the mixing of polymers. Other topics related to polymer blends are also covered. Specifically, miscibility, compatibility, phase separation and adhesion/interfacial tension are discussed briefly for a more fundamental understanding of blends.

2.2.1 Thermodynamics of Mixtures Overview

An understanding of polymer blends requires some knowledge of the thermodynamics of mixtures. Thermodynamic theories center around the idea that blends of two components are governed by the free energy equation given below.

$$\Delta G_{mix} = \Delta H_{mix} - T\Delta S_{mix} \qquad \textbf{Equation (1)}$$

In this equation, ΔG_{mix} is the free energy of mixing, ΔH_{mix} is the enthalpy of mixing, ΔS_{mix} is the entropy of mixing and T is the absolute temperature of the system. In order for the components to mix, a necessary condition is that ΔG_{mix} must be negative (<0) [42]. In order for this to occur the disorder of the system during mixing, represented by the entropy term, or the temperature of the system

should be relatively high. Another way to enhance mixing is to minimize the heat related to intermolecular interactions, represented by the enthalpy term.

For ideal solutions and for athermal mixing, the interactions amongst molecules are equal, yielding no change in volume and no heat exchanged ($\Delta H_{mix} = 0$) [42]. Thus the entropic portion of the free energy equation governs the behavior of ΔG_{mix} under these conditions. To determine the entropy of such a two-component system, statistical methods are employed to relate to the mole fractions of the species shown by equation 2 where x_i is the mole fraction of a particular species and n_i is the moles of a particular species and R is the gas constant [42].

$$\Delta S_{mix} = -R[n_1 \ln(x_1) + n_2 \ln(x_2)] \qquad \textbf{Equation (2)}$$

Thus the change in free energy (ΔG_m) would be equal to equation 3 where all variables are defined as before.

$$\Delta G_{mix} = RT[n_1 \ln(x_1) + n_2 \ln(x_2)] \qquad \textbf{Equation (3)}$$

Regular solutions where the change in enthalpy is not zero have to take into account intermolecular interactions [42]. For interactions that are not strong, or intermolecular forces such as van der waal forces, ΔH_{mix} can be defined by the

equation below. The total volume of the system is V, ϕ is the volume fraction of each component and δ is the solubility parameter for each component. All other variables are as defined earlier.

$$\Delta H_{mix} / V = (\phi_1)(\phi_2)[\delta_1 - \delta_2]^2 \qquad \textbf{Equation (4)}$$

The solubility parameter is the square root of the cohesive energy density. The cohesive energy density measures the strength of secondary bonds, thereby giving insight on specific interactions related to the enthalpy term [43]. The cohesive energy density is given by equation 5, where ΔE_v is the energy of vaporization and V_{molar} is the molar volume of the specific liquid.

$$CED = \Delta E_v / V_{molar} \qquad \textbf{Equation (5)}$$

Thus the solubility parameter incorporates all the internal molecular energies associated with the contacts between the polymer and solvent. There are different methods for estimating solubility parameters. Hoy, Van Krevelen and others have developed group contribution methods by which a non-polar polymer's solubility can be approximated within an acceptable range [44]. Using the group contribution method, the solubility of a polymer with mostly non-polar species in the repeat unit can be estimated by equation 6. In equation 6, p is the density, F_i is the sum of the molar attraction

$$\delta = \rho(\sum F_i) / M \qquad \textbf{Equation (6)}$$

constants and M is the molecular weight of the polymer repeat unit. While such solubility parameters are simple and convenient because they can be used to predict the mixing of two components, they do not take into account strong polar or hydrogen bonding, causing inaccuracy [44]. This led to the development of the Flory-Huggins theory.

For polymer-solution systems, the ideal solution often is not a good estimation because of the difference in sizes of the molecules. In addition, there is solvent-solvent interaction, polymer-polymer interaction and solvent-polymer interaction. The interaction between the polymer and the solvent requires some breaking of solvent-solvent and polymer-polymer contacts. These breaks and formations of contacts affect the enthalpy portion of the free energy equation. Thus athermal mixing does not occur. Flory and Huggins developed a theory to predict the change in free energy for polymer solutions. The relationship developed by Flory and Huggins includes lattice interaction parameters and the Gibbs free energy change between the polymer and solvent. Due to the inaccessibility of these parameters, the Flory-Huggins interaction parameter, χ, was defined to give the following enthalpic and free energy relationship for polymer-solvent mixtures (Equations 7 and 8).

$$\Delta H_{mix} = RT\chi_{AB}(\phi_2)n_1x_1 \qquad \textbf{Equation (7)}$$

$$\Delta G_{mix} = RT[n_1 \ln(\phi_1) + n_2 \ln(\phi_2) + n_1\phi_2\chi_{AB}]$$ **Equation (8)**

All variables are the same except that x_1 is representative of the degree of polymerization for polymeric solvents and is equal to one for monomeric solvents. In the second equation, the first two terms are the entropic portion of the free energy equation and the last term represents the enthalpic portion. While the relationship developed by Flory-Huggins has its drawbacks, dilute polymer solution mixes can be estimated adequately [44].

Flory-Huggins polymer-solution theory and the regular solution theory which incorporates solubility parameters are different in that Flory-Huggins uses an interaction parameter, χ, that relates to the interaction of components in a binary mixture to each other and themselves [44]. The solubility parameter has to be calculated for each component. In addition, one solubility parameter does not account for all interactions between both components. Also, regular solution theory uses mole fractions to determine the changing entropy of the mixture, whereas the Flory-Huggins polymer-solution model uses volume fractions to estimate the changing entropy of the mixture. Although the latter model proved satisfactory for polymer-solvent mixtures, polymer-polymer mixtures are more affected by molecular weight. Neither model completely satisfies and accurately describes all polymer-polymer systems, but they are the principles that govern the system and should be understood before tackling other models that may better predict the system at hand. This understanding of the thermodynamics involved is crucial to understanding the polymer blend system.

2.2.2 Polymer-Polymer Miscibility/Compatibility

In the discussion of polymer blends, miscibility and compatibility must be addressed. A blend being immiscible does not reflect the compatibility of the blend. A compatible polymer blend is a blend that exhibits macroscopically uniform physical properties throughout its whole volume [42]. Miscibility is the ability of a mixture to form a single phase over specific ranges of temperature, pressure and composition [42]. Complete miscibility requires the proper type of interactions, the proper number of interactions and the proper spacing of interactions [42]. In more practical terms, miscibility is often indicated by 1) transparent films displaying homogeneity even under magnification, 2) a single glass transition temperature (T_g) between the T_g values of the blend components, and 3) good mechanical integrity, especially in tensile strength [42]. Often associated with miscible blends is the synergistic increase in tensile strength, which is attributed to strong specific interactions leading to better packing on a molecular level [42].

Unfortunately, some incompatible blends exhibit these properties. Incompatible blends form transparent films due to similar refractive indices or due to the formation of two separate transparent films layered one on the other [42]. Another way that incompatible blends form transparent films is by the impediment of phase separation due to potential entanglement and/or the high viscosity of the polymer-polymer matrix [42]. If this small change in free energy were to occur it would lead to separation of the polymer-polymer matrix and films would not be transparent. Other issues that can cause incompatible blends to

demonstrate miscible behavior may be via an experimental technique. For example, it is well known that differential scanning calorimetry results may show one T_g (due to the other one not being as visible), while dynamic mechanical analysis results may show two because it is more sensitive to secondary transitions. These techniques help to identify immiscibility more so than miscibility [42]. Compatibility as defined in this work, on the other hand, relies more heavily on the properties achieved.

Regardless of the drawbacks, miscibility and compatibility is often assumed if a blend forms a film with optical clarity and has a single glass transition temperature. Equations have been developed relating the composition of the blend and T_g values of the homopolymers to predict the T_g of the blend as shown in Equation 9, Fox's Relationship. In this equation, T_g is the glass transition temperature and w_i is the weight fraction [46].

$$\frac{1}{T_g} = \frac{w_1}{T_{g_1}} + \frac{w_2}{T_{g_2}} \qquad \textbf{Equation (9)}$$

While this is characteristic of a miscible mixture, thermodynamics gives a necessary condition that for a two-component mixture with a homogenous single phase the change in the Gibbs free energy of mixing should be negative. Thus additional analysis of the resulting product (ex. mechanical testing) would be necessary in confirming, at the very least, the compatibility of the blend.

Kienzle [47] gives a mathematical description of polymer mixture properties. In Equation 10, P_1 is a property value and C_1 is the concentration of

$$P = P_1C_1 + P_2C_2 + IP_1P_2 \qquad \textbf{Equation (10)}$$

component 1, while I is the interaction coefficient. Figure 3 gives a graphical representation of the relationship being described in Equation 10. If I < 1, the property value is at its lowest at all blend compositions and the blend is considered incompatible. If I = 0, the property value varies linearly with

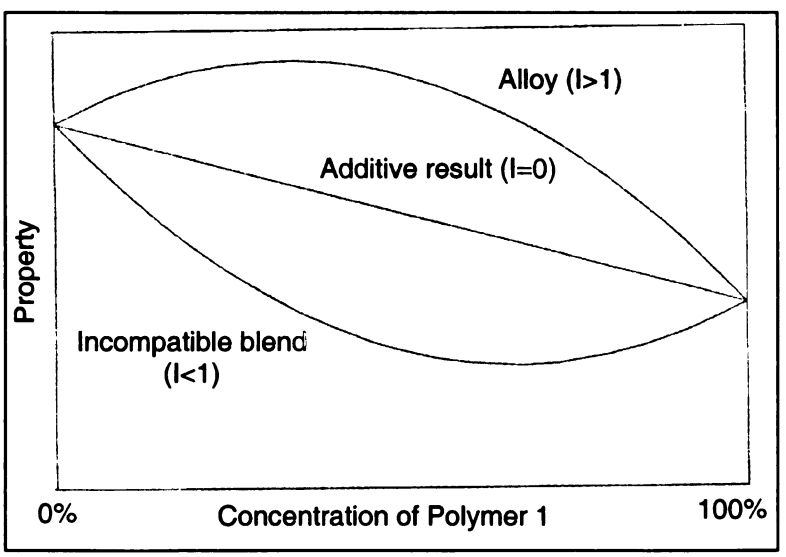

Figure 3. Graphical depiction of Equation 9 in regards to the Property of a Polymer Blend [47]

composition and exhibits higher property values than the incompatible blend. If I > 0, the property value is at its highest throughout the composition range. This

relationship provides another way to distinguish incompatible blends from compatible blends from compatible, potentially miscible blends.

Again, a miscible mixture is one in which the free energy of mixing is negative (<0) [42]. Fortunately, Flory-Huggins development inspired Scott and Tompa to apply the model to polymer-polymer systems. The free energy of a polymer-polymer system is given by Equation 11, where V_r is the reference volume close to the molar volume of the smallest repeat unit in a polymer, and x_i is again defined as the degree of polymerization for each polymer. All other variables are defined as before. The ΔG_{mix} being less than

$$\Delta G_{mix} = (\frac{RTV}{V_r})\left\{(\frac{\phi_A}{x_A})\ln\phi_A + (\frac{\phi_B}{x_B})\ln\phi_B + \chi_{AB}\phi_A\phi_B)\right\} \quad \textbf{Equation (11)}$$

zero is known as a necessary, but not sufficient criteria of miscibility because some incompatible systems also show a negative free energy [42]. A necessary and sufficient criteria of miscibility is that the second and third derivatives of free energy with respect to composition are equal to zero, as shown in Equation 12 [42].

$$\frac{\partial^2 \Delta G_{mix}}{\partial \phi_A^2} = \frac{\partial^3 \Delta G_{mix}}{\partial \phi_A^3} = 0 \quad \textbf{Equation (12)}$$

Setting both the second and third derivatives equal to zero results in the derivation of the critical conditions found in Equations 13-15. In these equations

$$(\chi_{AB})_{cr} = \frac{1}{2}\left[(\frac{1}{x_A^{1/2}}) + (\frac{1}{x_B^{1/2}}) \right] \qquad \textbf{Equation (13)}$$

$$(\phi_i)_{cr} = \frac{x_i^{1/2}}{x_i^{1/2} + x_i^{1/2}} \qquad \textbf{Equation (14)}$$

$$(\chi_{AB})_{sp} = \frac{1}{2}\left[\frac{1}{x_A(\phi_A)_{sp}} + \frac{1}{x_B(\phi_B)_{sp}} \right] \qquad \textbf{Equation (15)}$$

all variables are as defined earlier, with x_i continuing to be the degree of polymerization for component i. From the critical conditions it is apparent that for very large degrees of polymerization, the critical interaction parameter chi would be very small [42]. This makes sense because for polymers with large segments, more polymer A – polymer B interactions will take place more readily versus if there were fewer segments. This minimizes the enthalpy of interaction and thus decreases the critical interaction parameter. Also, for extremely large degrees of polymerization the critical compositions will be very small [42]. This predicts that even at very low compositions, very large polymers are incompatible and separate.

Molecular weight of the individual polymer components can affect the separation of the polymer blend [42]. Assuming the same molecular weight for

each component in order to simplify the relationship, ΔG_{mix} for a polymer-polymer mixture would be given by Equation 16. In Equation 16, M_{cr} is the critical molecular weight at which the second derivative of free energy with respect to composition is no longer greater than zero for all compositions, ρ is the density, M_i is the molecular weight of component i. The first

$$\Delta G_{mix} = \frac{\rho RTV}{M_{cr}} \left\{ \frac{M_{cr}}{M} [\phi_A \ln \phi_A + (1-\phi_A)\ln(1-\phi_A)] + 2\phi_A(1-\phi_A) \right\} \quad \textbf{Equation (16)}$$

two terms, then the last, are the entropic and enthalpic portions, respectively. It can be seen that for M less than M_{cr}, the entropic term dominates and Equation 16 is fulfilled, whereas for M greater than M_{cr}, the enthalpic term begins to dominate in comparison to the entropic term. A graphical representation of ΔG_{mix} versus volume fraction can be seen in Figure 4 for equal molecular weight polymer blends. As can be seen, free energy becomes more positive with decreasing M as compared to the M_{cr}. What is also interesting is that as free energy becomes more positive, polymer mixtures with large amounts of each component can phase separate even if the free energy is still negative. The mixture only maintains one phase at extreme compositions.

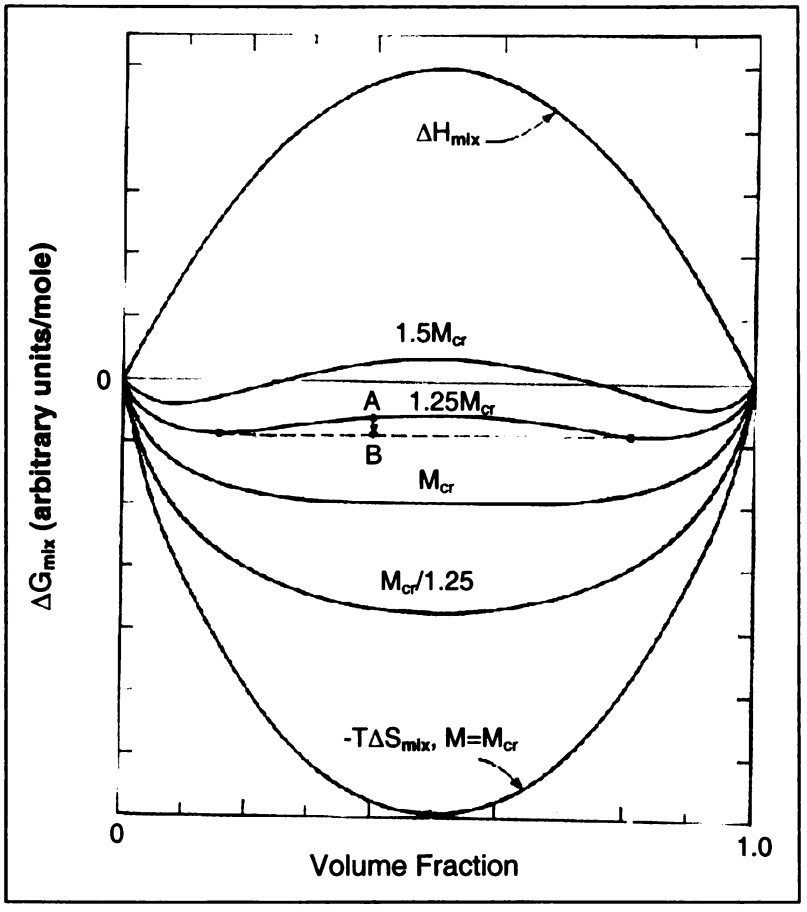

Figure 4. Free Energy of Mixing for Polymers A & B with the same molecular weight [37]

One way to enhance polymer-polymer miscibility at all compositions is to decrease the enthalpy. For endothermic systems, the lowest value of the enthalpic term is zero. For exothermic systems, however, enthalpy can be negative if certain specific interactions occur between polar groups within the mixture. In these systems, ΔG_{mix} will be negative despite the low entropy term caused by the large molecular weights of polymers. It is important to note that

even though there are specific interactions that support a negative enthalpy due to polarity, parts of the polymer chain will not be polar and will therefore cause a dispersive component of enthalpy to arise as seen in Equation

$$\Delta H_{mix} = \Delta H_{mix}^{(dispersive)} + \Delta H_{mix}^{(specific\,interactions)} \qquad \textbf{Equation (17)}$$

17. A moderate number of strong, well-dispersed interactions can help to maintain a negative enthalpy and avoid phase separation.

To help in predicting the behavior of polymer blend mixtures, molecular weight averages can be calculated for the blends using Equation 18 and 19 below. In these equations, w_i is the weight fraction of component I, $(M_n)_{mix}$

$$\left(\overline{M}_n\right)_{mix} = \frac{1}{\sum\left(\frac{w_i}{\left(\overline{M}_n\right)_i}\right)} \qquad \textbf{Equation (18)}$$

$$\left(\overline{M}_w\right)_{mix} = \sum w_i * \left(\overline{M}_w\right)_i \qquad \textbf{Equation (19)}$$

corresponds to the M_n of the blend mixture and $(M_n)_i$ corresponds to the M_n of the corresponding component. The same is true for $(M_w)_{mix}$ and $(M_w)_i$ in equation 19.

2.2.3 Phase Separation

While the intent is not to develop a phase diagram, understanding phase transitions and separations is a key to identifying immiscible or incompatible blends, and to understanding phase behavior in relation to temperature and changes in compositions. Phase diagrams for polymeric systems usually focus on the solid-liquid transition as shown in Figure 5 where the polymer goes from glassy to rubbery to the melt phase in the solid-liquid transition diagram [42]. In the liquid-liquid phase diagram shown, the effect of temperature on the blend at

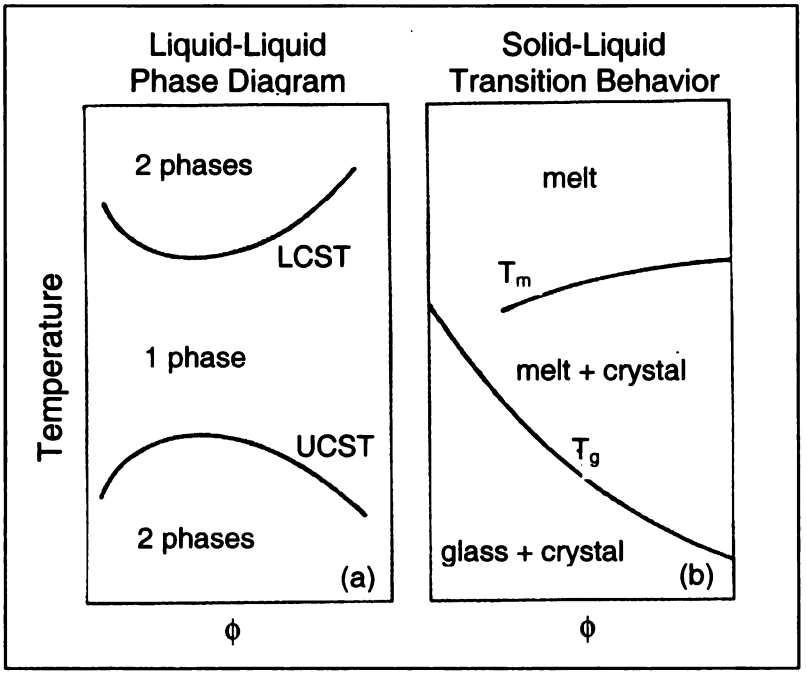

Figure 5. Phase and Transition Behaviors in Polymer Blends [42]

various composition causes the blend to either combine as one phase or separate. The liquid-liquid transition shows lower critical solution temperature

(LCST) above which liquid mixtures separate into two phases according to Figure 5. It also shows the upper critical solution temperature (UCST) below which the liquid mixture will again separate. Between these two points phase separation doesn't occur and one phase exists.

Phase separations within the amorphous region of polymer-polymer blends do cause mechanical failures and most likely can affect the attractiveness of the blend. It is important to note that miscibility in polymer blends is related to the amorphous phases of the blend as well [42]. There are cases where one polymer in a blend may start to crystallize. This may seem like it is phase separating when it may not be phase separating. While there is a solubility limit of one polymer in another, there is still value in developing partially miscible blends.

Phase diagrams of polymer blends give a better understanding of phase separations and provide insight on immiscible blends [42]. Figure 6 shows two types of phase diagrams for polymeric mixtures. The solid line represents the binodal curve boundary where stable polymer blends interface with their metastability. The dotted line represents the spinodal curve boundary where metastable polymer blends interface with unstability. The binodal and spinodal curves are also known as the limit of miscibility and metastability, respectively. In the metastable region, stable polymer blends can quickly separate into the compositions along the binodal with large fluctuations in composition as shown in figure 6 at compositions A, B, C. On the other hand, it can remain in the metastable phase indefinitely due to highly viscous, entangled, incompatible

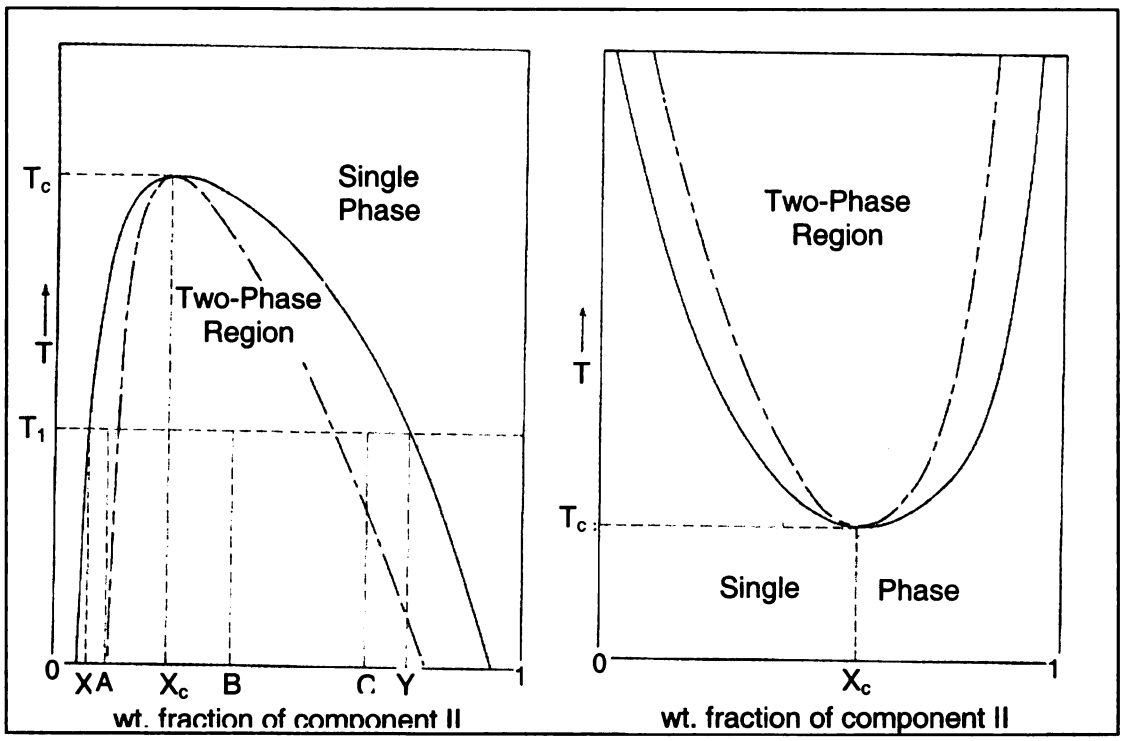

Figure 6. Phase Diagrams for Polymer Mixtures showing the binodal (solid) and spinodal (dashed) curves along with critical points [42]

polymer mixtures. At the same time, any small fluctuation in composition will immediately cause phase separation if within the spinodal boundary region.

Also, in phase diagrams for polymer blends (Figure 6) the apex of the curves where the binodal and spinodal curves meet are again the LCST and UCST points. If the curve is bent downward it exhibits a UCST, above which exists a single-phase blend. If the curve is bent upward it exhibits a LCST under which a single-phase blend exists. Endothermic (positive ΔH_{mix}) and positive entropy polymer mixtures usually display a UCST, while exothermic (negative H_{mix}) and negative entropy polymer mixtures usually display a LCST [42].

Molecular weight affects the LCST and UCST as well by increasing the UCST and decreasing the LCST with increasing molecular weight.

2.2.4 Interfacial Tension/Adhesion

While this work will not focus on interfacial and adhesion calculations, it is important to understand qualitatively how interfacial tension and adhesion plays an important role in polymer blends. Interfacial energies are thought to greatly affect dispersion, morphology and adhesion 42]. In turn, these areas (dispersion, morphology and adhesion) strongly affect the mechanical properties of a blend and, hence, the performance. The goal is to have low interfacial tension and high adhesion in polymer blends [42].

Interfacial tension is the energy barrier preventing one liquid from being immersed in another [48]. It is directly related to the work of adhesion by Equation 18, where $\square_i$ is the interfacial tension of component i, $\square_{ij}$ is the interfacial tension between two components and W_A is the work of adhesion.

$$W_A = \gamma_1 + \gamma_2 - \gamma_{12} \qquad \textbf{Equation (18)}$$

To maximize the work of adhesion, the interfacial tension of the combined blend must be minimized [42]. There are various methods for calculating the interfacial tension of the blend, some of which require knowing the surface tension of the each component of the blend. More important is the behavior of

interfacial temperature with different stimuli. For example, increasing temperature slowly decreases the interfacial tension between two polymers, whereas stimuli such as small amounts of additives and/or increasing polar interactions can dramatically decrease the interfacial tension. An increase in interfacial tension can be seen with regards to increasing molecular weight [42].

On the other hand, adhesion is the bonding or joining of dissimilar bodies (or cohesion is the joining of identical bodies) [42]. For polymers, the ideal adhesive strength is given as 15000 psi and it is reported that the practical adhesive strength is normally around 1500 psi [42]. This dramatic decrease in the practical adhesive strength shows imperfect molecular contact under practical situations. Interfacial contact is the first stage of forming an adhesive bond, followed by interdiffusion with or without chemical bonding.

Various theories of adhesion exist, including the fracture theory, the wetting-contact theory and the diffusion theory of adhesion. Each theory has strong points that relate to this work. The fracture theory states the difference between the ideal and practical strength of adhesion mentioned earlier is that practical fracturing is not reversible where as ideal fracturing is reversible [42]. From the wetting-contact theory, it is believed that adhesive strength increases with decreasing interfacial tension also mentioned earlier [42]. The diffusion theory makes several claims listed below [42].

1) Compatibility is necessary for interdiffusion to occur and increased compatibility yields increased interfacial thickness.

2) A decrease in solubility differences between the two component will minimize interfacial tension and increase adhesive strength.
3) Interdiffusion also strengthens adhesion.
4) Rate of adhesive bond formation can be expressed by a power law equation.
5) During bond formation, increasing applied pressure will increase adhesive strength because increased pressure promotes interfacial contact and provides larger interfacial areas for diffusion.

While interdiffusion plays a major role in adhesive bond formation, chemical adhesion is also a way to provide increased adhesion. It has been shown that through chemical adhesion, adhesive strength increases substantially. Adhesive strength gain from chemical adhesion is known to be 35 times greater than dispersive forces alone [42]. This value often happens to be the same as the ratio of a chemical bond to Van Der Waal bond dissociation energy. While an increase in functional groups such as carboxyls and hydroxyls has also been shown to increase adhesion to various substrates, too many functional groups may lower adhesive strength [42]. Once again, the goal in this work is to lower interfacial tension and increase adhesive strength.

2.2.5 Summary

The thermodynamics of polymer blends consists of many aspects. Understanding the fundamental equations, miscibility/compatibility and phase separation are key to developing a successful blend. Qualitative consideration of

interfacial tension and adhesion also increases knowledge about polymer-polymer blends and it provides insight into increasing the performance of those blends.

2.3 Polyester Synthesis

This segment will cover the literature review of polyesters from the 1800's to present. The literature review will be followed by a basic chemistry overview of polyesterifications closely associated with this study and a synopsis of Carothers' theory as it relates to polyester synthesis.

2.3.1 Synthesis Literature Review

The history of polyester synthesis can be dated back as far as 1847 when Berzelius reacted tartaric acid and glycerol to form a resin [13, 49]. Other scientists followed suit years after, reacting glycerol with camphoric and citric acids [49, 50]. According to Kienle, it was Baekeland's organized studies on the reaction between phenol and formaldehyde that sparked interest from General Electric (GE). This interest then led to Watson Smith's studies on the synthesis of a solid, clear resin from glycerol and phthalic anhydride that would gain significance commercially [50]. Callahan and other scientists at GE studied the glycerol-phthalic anhydride reactions and disclosed information about the process for preparing such a resin as well as specific findings that could lead to commercial applications [51]. One such finding was that using monobasic acids resulted in more flexible materials as compared to resins made with dibasic

anhydrides [49, 50]. These along with other breakthroughs led to the continued use of alkyd resins as coatings and the new use of alkyd resins commercially as adhesives [50].

Kienle did a significant amount of work on studying the kinetics and reported his work in a series of papers on the polyhydric alcohol-polybasic acid reaction [51 – 54]. First, Kienle set out to provide a systematic study on the glycerol-phthalic anhydride reactions in hopes that his results would be useful for other reactions and would disclose correlations with other sciences [51]. Using a 0.5:0.57 ratio of glycerol to phthalic anhydride, he reports details on the reaction setup, the process parameters and the isothermal kinetics of the reaction using acid and saponificaiton numbers [51]. He also reports on the viscosity, density, color and refractive index [51]. Kienle then repeated his work replacing glycerol with ethylene glycol and reveals numerous similarities between the reactions [52]. The major difference that he reports is that "...gelation of the resinous product does not take place at any temperature..." when ethylene glycol is used. Kienle continued his work by substituting the phthalic anhydride with phthalic acid and reacting with glycerol [53, 54]. The minor difference found by Kienle was that it took a slightly longer time for half of the volatile substance to be collected when compared to using phthalic anhydride. Otherwise he reports comparable results with the acid or anhydride of phthalate. The last two papers in Kienle's series on the polyhydric alcohol-polybasic acid reaction involve the reaction of glycerol with succinic acid and anhydride, maleic anhydride, adipic and sebacic acids [55, 56].

Slightly after or around the same time, Wallace H. Carothers decided to study molecular structures in order to identify any similarities with other polymeric materials. He chose to study aliphatic alcohols and carboxylic acids because they were commercially significant and relatively well studied scientifically. Carothers and others carried out esterifications with excess alcohol, and they were credited with the idea of reducing pressure to increase molecular weight. These studies eventually led to the Carothers' equation, which related the extent of reaction at the gel point to the average functionality of the mixture [57]. Carothers' expanded his work to include polyamides and was later credited with founding the very significant fibremforming polyamide, nylon. Carothers' success helped lead J. R. Whinfield and J.T. Dickson to the synthetic fiber still of major importance today, poly(ethylene terephthalate) (PET) [13].

In 1988 Jean Otton and Serge Ratton began publishing a series of papers that would study the formation of PET based on monofunctional compounds in order to "start to fill the gap" in regards to data on esterfication reactions at high temperatures [58 – 61]. Their first two papers study the esterification/alcoholysis reaction catalyzed solely by the carboxylic acid and, in another case, catalyzed by metallic derivatives [58, 59]. When catalyzed by carboxylic acids it was found that the reaction order was 2 and the reaction did not proceed with an order of 1 (or without a catalyst). In regards to metallic catalysts, Otton reports titanium compounds to be the most effective in both the esterification and alcoholysis reactions [58]. The activation energies, rate constants and the ester percent conversion for several metal catalysts are compared [59]. While other metal

catalysts show activities during esterification, their activities are low in the presence of carboxylic acid groups. In the alcoholysis reactions, some metal catalysts' activity decreases with decreasing ester content in the mixture, whereas antimony's (Sb) activity increases with decreasing ester content in the mixture [60]. It was also shown that while antimony and titanium metallic catalysts can both be useful in the formation of PET, antimony-based catalysts seem to require a higher concentration for the same effect as compared to titanium catalysts.

The works of many have contributed to the development of polyesters. In addition to the advances made by Berzelius, Kienle, Carothers, Whinfield, Otton and those associated with them, others today still contribute to the knowledge of polyesterifications involving glycerol. Such scientists as Kiyotsukuri, Tsutsumi and others have done extensive work with synthesizing polyester [62] and polyamide [63] films using multifunctional aromatic tricarboxylic acids with glycols, and aliphatic and aromatic diamines with acids, for polyester and polyamide formation, respectively. With increasing relevance to this current work, Kiyotsukuri and others have studied polyester films based on melt condensation of glycerol with aromatic and aliphatic acids in a 2:3 molar ratio to form cast films for further polymerization [64, 65]. They found that while films formed by the aliphatic dicarboxylic acids yielded a lower tensile strength than films fromed by aromatic dicarboxylic acids, they also displayed greater elongation characteristics. The opposite was true for films formed with aromatic dicarboxylic acids. Short preparation times were used for the prepolymer

formation and further polymerization as cast films continued at temperatures ranging from 270 – 210 degrees C for 0 to 6 hours. The method of prepolymer formation followed by film preparation and postpolymerization was continued by Tsutsumi with Nagata after first esterifying glycerol and sebacic acid to enhance enzymatic degradation of the polyester films formed [66]. They found that enzymatic degradation greatly decreased for mixtures of modified glycerol and terephthalic acid for an amount greater than 50 mol% of terephthalic acid.

The use of glycerol in mixtures has had both promising and less attractive outcomes. Pramanick and others incorporated glycerol into a mixture with trimellitic acid and poly(ethylene glycol) (PEG) and transesterified the mixture using $FeCl_3$ as a catalyst at various temperatures over six hours [67]. They claimed to have successfully synthesized a series of three dimensional copolyesters that could potentially be used as "bioerodable matrices for drug release in a controlled manner" [67]. Again, the addition of glycerol to a mixture of bisphenol A, phthalates and carbonate was claimed to improve "mechanical properties for film-substances, which also work well for high aromatic content systems" [68]. On the other hand unmodified glycerol was added to PET and the study attributed glycerol's poor reactivity, as compared to diethylene glycol and dipropylene glycol, to its inability to solvate PET efficiently.

Based on some studies, polyesterification products using glycerol have been classified as being hyperbranched polymers—part of the dendrimer macromolecular family. This group of macromolecular structures is characterized by their high degree of ordered (dendrimer) or disordered

(hyperbranched) branching, multifunctionality and low viscosities [69 – 72]. Studies by Hao and Lin of hyperbranched polyesters of the type X3-Y2 have shown reasonably low viscosities in the ranges of dendritic and hyperbranched polyesters [70]. On the other hand, Studies have shown that materials referred to as 'hyperbranched' that are formed from one monomer with three functional groups (X3) and another with two (Y2), sometimes do have an relatively high inherent viscosities [69].

Very few of the the X3-Y2 type reactions are carried out in the melt as suggested by Unal [72]. Carrying out polycondensations in the melt avoid the use of solvents that could be costly, economically and environmentally. Unal, Stumbe and Wyatt have carried out successful polycondensations in the melt. Unal reported that by discontinuing the X3-Y2 type reaction before gelation at 90%, one could obtain highly branched poly(ether esters) with weight average molecular weights averaging 450000 with a PDI of 13.7 [72 – 74]. More in line with the current study, Bruchmann reacted glycerol with adipic acid (similar to Kienle's work over half a century ago) varying the molar ratio of the reactants [73]. He found that while ratios above 1 of adipic acid to glycerol tended to gel, a ratio 1:1 of adipic acid to glycerol did not gel even after 8 hours. Similar to Unal, he obtained polymers with weight average molecular weights of up to 23,370 by increasing the ratio of acid to alcohol and stopping the reaction just before gelation. Most recently a study by the USDA on hyperbranched oligomers formed by the reaction of glycerol with three different acids (succinic, also studied earlier by Kienle, azelaic and iminodiacetic acid) claimed that branching is

evident via their mass spectra results [74]. The glycerol-based polyester weight average molecular weights ranged from roughly 1300 to 3000 Daltons with polydispersity indices around 1.3.

The use of glycerol to form polyester resins have been around since the mid 1800's. Extensive work has been done that led to the development of synthetic polyesters like poly(ethylene terephthalate) and poly(butylenes terephthalate). Studies continue on developing polyester resins that are useful and safe for the environment, with much of the published work involving polyesters based on glycerol coming largely from abroad with a number of studies from Japan, India and others from a number of European nations.

2.3.2 Chemistry

The chemistry involved in this study includes a combination of esterification and transesterification reactions, all part of step-growth polymerizations, although not all step-growth polymerizations involve condensation reactions. This section will cover the basics of polycondensation to form polyesters. Forming polyesters is a two step procedure including 1) Esterification or Transesterification where most of the monomers react and 2) Polycondensation where higher molecular weight is gained by the removal of low molecular weight species under vacuum at high temperatures. Classic polyesters, poly(butylene terephthalate) and poly(ethylene terephthalate), will be referred to as examples.

Esterification and Transesterification

In esterification reactions, mainly carboxylic acids, dicarboxylic acids or their anhydride derivatives are used in conjunction with other functional groups such as alcohols (diols, triols or polyols) to form ester linkages [49]. Acid catalysis enhances the ester reaction by adding electrophilic character to the carbonyl carbon atom, making it more attractive for the negatively charged oxygen of the alcohol. Base catalysts are used as well. The reactions in Figure 7 show esterification reactions using maleic acid,
maleic anhydride, and a transesterification reaction using dimethyl terephthalate, each with glycerol. Using maleic anhydride reduces the amount of water formed as compared to using maleic acid. The last reaction shows a transesterification reaction where one ester and one alcohol form a different ester and different alcohol. Equilibrium exists in these reactions and in order to drive polycondensation, the reaction must be pushed toward polycondensation by the removal of by-products. The atoms connected in the ovals represent ester linkage formations. PBT production transesterification is used and methanol is distilled off as a by-product.

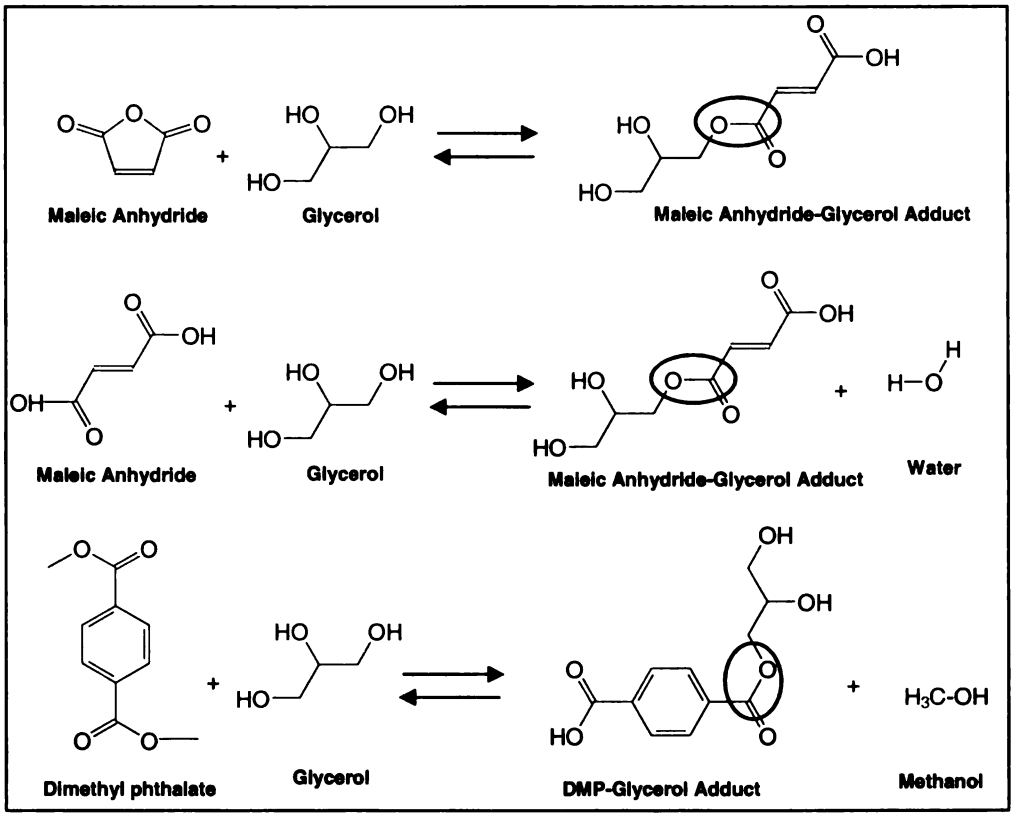

Figure 7. Esterification reactions using Maleic Acid and Maleic Anhydride as examples and Transesterification reaction using dimethyl terephthalate

Polycondensation

Polycondensation is where the reaction is driven to form high molecular weight polyesters. Polycondensation in the melt occurs in a vaccum at high temperatures. Lower molecular weight species or excess glycol are removed at these high temperatures and under intense mixing. Even under these conditions, oligomers may still be present. In fact, PET and PBT contain some oligomers even on the commercial scale.

Polycondensation reactions take time to form high molecular weight species and they require high conversions. In polycondensation reactions, reactivity is assumed to be independent of molecular weight under the principle of "equal reactivity" [49]. Very viscous mixtures form in polycondensation [50]. Hence flowing a dry, inert gas through the mixture aids in the removal of the appropriate components from the mixture and in the suppression of oxidative decomposition due to the presence of oxygen.

2.3.3 Carothers' Theory

Relation of polymer size, percent conversion and feed molar ratios, groups in step-growth polymerizations can be attributed to what is known as Carothers' equation. Carothers' equation is a guiding principle in polyester synthesis, helping to design reactions having appropriate yields with respective molecular weights. The basic assumptions associated with Carothers' theory are summarized below:

1) Equal reactivity of functional groups of the same kind or on the same molecule independent of the size of the molecules reacting
2) Equal reactivity of functional groups even after other functional groups on the same molecule have reacted
3) Homogenous, single-phase reaction mixture

To arrive at the number-average degree of polymerization, two different functional groups must be present (A-type and B-type functional groups). Functionality is defined by Rudin as the number of positions in the monomer

available for reaction under specific conditions [43]. For a given monomer, a certain average functionality exists. Equation 20 defines the average functionality (f_{av}), where f_i is the functionality of the monomer and N_i is the number of moles. This equation is specifically for when two types of functional groups reacting are present in equal concentrations. When there is an excess of one functional group, the other type of functional group will be the limiting functional group and the average functionality can be calculated using Equation 21, where n_a is the limiting

$$f_{av} \equiv \frac{\sum N_i f_i}{\sum N_i} \qquad \textbf{Equation (20)}$$

$$f_{av} = \frac{2n_A}{\sum N_i} \qquad \textbf{Equation (21)}$$

number of equivalents (given by the moles multiplied by the functionality of the reactant), and N_i is the moles of reactant i.

The derivation of Carothers' equation requires an expression for the extent of conversion (p). The extent of conversion can be defined as the ratio of the number of functional groups reacted to the number of functional groups initially present. This ratio can be seen in Equation 22, where N_o is the initial total number of moles and N is the final number of moles. The numerator represents

$$p = \frac{2 \cdot (N_o - N)}{N_o f_{av}} \qquad \textbf{Equation (22)}$$

the amount of functional groups used in the formation of polymer-polymer linkages.

To get the degree of polymerization (X_n) associated with the mixture, the initial number of monomer unit (N_o) and the remaining number of moles (N) must be known. Since the total moles is known, the N_o is known. To find N, Equation 22 can be arranged to give Equation 23 where all the variables are as defined

$$N = (\frac{1}{2}) \cdot (2N_o - N_o pf_{av}) \qquad \textbf{Equation (23)}$$

before. Therefore X_n can be quantified as shown in Equation 24 where X_n is the

$$\overline{X_n} = \frac{N_o}{(\frac{1}{2}) \cdot (2N_o - N_o pf_{av})} = \frac{2}{2 - Pf_{av}} \qquad \textbf{Equation (24)}$$

degree of polymerization and all variables are as defined earlier. This is Carothers' equation and it can aid in predicting the gel point in step-growth reactions, choosing an optimal ratio of reactants and more. The degree of polymerization (X_n) will go to infinity when a gel is formed. Thus, by setting the denominator of Equation 22 equal to zero, the percent conversion at which the reaction will gel can be found. Since gelation actually occurs when the weight-average degree of polymerization (X_w) becomes infinite (not when the X_n is infinite as predicted by Carothers) and X_w is greater than or equal to X_n the mixture will reach its gel point at conversions lower than predicted [43].

Chapter 3

Materials and Methods

This chapter lists all the materials used in the production of CA blends and glycerol-based polyesters along with the supplier information. It also includes basic information on materials used in various characterization techniques.

The second half of this chapter briefly discusses the processing equipment used in blend preparation or in producing test specimens. All characterization techniques used are summarized in general and, when possible, general procedures are described.

3.1 Materials

This section divides the materials into the following three categories. The bulk

1) Bulk Materials
2) Catalysts
3) Chemicals

materials include cellulose acetate, triacetin, poly(butylene adipate-co-terephthalate) and glycerol. The catalysts are sodium carbonate and dibutyltin oxide and the chemicals are pyridine, acetic anhydride, n-butanol and tetrahydrofuran.

3.1.1 Bulk Materials

Cellulose Acetate

Sleek, vibrant, modern, and shiny are words that all describe some positive attributes of CA. Cellulose acetate has the ability to produce products that are sleek and smooth with a shine or a reflection, making something seem modern. While demand for cellulose acetate-based products has decreased, it has never been completely eliminated from the market, speaking to its longevity. Cellulose acetate has still found use in various markets due to aesthetics coupled with strength. Typical cellulose acetate-based products include or are used in eyeglass frames, tool handles, cigarette tows, toys, clear adhesive tape, writing instruments, and face shields.

Clarity, toughness, compatibility with dyes and resistance to grease are among some of the advantages of using CA and why CA is used in many of these items [10]. Aside from aesthetics and excellent mechanical properties for various applications, cellulose acetate is produced from renewable natural resources and has the ability to biodegrade, making it an ideal raw material source for bio-based research and development of polymer products. Unfortunately, there are some drawbacks that come with cellulose acetate including engineering issues related to processing, along with the miscibility and compatibility of its blends. Table 1 shows some basic properties of CA and Figure 2 gives the structure of CA . The cellulose acetate, (CA-398-30, DS of 2.46, 50lb bag) was purchased from Eastman Chemical Co. (Kingsport, TN).

Acetyl Content (%)	39.7
Thermal Decomposition (°C)	304
Specific Gravity	1.31-1.32
Melting Point (°C) DSC	230-250
Glass Transition (°C) DSC	189

Table 1. Eastman Cellulose Acetate Properties

Triacetin

Triacetin or glyceryl triacetate ($C_9H_{14}O_6$, ~240 kg) was purchased from Chemical S.P.A in Italy. Triacetin structure can be seen in Chapter 4, Figure 12, with other plasticizers for cellulose acetate. It has a formula weight of 218.21 g/mol, a boiling point of 258 °C, a melting point of 3.2 °C and a freezing point of –78 °C.

Poly(butylene adipate-co-terephthalate) (PBAT)

Poly(butylene adipate-co-terephthalate) is a biodegradable, aliphatic-aromatic copolyester introduced by BASF to address the demands of growing domestic waste issues. The structure of PBAT can be seen in Figure 8. The copolymer is made

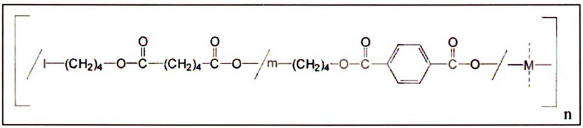

Figure 8. Structure of BASF Poly(butylene adipate-co-terephthalate) [40]

up of 22.2 mol% terephthalic acid, 27.8 mol% adipic acid and 50 mol% butanediol as determined by CNMR [40]. Unfortunately, PBAT is not made from renewable resources. Nevertheless, PBAT boasts a faster degradation rate than cellulose acetate on composting, as shown in Figure 9.

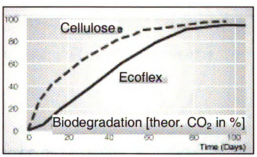

Figure 9. Biodegradation of Cellulose Compared to that of PBAT [41]

It also exhibits properties similar to LDPE, having high molecular weight and a long chain branched molecular structure [41]. The toughness and flexibility of PBAT has made it a natural pick for blends with other biodegradable polymers like starch and PLA [42,43]. Table 2 gives a summary of some properties of

PBAT. These properties have allowed the use of PBAT in various areas. Currently PBAT is used in making films applicable to agricultural, packaging and composting uses. Some other benefits of PBAT include its good thermostability (up to 230 °C), and its ability to be easily processed with no predrying of the pellets. The grade of Ecoflex (~55 lbs) purchased from BASF (Mount Olive, NJ) is F BX 7011.

Mass Density (g/cm^3) ISO 1183	1.25-1.27
MFR 190°C, 2, 16 kg ISO 1133	2.7-4.9
Melting Point (°C) DSC	110-120
Glass Transition (°C) DSC	-30
Shore D hardness ISO 868	32
Vicat VST A/50 (°C) ISO 306	80

Table 2. BASF PBAT (also known as Ecoflex) Properties

Glycerol

Glycerol, also known as glycerine, is a hygroscopic, trihydric alcohol, as shown in Figure 10. It is made naturally as a by-product of soaps and synthetically from propylene. It is an odorless, colorless, sweet, viscous liquid.

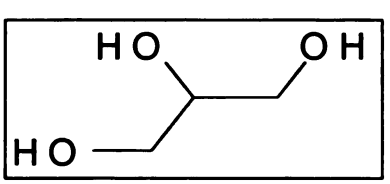

Figure 10. Structure of Glycerol

Glycerides, the esters of glycerol, are found naturally in animal and/or vegetable fats and oils. More currently, glycerol has been produced as a by-product in biodeisel production [44]. Figure 11 shows the associated reaction of the

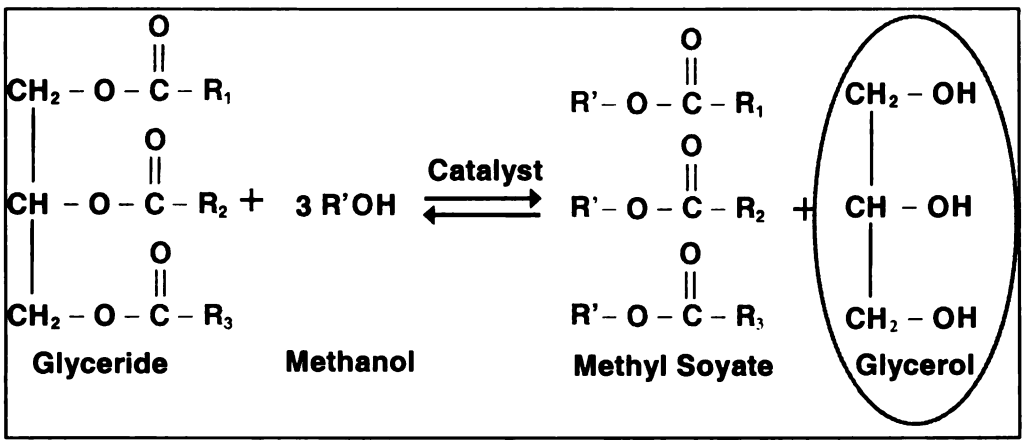

Figure 11. Biodiesel production chemical reaction showing Glycerol as a by-product [45]

process. A triglyceride reacts with methanol to give methyl esters used in biodeisel production and glycerol, the by-product. With an increasing interest in biodiesel production, the development of glycerol esters can play a key role in the efficiency of biodiesel production, adding giving value to the overall production. Glycerol properties are summarized in Table 3.

Melting Point (°C)	17.8
Boiling Point (°C)	290
Flash Point (°C) Closed Cup	160
Density (g/cm3)	1.261

Table 3. Properties of Glycerol

Some common products that use glycerol in the food and personal care industries include toothpaste, skin care, hair care, icing, food coloring and more. In the plastics industry, glycerol is often used as a plasticizer or lubricating agent. Nabar et al. used glycerol in the production of starch foams via reactive extrusion [4]. In addition to its softening capabilities, glycerol can increase flexibility and toughness. The anhydrous glycerol (4L) with a density of 1.257 g/cm3 and a formula weight of 92.10 g/mol was purchased from J.T. Baker.

3.1.1 Catalysts

The two catalysts used were sodium carbonate and dibutyltin oxide. Both are useful in transesterification reactions. Sodium carbonate (Na_2CO_3), ACS grade with greater than or equal to 99.5% purity was purchased from Sigma Aldrich in a 500g batch. It's formula weight, melting point and density are 105.99 g/mol, 851 °C and 2.532 g/cm^3, respectively. Dibutyltin oxide ($C_8H_{18}OSn$) with a purity of 98% was also purchased from Sigma Aldrich in a 100g batch. Its formula weight is 248.92 g/mol and it's melting point is greater than 300 °C.

3.1.3 Chemicals

A number of chemicals were used in the synthesis of glycerol-based pre-polymeric materials and for the characterization of samples (synthesized or extruded) depending on the method used. Dimethyl terephthalate ($C_{10}H_{10}O_4$) was a main component reacting with glycerol in the esterification process. The

chemical was purchased from Sigma Aldrich in 3 kg batches. The formula weight and melting point of DMT are 194.19 g/mol and 140 °C, respectively.

The use of acetic anhydride, pyridine and n-butanol was necessary for characterization of polyester prepolymer via the hydroxyl value calculation. Acetic anhydride ($(CH_3CO)_2O$, 500mL) with greater than 97% purity was purchased from Columbus Chemical Industries meeting ACS specifications. The formula weight of acetic anhydride is 102.09 g/mol. ACS reagent grade pyridine (C_5H_5N, 500 mL) was purchased from J.T. Baker. It's formula weight and boiling point are 79.10 g/mol and 115.3 °C, respectively. The ACS reagent n-butanol ($CH_3(CH2)_3OH$, 500mL) with a formula weight of 74.12 g/mol was also purchased from J.T. Baker.

Tetrahydrofuran was used in titration studies and as the solvent mobile phase in gel permeation chromatography (GPC). The tetrahydrofuran (C_4H_8O, 500 mL) used in titrations was purchased from J.T. Baker. The ACS reagent grade tetrahydrofuran has specific gravity of 0.884, formula weight of 72.11 g/mol and a distilling temperature of about 66°C. The tetrahydrofuran (C_4H_8O, 4L) was inhibitor free, CHROMASOLV Plus specifically for use with GPC experiments. This tetrahydrofuran was greater than 99.9% pure, and was purchased from Sigma Aldrich. Its boiling point, melting point and density are 66 °C, -108 °C and 0.889 g/cm^3, respectively.

3.2 Processing and Characterization Methods

The processing methods discussed include reactive extrusion with a twin-screw extruder for blending of polymers and extrusion/injection molding with the DSM Micro extruder and injection molder for test specimens. The characterization techniques mentioned are categorized by chemical, thermal, dynamic mechanical and morphological analysis. It is important to note that most experiments most experiments were repeated at least once. Further repeat experiments were done based on judgement.

3.2.1 Processing Equipment & Procedures

Century Extruder

A Century ZSK-30, twin-screw co-rotating extruder was used for all polymer blending. The extruder has a screw diameter of 30 mm and an length to diameter (L/D) ratio of 40. The extruder system is equipped with an extruder driver with a speed control gearbox, a main AccuRate, single-screw bulk metering feeder, another AccuRate single screw side-feeder, a cylindrical filament die with a diameter of 2.7 mm and a length of 8.1 mm, and a cooling system for the nine zone heating blocks of the extruder. Cooling of the extruder barrel can be controlled by adjusting the flow rate of the cooling water supply manually via nine valves for the nine zone heating blocks. There is a thermocouple and pressure sensor affixed downstream the extruder to measure the temperature and pressure of the melt and a venting/vacuum port located downstream over zone heating block number 8. Other parts of the extrusion

system include a water-bath equipped with a hose for draining and filling, a Scheer Bay Co. pelletizer (Model # BT25) for solids handling and a MasterFLex pump (Model # 7524-40) from Cole Parmer Instrument Co for addition of liquid additives to the mixture.

In general, processing of blends included the use of one or two feeders at certain calibrated speeds for the feeders. The material entered the extruder via a hopper. The feed for any liquid additives is located right after the main feed through zone 1 of the extruder. The material passes through a series of compounding and conveying screws, a venting zone and eventually the die exiting the extruder. As the polymer strand exited the extruder, it was quenched in a water bath and continued downstream in the water bath to the pelletizer. The material was then collected and stored or dried for future use.

DSM Micro Extruder and Injection Molder

The DSM Micro Extruder and Injection Molder is a micro-mixing and -molding piece of equipment from the Netherlands. The DSM Micro 15 cc consists of (1) the micro-extruder with twin co-rotating screws for mixing and conveying, (2) a tiny cylinder attached to a mini feed hopper for feeding material into the barrel of the extruder, (3) a transfer cylinder for moving the product from the micro-extruder to be injection molded and (4) the mini-injection molder for making common molded parts such as tensile bars, rectangular bars of various sizes and discs.

In general about 10 – 15 g of material (depending on polymer pellet or powder density) was placed in the hopper and plunged directly into the mini-extruder barrel. The material was allowed to mix until the viscosity began to fall suggesting good mixing had occurred. The transfer cylinder was then used to store and transport the polymer melt exiting the micro-extruder. As the transfer cylinder was being filled, the piston in the cylinder was pushed out. The transfer cylinder was placed in the mini-injection molder and a high-pressure cylinder forced the transfer cylinder piston to push the material from the transfer cylinder to the DSM mould. The mould was removed and the injection moulding process was repeated until the micro-extruder was empty. At this point the micro-extruder was refilled and the process continued as before.

3.2.2 Synthesis Procedure

A 1:1 molar ratio of glycerol and DMT was combined in a reaction kettle. The reaction kettle was equipped with reaction kettle cover containing three 24/40 joint openings and one 29/42 joint in the center. The center joint opening was used for the glass or metal (recommended) stirrer. For the metal stirrer a poly(tetrafluoroethylene) (PTFE) bearing was required. The other three joint openings were used for the (1) D&S trap, (2) nitrogen inlet and (3) thermometer/temperature controller probe combined. Above the D&S trap was a condenser and at the top of the condenser was an outlet flowing to a container of silicon oil to ensure nitrogen flow out of the system and no airflow into the system. Before the cover was placed over the kettle, silicon grease or an o-ring

was placed between the cover and the kettle for a tight seal when clamped together.

Once the system was contained, nitrogen was allowed to flow through the system for ten to fifteen minutes. The temperature controller was set to 100 at a power attenuation of 5 (this means that only 50% of the full power was being sent to the reaction mantle). The slow heating was used to aid in lower sublimation of the DMT by allowing uniform heating throughout the vessel. At 100°C a certain amount of catalyst was added to the mixture and the temperature was increased after fifteen minutes to 200°C. Once the temperature equilibrated to the set point, it was held there for four hours to allow for a higher rate of reaction and more methanol formation. After four hours, the reaction was stopped and the pre-polymer was collected and cooled.

3.2.3 Characterization Techniques

Characterization of the reaction product and of the blends can be broken down into three categories. Studying the structure, analyzing the thermal behavior and assessing dynamic mechanical and morphological equipment will assess polymer blend characteristics.

Chemical Analysis

The chemical characterization techniques help to identify percent conversion in synthesis development and average molecular weight data for both synthesis products and polymer blends.

A. Acid/Base Titration

Titration is a method used to quantify an unknown amount of acid in a solution by using a known concentration of standard solution (also known as the titrant) that reacts with the unknown. With a few drops of an end-point indicator (phenolphthalein) in the unknown acidic solution, the end of the reaction can be identified via a color change. The amount of titrant added to the unknown solution to bring about a color change can then be related to the unknown amount of acid on a molar basis via a balanced chemical equation, molarity of the standard and volume of the unknown solution to give molarity of the reagent in question. Acid number procedures were determined per the ASTM D1980 Standard [75] with minor changes. About 7-8 grams of each sample was dissolved in 100 mL of THF for the acid value titrations.

B. Hydroxyl Value

Hydroxyl value is a technique used to quantify hydroxyl groups in a sample. In the case of this study, it was being used as a measure of conversion for polyester synthesis. All hydroxyl values were calculated per the ASTM D1957 standard [76] using about 0.4 grams of each sample. The samples were heated for two hours on the water bath.

C. Average Molecular Weights

Gel permeation chromatography measures a polymer's molecular weight distribution as compared to a standard. The material is dissolved in a solvent

and the solute particles of the specified materials flow through a column of porous particles in which larger solute particles elute from the column faster than smaller solute particles because they pass through less of the porous particles due to their size. The information gathered from this experiment is important because it provides valuable information that can be indicative of a polymer's mechanical properties and processing behavior. In addition, the breadth of distribution given by the polydispersity index can potentially yield information on whether there may be significant branching of the polymer sample.

Molecular weight averages and distributions of all samples were carried out on a 600 multisolvent gel permeation chromatography (GPC). The GPC was equipped with a 2410 refractive index detector, a 717 auto sampler and the Breeze software from Waters. Three Waters Styragel Columns ranging from 500 to 500,000 Daltons were used in the GPC. HPLC grade tetrahydrofuran (THF) was used as the mobile phase and the calibration was performed against narrow polystyrene standards. Each sample was dissolved in THF at about 2 to 3 mg/mL and filtered into clear vials with snap caps with 0.45 mm PTFE filters.

Thermal Analysis

The thermal analysis techniques used were differential scanning calorimetry (DSC) and thermogravimetric analysis (TGA). Determination of transitions helped in developing processing parameters and to explain behaviors seen in the blends.

A. Thermogravimetric Analysis (TGA)

Thermogravimetric Analysis reveals the thermal stability of a material by monitoring weight percent and weight percent per degree as a function of temperature. A high resolution TGA 2950 from TA Instruments was used to determine the ultimate degradation temperature of all the materials, assessing the thermal stability.

In general an empty pan was tared in the TGA chamber under nitrogen and after taring was completed, the sample was added to the pan and enclosed in the chamber. The confined chamber was purged with nitrogen gas. For all samples the sample purge of nitrogen was set at 60 ml/min and the balance purge at 40 ml/min. All samples were studied by heating to 500 °C at a rate of 20°C/min.

B. Differential Scanning Calorimetry (DSC)

Differential scanning calorimetry provides information on the thermal transitions within a material. It measures the heat flow to the material and compares it to a standard, identifying the thermal transitions from the comparison. It also records values of temperature and time. It has been used to identify glass transition, melting and crystallization temperatures, and melting and crystallization enthalpies. Analysis is done in a confined chamber with a nitrogen purge at 100 ml/min.

In this study a DSC 2920 from TA Instruments with a cooling unit was used to identify phase change temperatures (T_g, T_m, T_c, ΔH_m and ΔH_c , where T_g

is the glass transition temperature, T_m and T_c are melting and crystallization temperatures, and H_m and H_c are the melting and crystallization enthalpies).

Dynamic Mechanical Behavior

Dynamic Mechanical Analysis assesses the mechanical properties of a material as it relates to time, temperature, and frequency. DMA also provides a variety of modes in which to mechanically deform a material. Specifically, a DMA 2980 from TA Instruments was used to measure the storage modulus, loss modulus and tan delta, to gain insight on the mechanical, glass transition and viscoelastic behavior, as well as the homo-/heterogeneity of the materials. The DMA was equipped with a liquid nitrogen tank to allow attaining very cold temperatures.

The three-point bending mode was used in all tests to facilitate measurements without grip interference. All DMA tests carried out in this study utilized rectangular test specimens from the DSM micro-extruder and mini-injection molder that were cut to have dimensions of about 38 x 12 x 3.6 mm (l x w x h). The DMA tests were all performed under the same conditions. The method used for all the samples is listed below.

1) Initial temperature: -100.00 °C
2) Isothermal for 10.00 min
3) Ramp 3.00 °C/min to 85.00 °C

Morphology

A Phillips Electroscan 2020 environmental scanning electron microscope (ESEM) was used to study the surface morphology of pellets. Polymer pellets were sectioned using a razor blade. The sample was then mounted on an aluminum stub with graphite tape.

Chapter 4

Cellulose Acetate Blends with Ecoflex

4.1 Overview

The need for bio-based bioplastics is evident. With the opportunity to design blends with bio-based content comes the ability to be proactive and integrate biodegradable materials in the design phase. The materials being introduced in this blend have the potential to meet the need for bio-based, biodegradable plastics that have the properties necessary to compare to plastics on the market.

Cellulose acetate is a bio-based, biodegradable raw material that maintains presence in the market even after being replaced in several areas by cheap, synthetic plastics [13]. This organic ester's prime properties include hardness, good impact resistance, smooth texture, high clarity, and an ability to incorporate several pigments. Cellulose acetate as a main component in bio-based plastics is a natural selection.

Also a natural selection for blends with CA is PBAT, a biodegradable, aliphatic-aromatic copolyester. Both tested for biodegradability in composting environments, and both containing esters, CA and PBAT would seem good choices for blending. Good toughness and flexibility, due to the aromatic and aliphatic components, respectively, are traits of PBAT and should help to maintain the toughness of CA while offering some flexibility to the blend. Also, with PBAT having a T_g of –30°C, blends of CA and PBAT could possibly cause a

decrease in the blend T_g if the materials are miscible or even partially miscible. It is important to note that there are many polymer pairs that are not miscible, but studying these blends (miscible or immiscible) can lead to an understanding of what is needed to promote compatibilization of the blend.

BASF developed PBAT as an answer to the need for more environmentally-friendly plastics. They noted that bio-based products could not perform at the level of synthetic products, and, hence, decided to use synthetic materials to design their final product [40]. Regarding CA, external plasticizers have often been used to increase the processing range of CA by decreasing the T_g. Brydson notes that some of the most important plasticizers for CA are dimethyl phthalate (DMP) and triacetin (TA) [42]. More recently, triethylcitrate (TEC) has also been recognized as a good plasticizer for CA. The structures for DMP, TA and TEC are shown in Figure 22 and calculated solubilities using equation 6 are shown in Table 9. Although these are great external plasticizers for processing CA, they tend to leach or bleed out, thereby altering the properties of the blend.

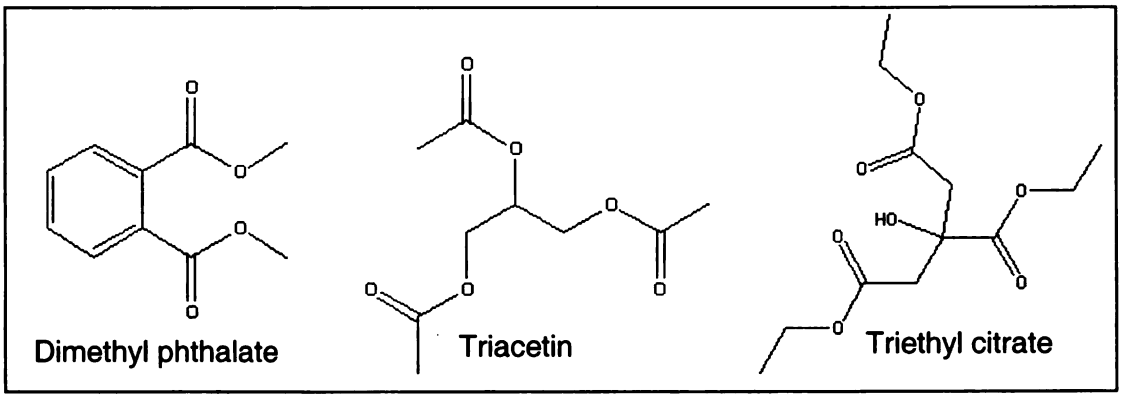

Figure 12. Important External Plasticizers for Cellulose Acetate

A successful blend of CA and PBAT could potentially address two fundamental issues in CA and in PBAT. The first issue is the lack of bio-based content in PBAT and the second issue deals with the small temperature processing range of CA. Adding CA to the blend can increase the biobased content of PBAT making it more attractive from a biobased perspective. Also, a compatible blend of CA with PBAT can broaden the processing range of CA and eliminate the need for the plasticization of CA with low molecular weight plasticizers.

Plasticizers	Calculated Hoy Series Solubility Parameter	Paper by Ljungberg, Nadia using Hoy Series
TA	19.2	19.1
TEC	19.7	19.7
ATEC	18.9	18.9
ATBC	18.0	18.0

Table 4. Calculated solubilities compared to literature using Hoy parameters

4.2 Materials & Methods

The materials used in this study include cellulose acetate, triacetin, poly(butylene adipate-co-terephthalate), dibutyltin oxide and inhibitor-free tetrahydrofuran. The methods for processing include a reactive extrusion system and the DSM for preparation of test specimens. The characterization techniques employed include gel permeation chromatography, differential scanning calorimetry, thermogravimetric analysis, dynamic mechanical analysis and environmental scanning electron microscopy.

4.2.1 Specific Processing Methodology

The CA used in the blends was dried for at least twelve hours to remove moisture. The Ecoflex used in the blends was dried for the same amount of time only if the amount in the mixture was less than 70%. Reactive extrusion of CA and PBAT occurred using the following temperature profile from feed to die: 30/145/200/220/225/230/230/230/225/220 (°C). The melt temperature ranged from 220-226°C and the motor speed was set at 180 RPM. Blends ranging from 50% to 70% Ecoflex were prepared using the twin-screw extruder under the given conditions

In the second set of CA-Ecoflex blends, the blend of just 30% CA and 70% Ecoflex was extruded using the following temperature profile from feed to die: 15/40/80/150/190/220/230/230/230/220 (°C). The melt temperature was about 227 °C and the motor speed was 250 RPM. CA with 30% triacetin was extruded with the following temperature profile from feed to die:

15/40/100/150/180/210/210/210/210/200 (°C). The melt temperature was 203 °C and the motor speed was 200 RPM. The blends of plasticized CA (30% and 50%) and Ecoflex (70% and 50%) with and without catalyst were extruded at the same temperature profile as was used to plasticize CA. The melt temperatures ranged from 203 – 210 °C and the motor speed was set at 250 RPM.

4.2.2 Specific Characterization Methods

For DSC, the sample was heated to 210 °C at a rate of 20 °C/min followed by quenching to –55 °C where it was held isothermally for 1 min. The sample went through the first heat scan to erase the thermal history and allow for the removal of moisture from the blend. The melting and cooling data were gathered from the second heat scan when the sample was reheated to 255 °C at a rate of 20 °C/min followed by cooling to 20 °C at 20 °C/min.

The GPC, TGA, DMA and ESEM methods used are as described earlier in the general characterization section. ESEM images of the blends were taken at magnifications of 1000, 2000 and 5000.

4.3 Results and Discussion

4.3.1 Summary of Runs

Various compositions of CA and PBAT were extruded with no additives simply to study the effect of composition on the blends. These samples are listed above the darkened line. Blends with higher than 50% CA by weight could not

be extruded. Below the darkened line, in the same table, are the samples used to study the effects of plasticization, catalyst and composition. These samples were subject to the corresponding processing and characterization methods discussed in section 4.2. The naming convention for samples below the darkened line was developed by using the first letter of each material ("C" for CA, "CT" for plasticized CA and "P" for PBAT), followed by numbers representing the percentage of each component in the order that the component is listed in the sample name. These runs were used to help elucidate the effects of composition and plasticizer on CA-PBAT blends, as well as the effects of catalyst and composition on plasticized blends of CA-PBAT.

Sample	Cellulose Acetate (CA)	Triacetin	Ecoflex (PBAT)	DBTO (phr)
30% CA	30	---	70	---
40% CA	40	---	60	---
50% CA	50	---	50	---
CP37	30	---	70	---
CT73	70	30	---	---
CTP37	21	9	70	---
CTP55	35	15	50	---
CTPD37	21	9	70	1
CTPD55	35	15	50	1

Table 5. Extruded Blends of CA and PBAT without modification

Effect of Composition on Thermal Properties of CA-PBAT

The effect of composition on the degradation temperature of the blends can be seen in Table 6. Note t hat PBAT is directly from the manufacturer and NPBAT is PBAT that has been extruded one time. Figure 13 shows an example of the two distinct derivative weight loss curves formed for 30% CA. Samples at all loadings of CA showed similar curves. This confirms that CA and PBAT do not form a miscible blend at the weight percentages of CA studied. In fact, a closer look at Table 6 shows that the CA blend component degradation temperature shifts towards the degradation temperature of 100% CA, while PBAT temperatures remain about the same as that of neat PBAT (NPBAT). At a composition of 30 wt. % CA, however, the blend displays a slightly higher degradation temperature for the CA component. This suggests that there may be some compatibility between the two components.

Sample	CA	PBAT
100% CA	344.59	---
50% CA	344.73	374.29
40% CA	349.05	374.63
30% CA	350.49	376.02
100% PBAT	---	373.68
100% NPBAT	---	375.24

Table 6. Preliminary CAPBAT degradation values as retrieved by TGA

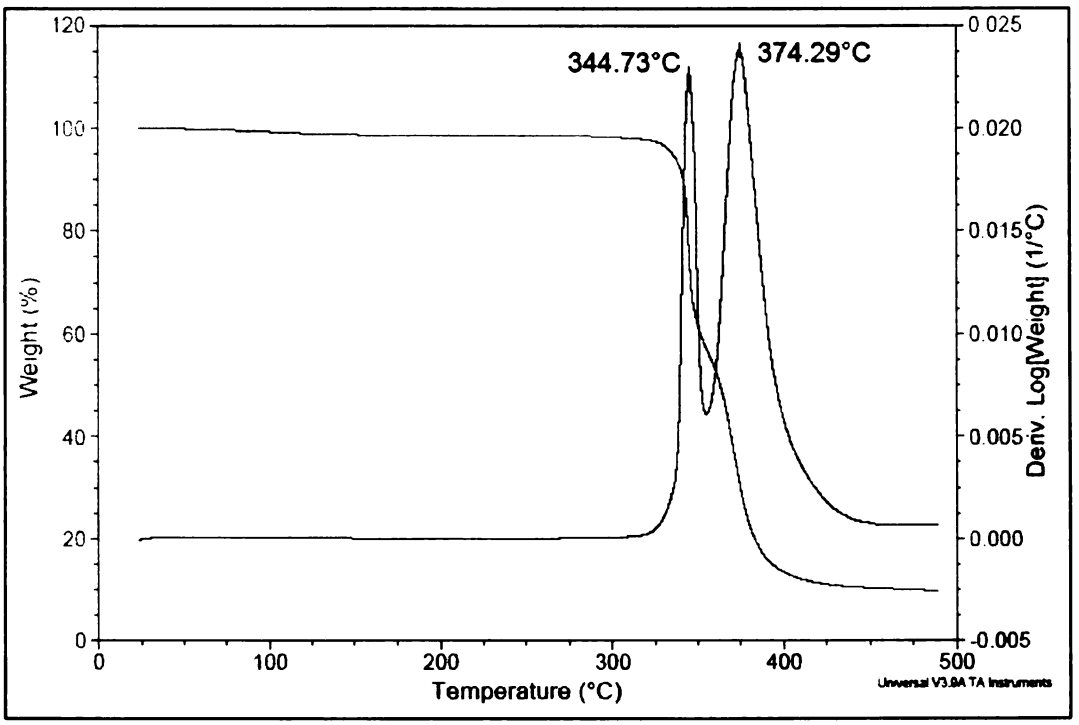

Figure 13. Weight loss and derivative weight loss (represented by two maximas) curve of CAPBAT sample to illustrate the two component blend of CA and PBAT

Comparison of the samples' weight loss curve show that the blends first mimic the weight loss curve of CA (the component with the lower degradation temperature) and later the PBAT (the component with the higher degradation temperature) weight loss curve is followed. Weight loss curves shifts toward the higher degradation temperature weight loss curve (PBAT) with increasing PBAT content, exhibiting more PBAT-like characteristics and possibly indicating increased compatibility. These trends can be seen in Figure 14.

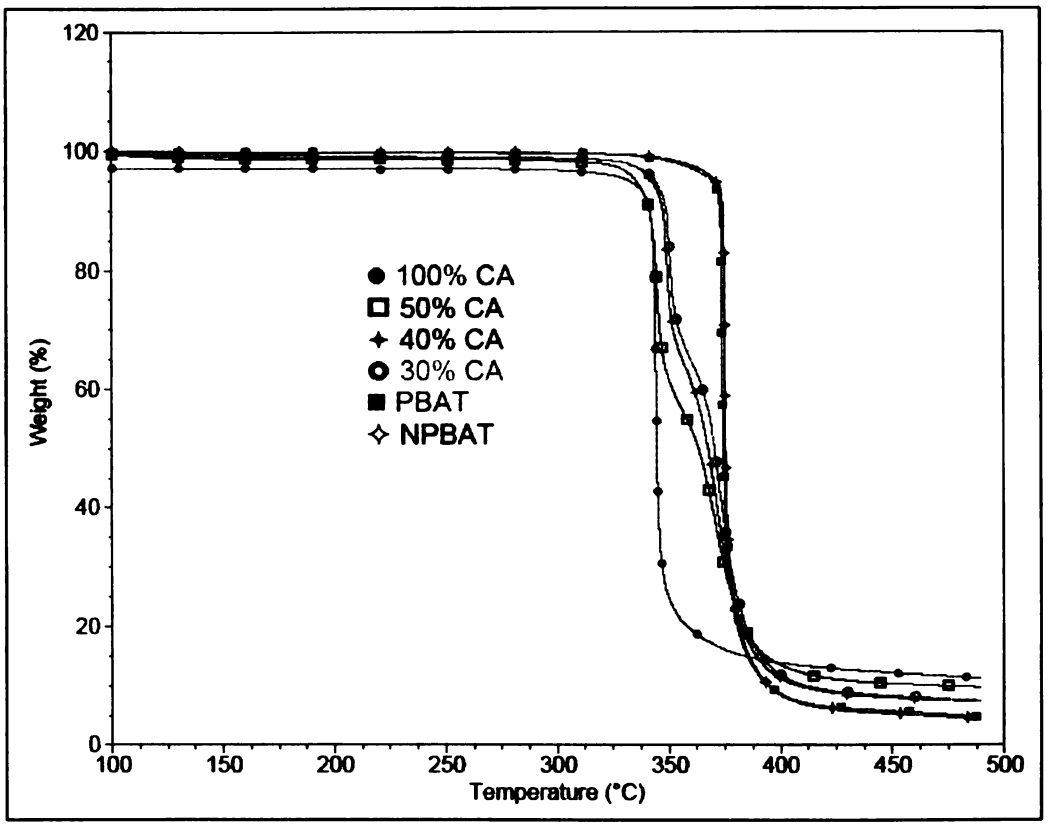

Figure 14. Weight loss curves of preliminary CAPBAT samples

Thermal transitions in DSC support the claims of non-miscible blends by exhibiting two glass transitions and two crystallization peaks as shown in Table 7. Plasticization of CA with the addition of PBAT is evident in the decrease of the glass transition temperature to 189°C from 207°C and in the elimination of the CA melting peak. While melting temperatures of the PBAT component remain somewhat unaffected as compared to NPBAT, the melting endotherm, crystallization temperature and crystallization endotherms of PBAT decrease with increasing CA content in the blend.

Sample	T_{gPBAT} (°C)	T_{gCA} (°C)	T_m (°C)	H_m (J/g)	T_{cPBAT} (°C)	H_{cPBAT} (J/g)	T_{cCA} (°C)	H_{cCA} (J/g)
100% CA	---	207.00	234.25	9.39	---	---	202.35	5.48
50% CA	-29.62	194.94	122.38	8.08	64.20	9.19	202.28	4.00
40% CA	-30.93	192.35	120.97	9.67	69.97	11.41	201.22	3.51
30% CA	-30.97	189.20	121.72	10.92	68.64	12.25	202.44	3.82
100% PBAT	-28.28	---	115.27	18.49	25.88	13.99	---	---
100% NPBAT	-29.85	---	123.31	13.33	76.55	17.09	---	---

Table 7. Summary of DSC thermal properties for preliminary CAPBAT blends

The phenomenon occurring begins with CA particles dispersed in the PBAT. As PBAT begins to melt, CA particles increasingly interfere with the PBAT crystals and successfully disrupt the crystallinity of some PBAT chains, lowering the enthalpy of melting. There is no effect on PBAT melting since the interaction between CA and PBAT occurs as the PBAT enters the melt stage. As PBAT in the blend melts, PBAT chains interfere with the hydrogen bonding in CA, effectively separating CA chains, leading to the elimination of the CA component melting curve. On cooling, CA crystallizes first and thus its crystallization temperature is not affected. However the extent of crystallization is slightly decreased with increased PBAT content. Crystallized CA chains then inhibit the crystallization rate of PBAT, effectively reducing the extent of crystallization as well as the crystallization temperature as shown in Figure 15. Thus, both CA and PBAT have effects on the crystallization properties of the other. This, again, indicates that there is some interaction occurring between CA and PBAT.

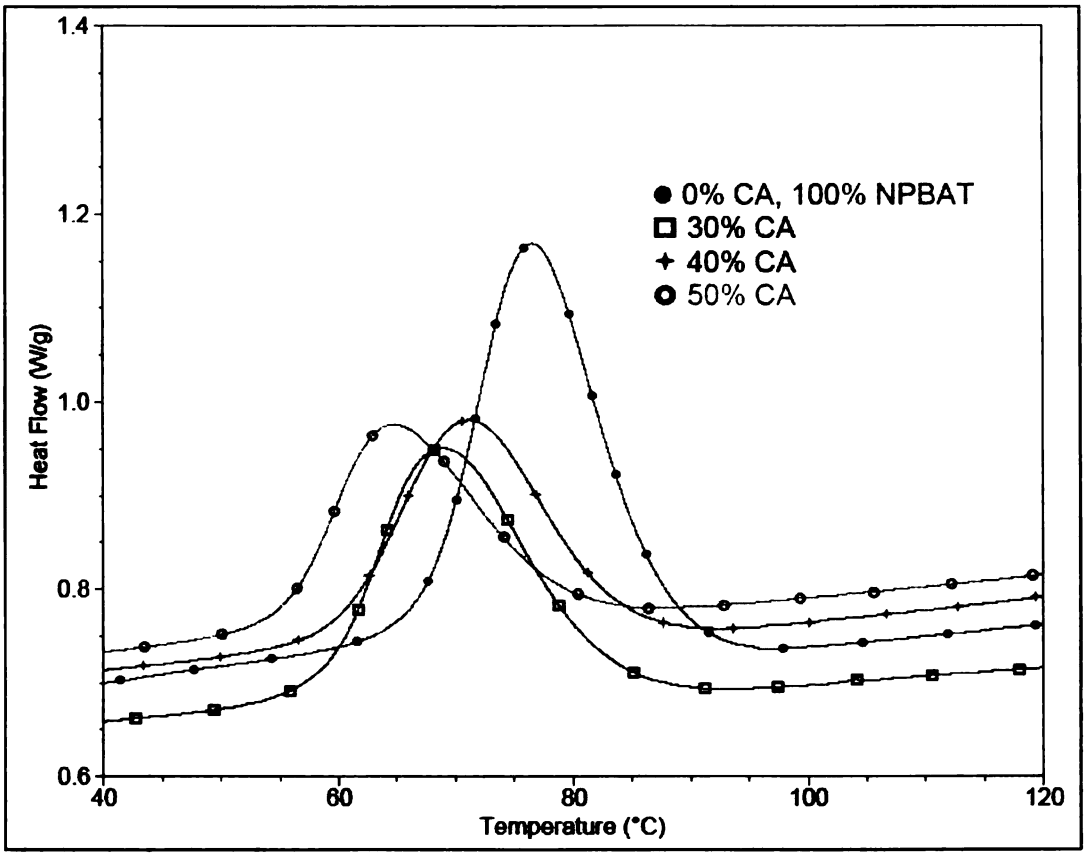

Figure 15. DSC crystallization temperatures of preliminary CAPBAT blends

This compositional study has shown that a blend with 30% CA shows some interaction with CA and is possible a compatible blend. Using the compositions in this study, we will look at the effects of plasticizer, catalyst, and the compositional effects of both plasticized and catalyzed samples. Materials, processing equipment and procedures, and characterization descriptions are as described earlier.

Effect of Plasticization and Composition

The compositional make-up of the samples in this segment can be found in Table 8. The effect of plasticization will be looked at simultaneously with the effect of composition on plasticized CA samples. All the materials and methods used are as described earlier. It should be noted that reactive carboxylic end groups of PBAT may react with accessible hydroxyl groups of CA under reactive extrusion of two without catalyst.

Molecular weight data for all samples in this segment are shown in Table 8 and Figure 16. CA is cellulose acetate, CT73 is plasticized cellulose acetate (30% plasticizer), CP37 is unplasticized cellulose acetate and PBAT in a 3:7 ratio, CTP37 is plasticized cellulose acetate and PBAT in a 3:7 ratio, and CTP55 is plasticized cellulose acetate and PBAT in a 5:5 ratio. The physical blend of CA and PBAT at 30 wt. % CA (CP37) was compared with the plasticized CA and PBAT blends at 30 (CTP37) and 50 (CTP55) wt. % plasticized CA. The number-average molecular weight for CP37 decreased dramatically as compared with CA, and had a slight increase in PDI due to the addition of a lower molecular weight component, as expected. Compared to NPBAT there was an increase in M_n and decrease in PDI. Plasticized blends of CA show higher molecular weight values due to the breaking up of the hydrogen bonding and increasing access to available CA hydroxyl groups to react with PBAT carboxylic end groups.

Sample	M_n (Dalt.)	M_w (Dalt.)	PDI	M_{nmix}	M_{wtheo}	% diff. M_n	% diff. M_w
CA	76640	145521	1.90	---	---	---	---
CT73	66406	126976	1.91	---	---	---	---
CP37	48800	95531	1.96	50755	105579	4%	11%
CTP37	51851	101667	1.96	49248	100016	-5%	-2%
CTP55	54868	110160	2.01	53173	107719	-3%	-2%
NPBAT	44338	88462	2.00	---	---	---	---

Table 8. Molecular weight data for "unplasticized" and plasticized CA-PBAT samples showing actual and theoretical M_{nmix} and M_{wmix} values and their % difference values

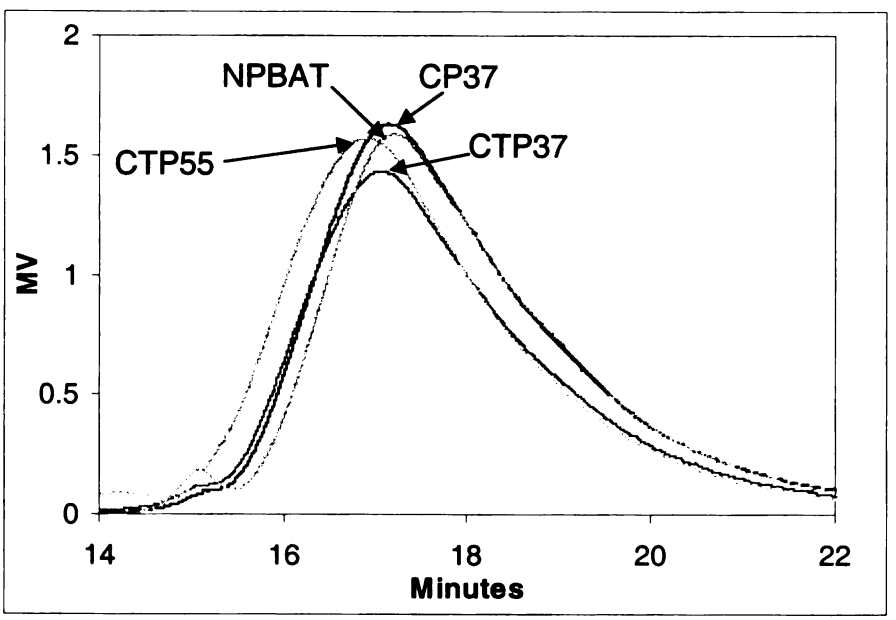

Figure 16. Chromatogram of samples affected by varying contents of plasticizer and cellulose acetate: CP37 (0% plasticizer, CTP37 (9% plasticizer), CTP55 (15% plasticizer)

It can be seen from Table 8 and Figure 16 that amongst the blends, the unplasticized blend had the lowest average molecular weight, while the plasticized blend had higher average molecular weight properties for reasons explained earlier. The theoretical values of M_n and M_w for the samples are shown in Table 8 with the percent differences as compared to the actual values

(first set of average molecular weights). Theoretically, since plasticizing CA allows for higher reactions between PBAT and CA, blends of CA and PBAT will naturally exhibit better than additive properties, and will not follow the incompatible curve as predicted by the Kienle equation.

Effect of plasticizer and plasticized compositions on the thermal stability of the blend can be seen in Figure 17 and Table 9. Addition of plasticizer decreases the thermal stability of the blend by being easily volatilized or forced out of the blend. The lower degradation temperatures could also be due to small amounts of triacetin reacting as well. This decrease in thermal stability is increased for higher CA loadings because increased CA in the blend increases the overall percentage of plasticizer in the blend as well.

Sample	T_{DTA} (°C)	T_{DCA} (°C)	T_{DPBAT} (°C)	T_{DCA-TA} (°C)
CA	---	344.59	---	---
CT73	267.24	351.26	---	---
CP37	---	353.03	376.70	---
CTP37	140.98	352.68	375.73	---
CTP55	160.65	350.88	383.04	---
PBAT	---	---	373.68	---
NPBAT			375.24	---

Table 9. Degradation temperatures for "unplasticized" and plasticized blends

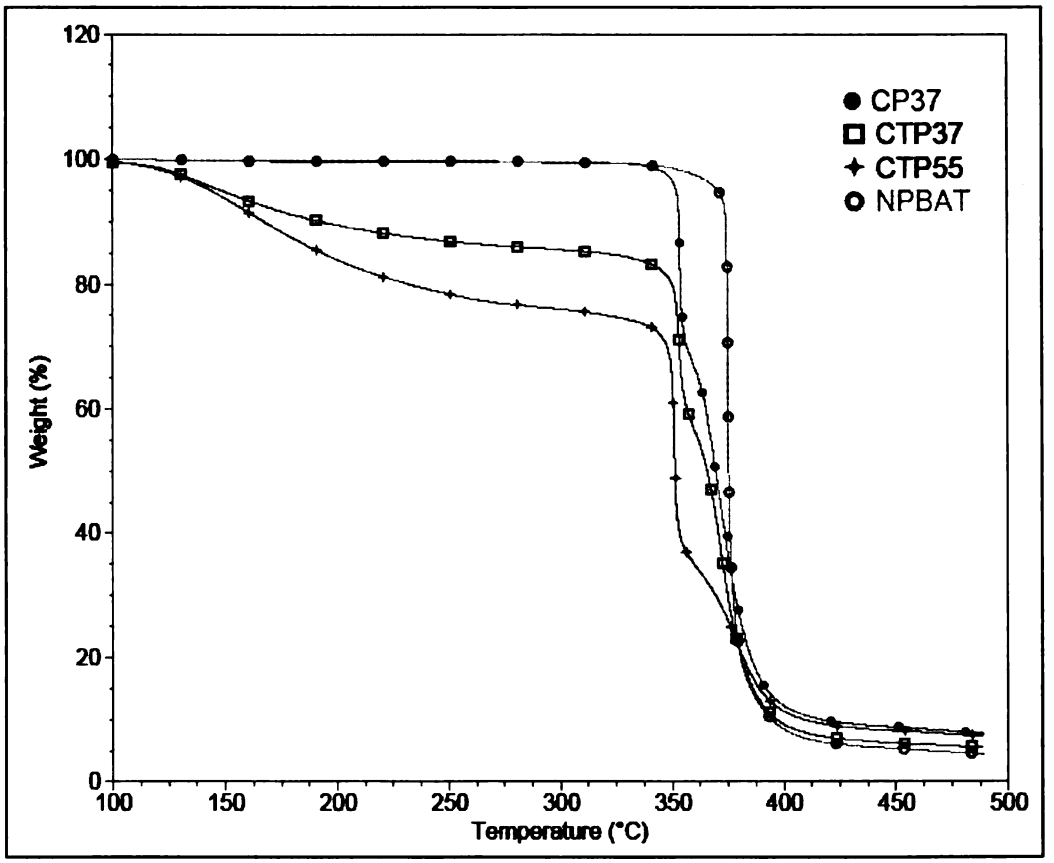

Figure 17. TGA weight loss curves for "unplasticized" and plasticized samples

Similar to compositional trends earlier, as the CA component increases, degradation temperatures shift towards the degradation temperature of 100% CA, while PBAT component temperatures remain about the same for all blends except CTP55. The derivative weight loss curves, whose peak gives the degradation temperature, seem to be shifting apart as shown in Figure 18. Again, at a composition of 30 wt. % plasticized CA, the blend displays a slightly

higher degradation temperature for the CA component suggesting some compatibility between the two components.

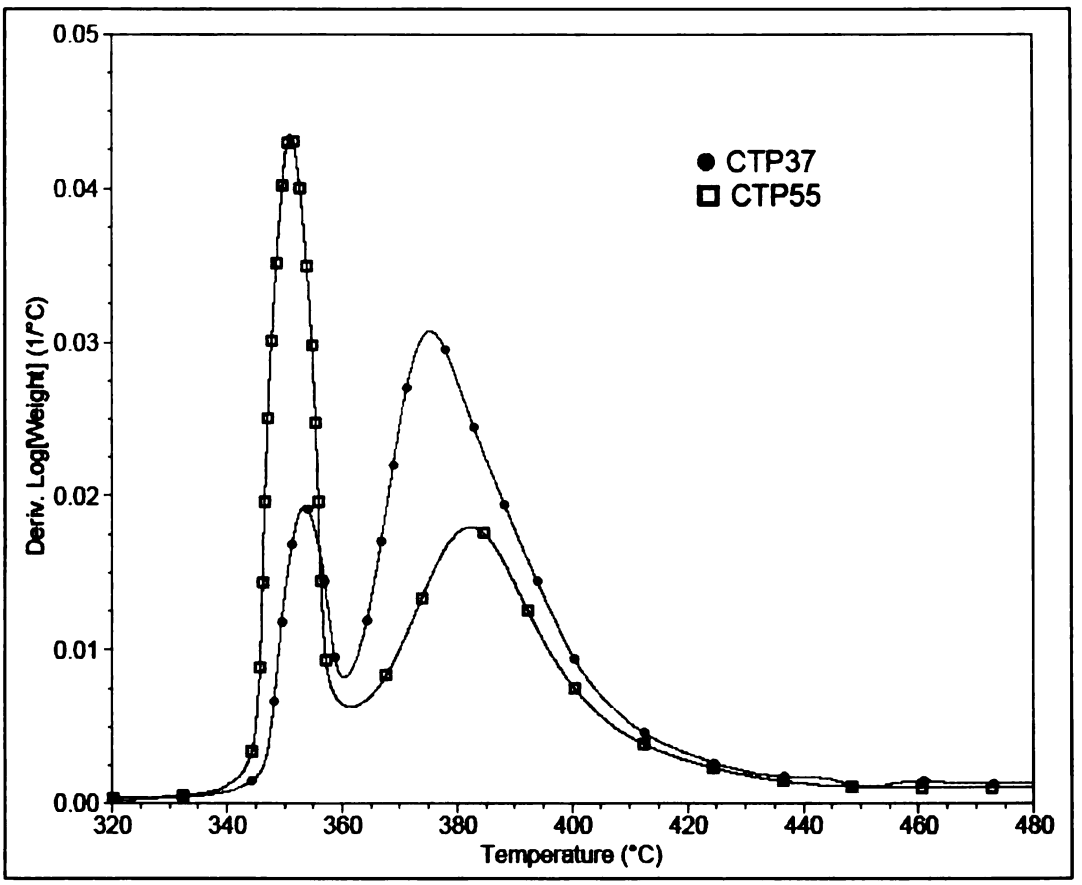

Figure 18. TGA derivative weight loss curves comparing plasticized compositions

Unlike thermal transitions in DSC for physical blends of CA and PBAT without plasticizer, the DSC results for plasticized blends of CA and PBAT show no transitions for the CA component of the blend, as shown in Table 10. The glass transition temperatures in Table 10 that are below zero were taken from DMA results for a better approximations of T_g. Values of T_g above zero

Sample	T_{gPB} *(°C)	T_{gCA} (°C)	T_{mPB} (°C)	ΔH_{mPB} (J/g)	T_{cPB} (°C)	ΔH_{cPB} (J/g)	T_{cCA} (°C)	ΔH_{cCA} (J/g)
CA	---	207.00	234.25	9.39	---	---	202.35	5.48
CP37	-24.37	193.81	115.44	10.17	59.67	11.72	203.21	2.48
CTP37	-39.63	---	105.95	5.95	61.91	8.29	---	---
CTP55	-36.46	---	101.79	4.46	54.36	4.48	---	---
PBAT	-26.26	---	115.27	18.49	25.88	13.99	---	---
NPBAT	-27.90	---	123.31	13.33	76.55	17.09	---	---

Table 10. DSC results for "unplasticized" and plasticized blends with varying plasticized blend compositions; * indicates values from DMA

were similar for both DSC and DMA. Blends that were plasticized showed a decrease in the PBAT component T_g values with no identified glass transition temperatures present for CA, while unplasticized blends had the opposite effect on PBAT component T_g values and did have glass transition temperature for CA. Plasticized CA and PBAT blends also showed an appreciable decrease in melting temperatures and extent of crystallization of PBAT as compared to unplasticized blends. The higher crystallization rates temperatures of PBAT are attributed to the more flexible amorphous segments of PBAT and smaller plasticizer molecules allowing for chains to order themselves quickly, but not necessarily to the extent that they would have without the increased flexibility. Compositionally, melting and crystallization properties (temperatures and enthalpies) of the PBAT component decrease with increasing CA content in the blend.

Dynamic mechanical results of the blends in this segment are shown in Figures 19, 20 and 21. The storage modulus (Figure 19) is higher for plasticized blends in agreement with molecular weight data. Increasing the amount of CA in the blend, increases the storage modulus. Plasticized samples show higher

storage moduli's due to the enhanced reactions occurring as compared to unplasticized blends of CA and PBAT. This is the cause for the great difference in the storage modulus at low temperatures. It is interesting to note that the storage modulus for the unplasticized blend of CA is about the same as NPBAT at cooler temperatures. The difference in the slopes of the storage modulus curves can be seen in the loss modulus curves (Figure 20) which show lower T_g values for the plasticized samples, as discussed earlier. This difference in the slopes of the storage modulus curves, as well as the difference in the width of the loss modulus curves results in broad tan delta curves for the samples with higher CA loading, as shown in Figure 21. Broader curves indicate less interaction between the two components. Broadening of the curve usually lowers the curve peaks as well [77].

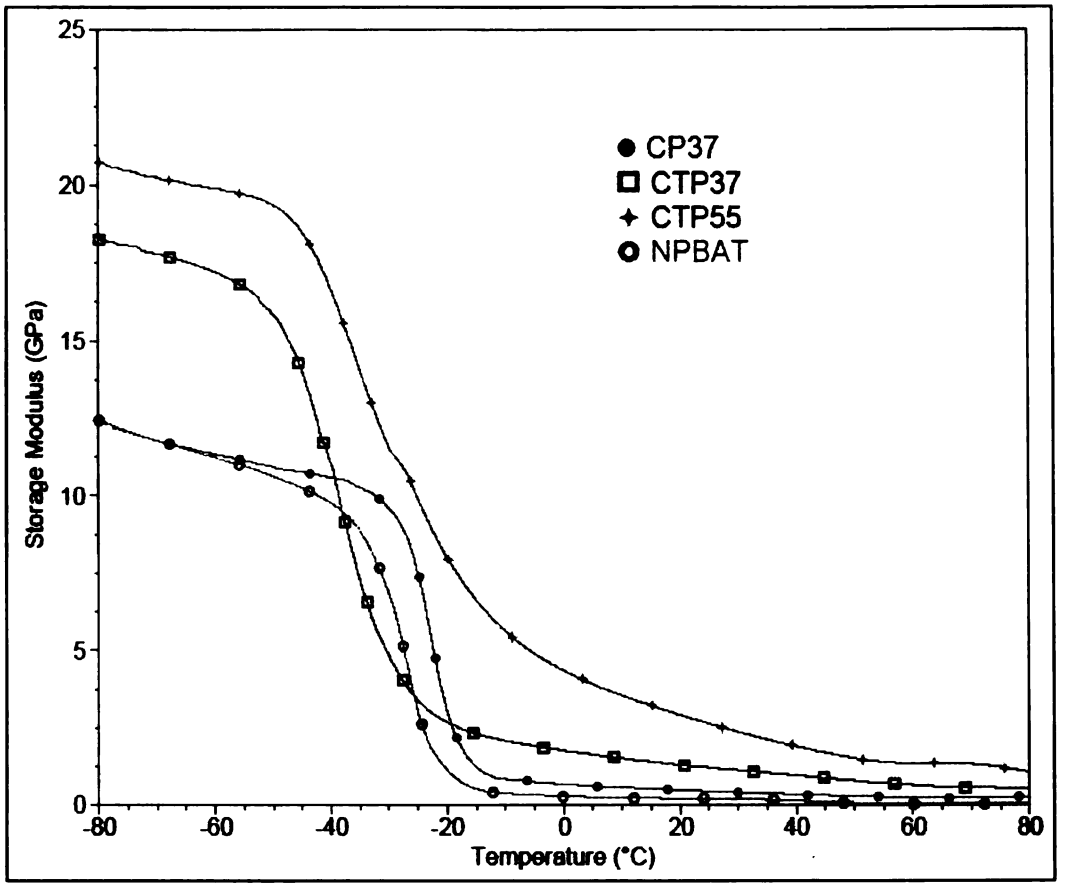

Figure 19. DMA storage modulus of "unplasticized" and plasticized blends along with varying compositions of plasticized blends

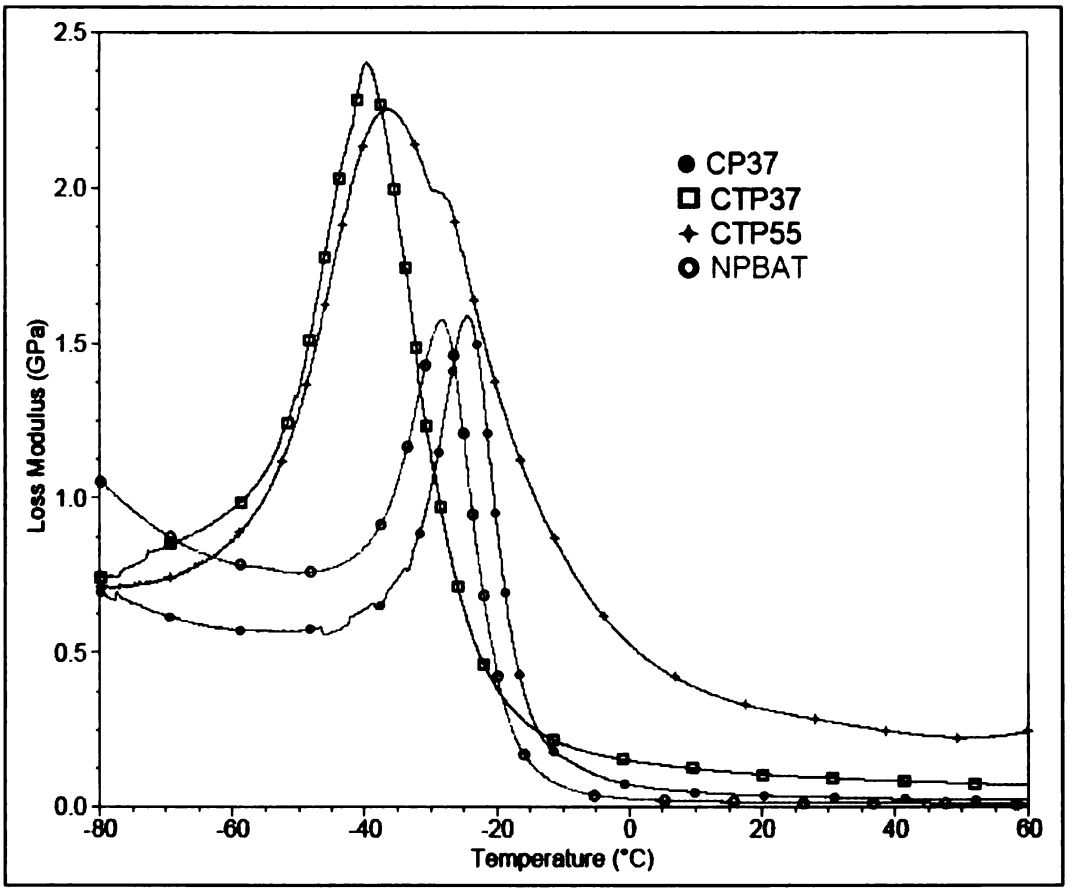

Figure 20. DMA loss modulus of "unplasticized" and plasticized blends along with varying compositions of plasticized blends

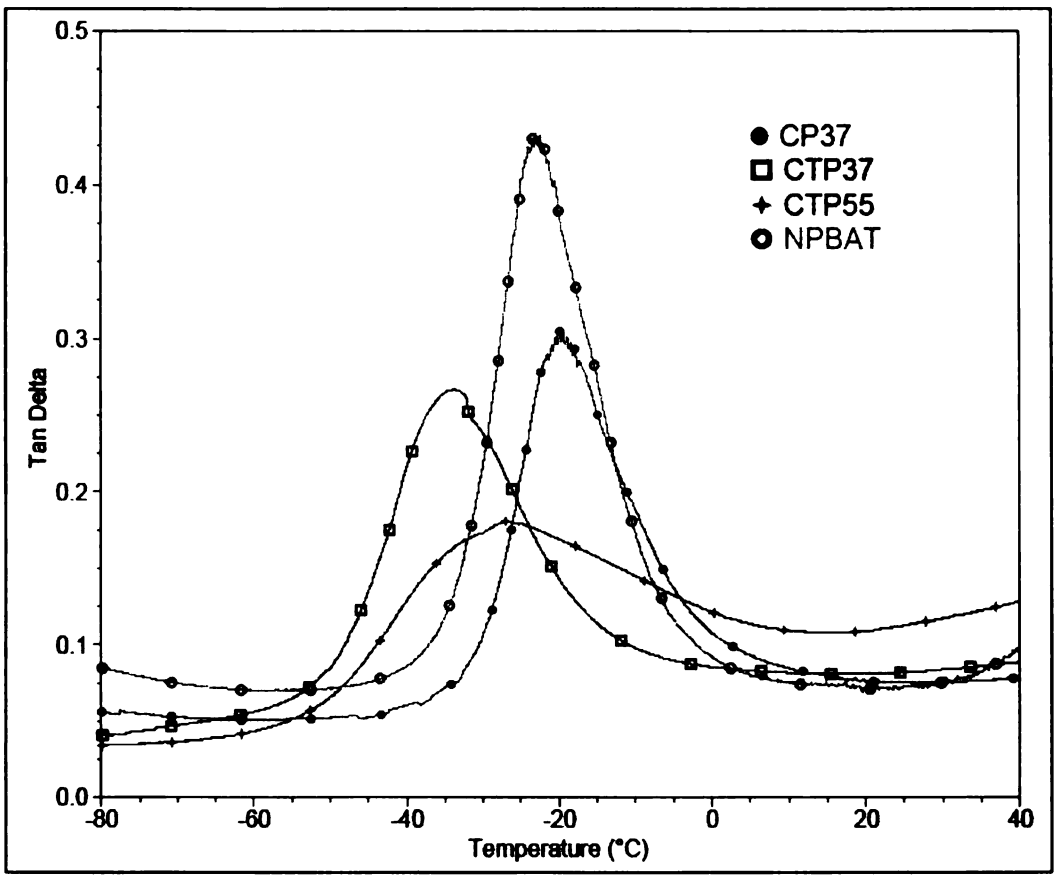

Figure 21. DMA tan delta of "unplasticized" and plasticized blends along with varying compositions of plasticized blends

The use of ESEM images of the surface of blend pellets from reactive extrusion allowed for an enhanced view of the morphology. The results from ESEM are in Figure 22 at magnifications of 1000x, 2000x and 5000x. Each column represents a different sample while each row represents the magnification. Cellulose acetate and PBAT form a heterogenous blend from two homogenous polymers. In these images spherical particles of CA are dispersed in a PBAT matrix. Only shape and size of particles are discussed.

In Figure 22, at 1000x magnification, samples CP37 and CTP37 both show some distinct spherical particles, whereas sample CTP55 shows expanded, distorted spherical shapes suggesting CA aggregation. At 2000x magnification, there seems to be some adhesion and deformation of CA particles in CP37 and CTP37. The plasticized blend (CTP37) shows increased interaction and deformation over the unplasticized (CP37) blend. Thus the addition of plasticizer helps increase the deformation of CA particles, and enhance the interaction between CA and PBAT phases. Compositionally, additional CA seems to decrease interactions between the two components and increase the interactions of CA with itself as seen for CTP55 at a 2000x magnification. The spherical particles are less distinct and CA material is spreading across the matrix. Magnifications at 5000x estimates particle size to be the lowest for the plasticized blend of CA and PBAT at 30 wt. % plasticized CA at 1 – 2.5 μm. The unplasticized blend had comparable particle size results (1 – 3 μm). Increased CA content showed higher range of particle sizes (2.5 – 4 μm). Smaller particle sizes are associated with higher dispersity of one phase in another [42].

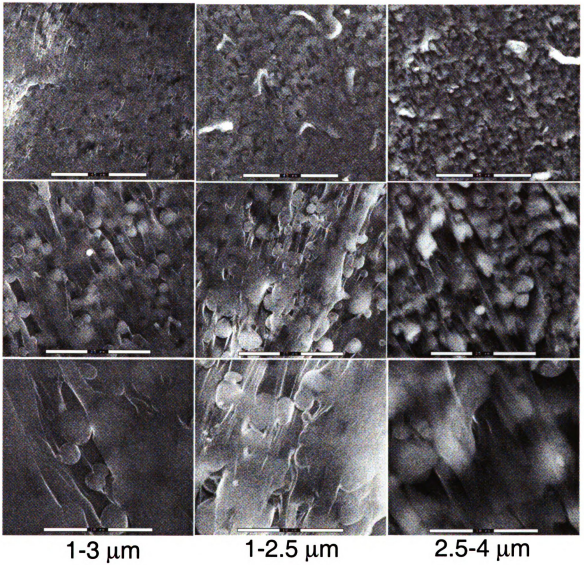

Figure 22. ESEM images of CP37, CTP37 and CTP55 by column from left to right, at 1000x, 2000x, 5000x by row from top to bottom. Values displayed at the bottom represent particle sizes for each sample

Effect of Catalyst and Composition of Plasticized Blends

Catalyst addition was expected to cause transesterification reactions between the CA and PBAT. Table 11 shows the average molecular weight values and Figure 23 shows the chromatogram for the uncatalyzed and

catalyzed blends. In Table 11, CTP37 is plasticized cellulose acetate and PBAT in a 3:7 ratio, CTP55 is plasticized cellulose acetate and PBAT in a 5:5 ratio, CTPD37 is plasticized cellulose acetate and PBAT in a 3:7 ratio with catalyst, and CTPD55 is plasticized cellulose acetate and PBAT in a 5:5 ration with catalyst. The "D" in the sample names represent the catalyst dibutyltin oxide.

Transesterification is expected to be the main reason for the significant decrease in both M_n and M_w values, and the increase in PDI for catalyzed blends, as compared to uncatalyzed blends of the same composition. Differences in composition of catalyzed blends are similar to before in that increased CA content increases average molecular weight properties of the sample. The significant decrease of the molecular weight properties of the catalyzed blends is also expected to be affected by the triacetin in the blend. This is because triacetin also has ester components and is most likely involved in the transesterification reactions.

Sample	M_n (Dalt.)	M_W (Dalt.)	PDI
CTP37	51851	101667	1.96
CTP55	54868	110160	2.01
CTPD37	36930	78492	2.13
CTPD55	42135	91302	2.17
NPBAT	44338	88462	2.00

Table 11 . GPC average molecular weight data of uncatalyzed and catalyzed blends

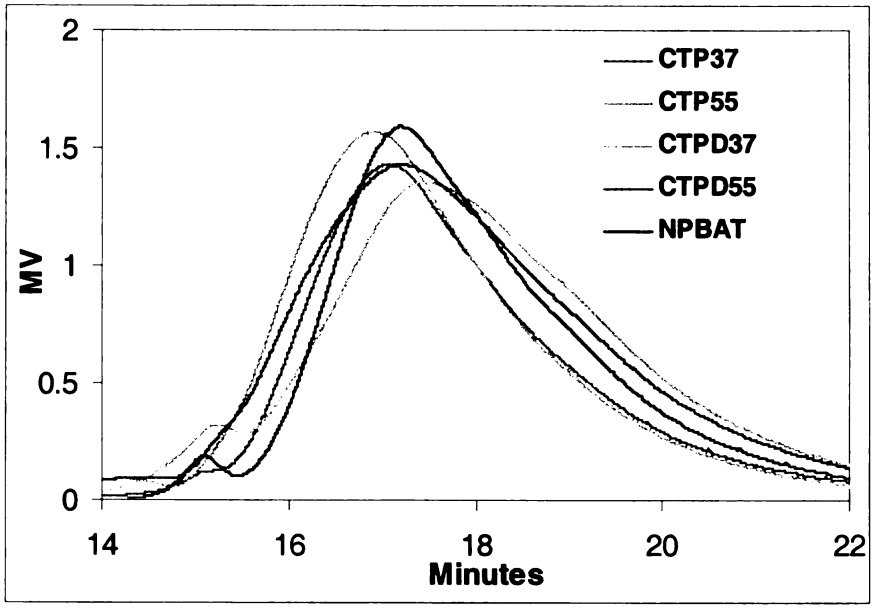

Figure 23. GPC chromatogram of uncatalyzed and catalyzed blends

Thermal properties give an even greater indicator that plasticizer is participating in transesterification reactions. The degradation temperatures are tabulated (Table 12) for the uncatalyzed and catalyzed samples. Catalyzed samples show the least stability of all when compared to the unplasticized and plasticized blends (Figure 24). Cleavage of the triacetin chains within the catalyzed blends causes the volatile triacetin molecules to escape and/or

Sample	T_{DTA} (°C)	T_{DCA} (°C)	T_{DPBAT} (°C)	$T_{DCA\text{-}TA}$ (°C)
CTP37	140.98	352.68	375.73	---
CTP55	160.65	350.88	383.04	---
CTPD37	127.51	346.81	375.44	307.02
CTPD55	137.65	346.18	381.82	293.14
NPBAT			375.24	---

Table 12. TGA degradation temperatures of uncatalyzed and catalyzed blends

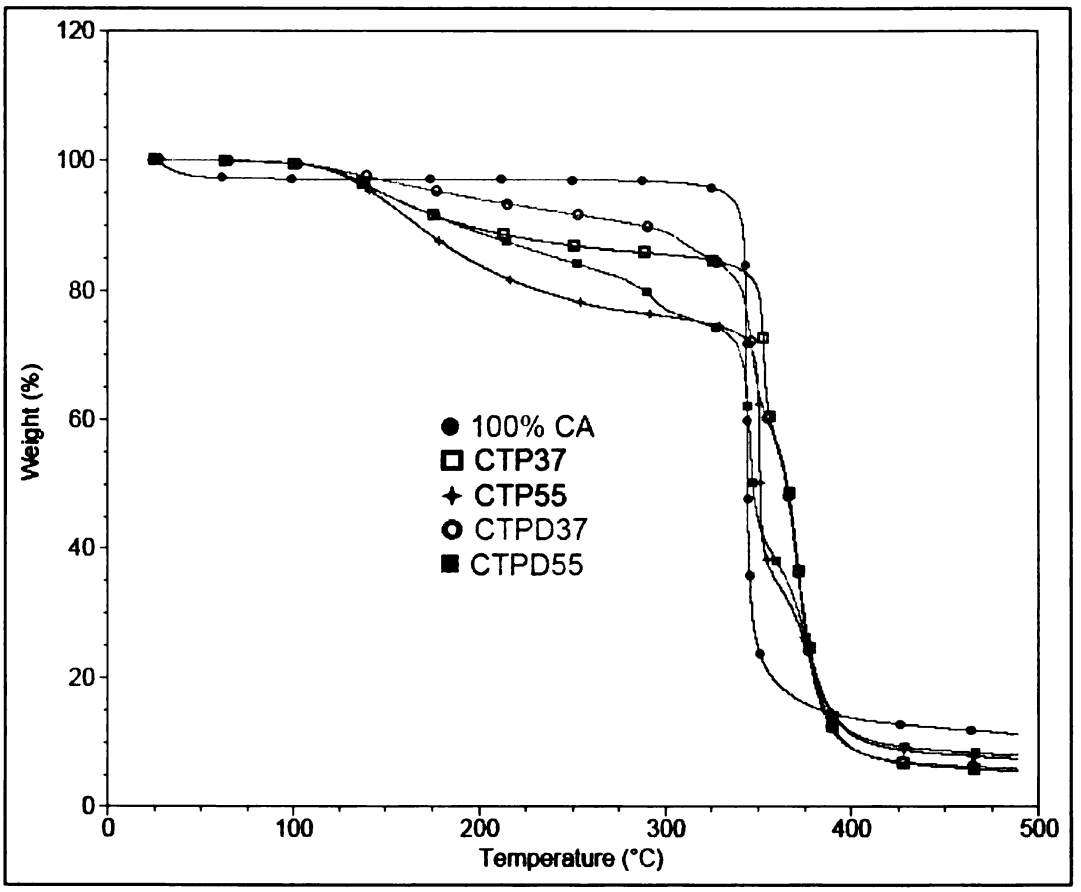

Figure 24. TGA weight loss curve of uncatalyzed and catalyzed blends

degrade at lower temperatures as compared to uncatalyzed blends. The degradation temperatures of the CA component are lower for catalyzed blends than they are for the uncatalyzed blends. Degradation temperature effects on the composition of catalyzed blends are the same as before in that the TGA derivative weight loss curves of each component shift apart from each other suggesting increased incompatibility (Figure 25).

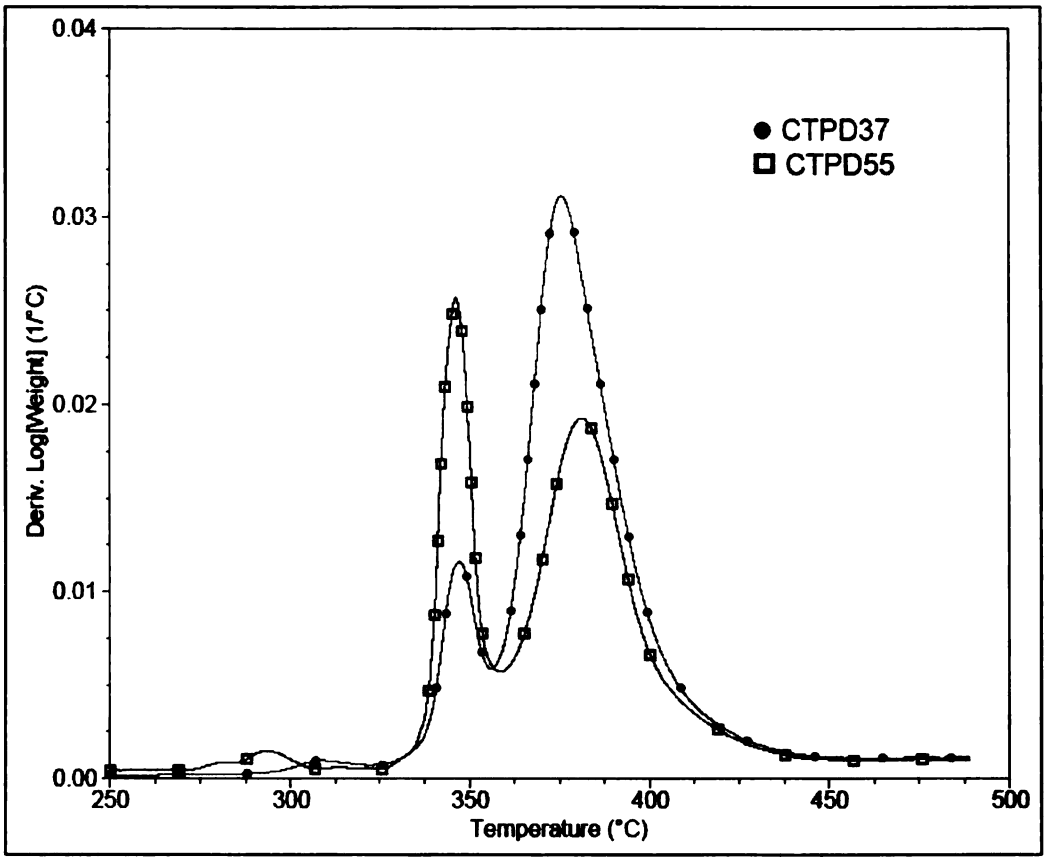

Figure 25. TGA derivative weight loss curve comparing compositions of catalyzed blends

Thermal transitions from DSC show that catalyzed blends decrease T_g further as compared to the uncatalyzed blend (Table 13). The glass transition

Sample	T_{gPB} *(°C)	T_{mPB} (°C)	ΔH_{mPB} (J/g)	T_{cPB} (°C)	ΔH_{cPB} (J/g)
CTP37	-39.63	105.95	5.95	61.91	8.29
CTP55	-36.46	101.79	4.46	54.36	4.48
CTPD37	-40.87	110.58	7.62	68.89	9.95
CTPD55	-41.56	105.01	4.89	61.59	5.31
NPBAT	-27.90	123.31	13.33	76.55	17.09

Table 13. DSC transitions for uncatalyzed and catalyzed blends; * indicates values from DMA

temperature below zero is obtained from DMA. The decrease in Tg between the uncatalyzed and catalyzed blend with higher CA wt. % is greater than the Tg of the catalyzed and uncatalyzed blends at lower CA wt. %. These lower T_g values are a result of shorter chains from transesterification. These shorter chains are also responsible for increased crystallization and melting properties of catalyzed blends as compared to their uncatalyzed counterparts. The differences in the melting and crystallization properties of the uncatalyzed and catalyzed blend with higher CA wt. % are, again, greater than the differences for the uncatalyzed and catalyzed blend with lower CA wt %. Compositionally, melting and crystallization properties (temperatures and enthalpies) of the PBAT component decrease with increasing CA content in the blend.

Dynamic mechanical results of the blends in this segment are shown in Figures 26, 27 and 28. The storage modulus (Figure 26) shows opposite effects for uncatalyzed versus catalyzed blends at the varying compositions. The blend that is somewhat compatible (30% plasticized CA content) shows a higher storage modulus at low temperatures compared to its uncatalyzed counterpart.

On the other hand, the blend that is less compatible or even incompatible (50% plasticized CA content) shows a lower storage modulus at low temperatures compared to its uncatalyzed counterpart. The reason for this is that the catalyzed sample with higher CA loading may have greater aggregation that forced the triacetin to separate out and reduce the overall plasticizer in the blend, reducing the storage modulus at low temperatures. The difference in the slopes of the storage modulus curves can be seen in the loss modulus curves (Figure 27) which show lower T_g values for the catalyzed samples as discussed earlier. This difference in the slopes of the storage modulus curves, as well as the difference in the width of the loss modulus curves result, again, in broad tan delta curves for the samples with higher CA loading as shown in Figure 28. Again, broader curves indicate less interaction between the two components and more interaction among the chains within their respective components.

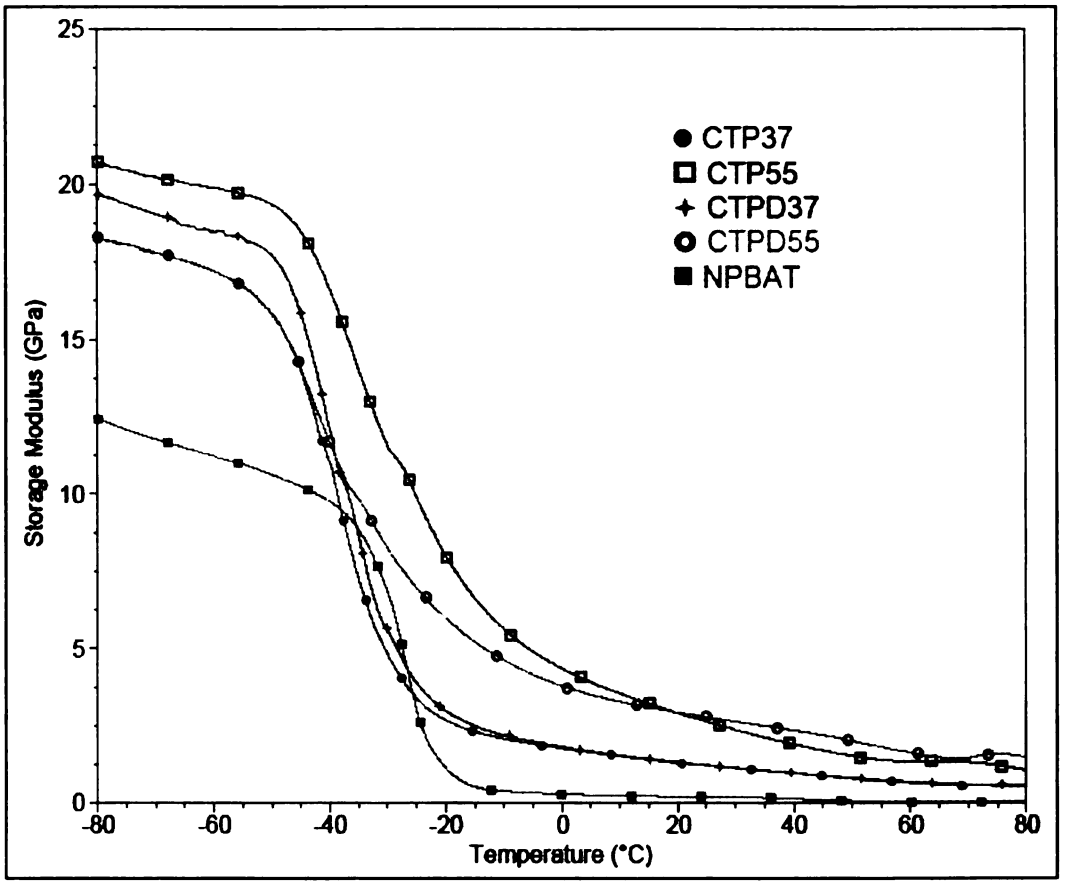

Figure 26. DMA storage modulus curves for uncatalyzed and catalyzed blends

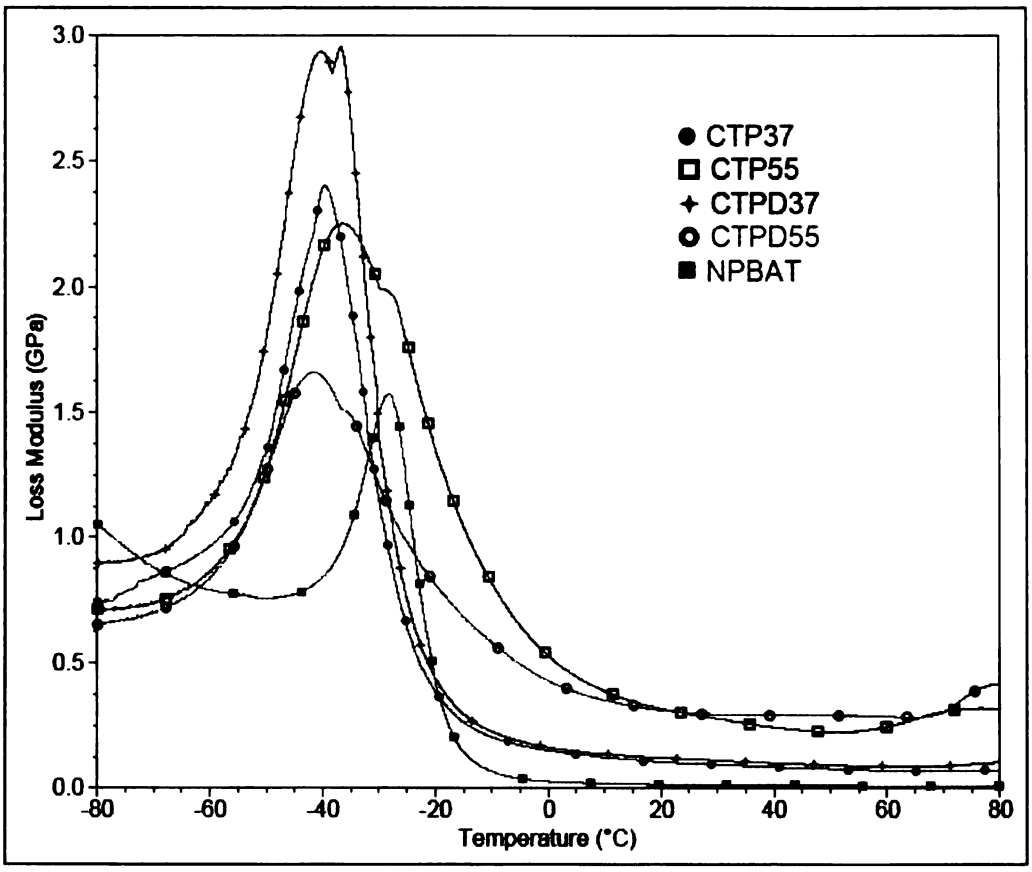

Figure 27. DMA loss modulus curves for uncatalyzed and catalyzed blends

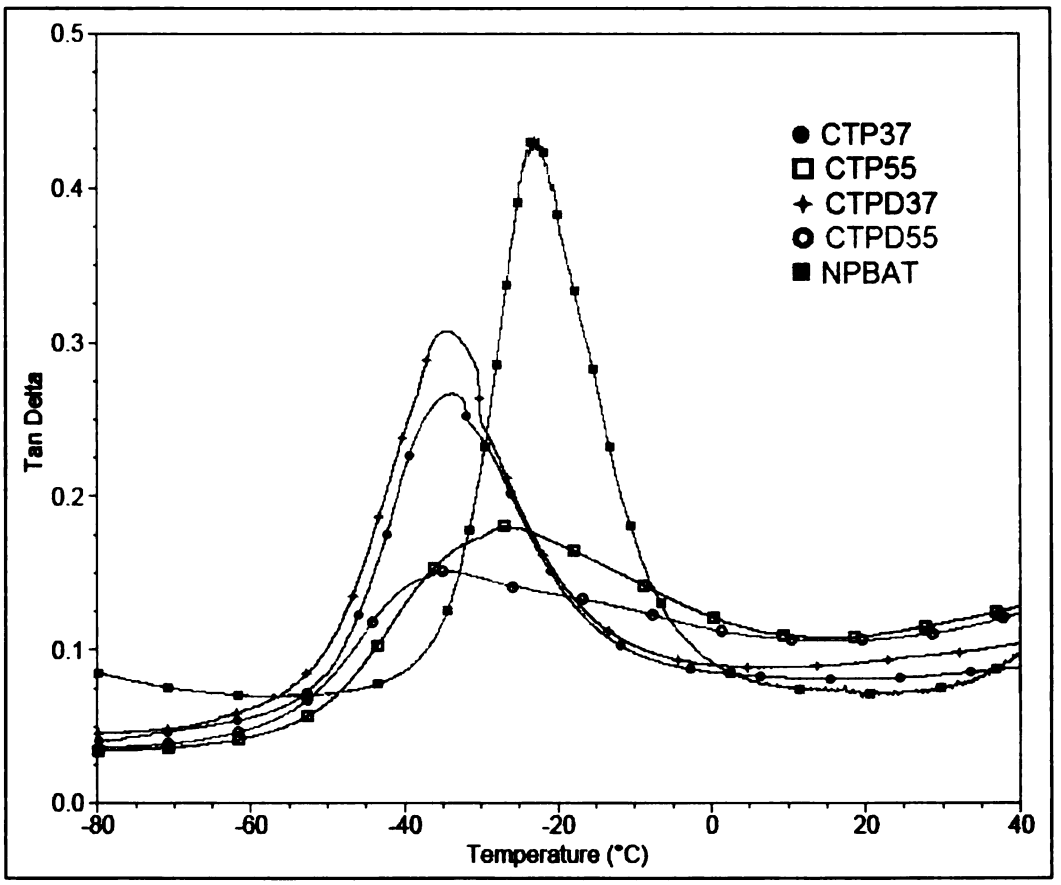

Figure 28. DMA tan delta curves for uncatalyzed and catalyzed blends

The results from ESEM are in Figure 29 at magnifications of 1000x, 2000x and 5000x. Each column represents a different sample while each row represents the magnification. Each column representing the catalyzed sample images is labeled as such. Again, in these images spherical particles of CA are dispersed in a PBAT matrix. Only shape and size of particles are discussed with a focus on the catalyzed samples since the uncatalyzed samples were discussed earlier.

In Figure 29, all the images of the catalyzed samples show less interaction with PBAT. Spherical particles are clearly defined and aggregated in the CTPD37 sample unlike in the uncatalyzed counterpart. Further distorted, (as compared to uncatalyzed counterpart) spherical shapes suggests increased aggregation of CA in CTPD55. The same results are seen at 2000x magnification and with evidence of less adhesion and interactions of the two components with each other and more adhesion and interaction of the two components with themselves. Compositionally, the CTPD55 shows even further spreading of CA material across the matrix. Magnifications at 5000x shows enlarged particle size for catalyzed blends with largest particle size of ~ 4μm related to CTPD55. The particle shapes in this sample almost seems cylindrical with spheres being hard to identify.

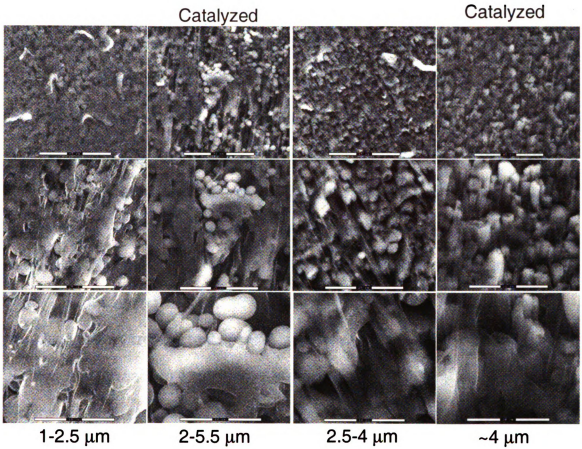

Figure 29. ESEM images of CTP37, CTPD37, CTP55 and CTPD55 by column from left to right, at 1000x, 2000x, 5000x by row from top to bottom. Values displayed at the bottom represent particle sizes for each sample.

4.4 Summary

Blends of CA with PBAT were studied as unplasticized and plasticized blends at different compositons, and as uncatalyzed and catalyzed blends at varying composition. Experimental results show that CA and PBAT can be reactively extruded to yield a compatible blend. Interactions between the polymers are confirmed by various characterization techniques. One example is the increased molecular weight and decreased PDI values of the blends as

compared to PBAT alone along with other characterization identifiers. Regardless, there is a limit to the compatibility of CA in PBAT.

The overall results show cellulose acetate and PBAT do in fact disrupt the crystallinity of each other. Thus, increasing CA content increases the disruption of PBAT crystallinity. In this study, PBAT proved to be a polymeric plasticizer for CA in that the melting endotherm was eliminated and the T_g of CA was reduced with increasing PBAT content. While external plasticizers did show increases in molecular weight as compared to unplasticized blends and to PBAT, they also resulted in decreased thermal stability most likely due to their high volatility. An increase in plasticizer content seemed to increase access to CA hydroxyl groups allowing for the reaction with PBAT acidic end groups. While higher average molecular weight properties were attained with higher CA loading, TGA results suggested decreased compatibility with increased CA loading.

The addition of catalyst in the blends showed a decrease in blend Tg values and an increase in crystallization properties as compared to uncatalyzed blends. The morphology of the blends was significantly affected by catalysts. Catalyst addition promoted decreased interaction between the two components. Triacetin was assumed active in transesterification reactions and, also believed to play a role in how the properties of the blends were affected.

While plasticization seemed to increase compatibility, it severely decreased thermal stability. Comparing the unplasticized and plasticized samples at a ratio of 3:7 CA (or plasticized CA) to PBAT, both showed promising behavior in terms of interaction with PBAT. In line with the goals of this study,

however, the unplasticized blend of CA and PBAT would be further developed in order to yield a higher amount of biobased material being incorporated into PBAT. Therefore, the physical blend of CA and PBAT, with a 30 wt. % loading of CA, proved to be the best blend suiting the purposes of this work.

Chapter 5

Synthesis of Glycerol-based Materials

5.1 Overview

The development of biobased, biodegradable blends plays an important role in the overall success of sustainability in the 21st century. While polymer blending is a common route to achieving polymers with desired properties, synthesis of new polymers is another essential route to producing sustainable polymers. Development of these new polymers can increase the possibilities for many more blends to achieve desired properties.

To develop such a polymer, Carothers' theory, as described earlier, is used to determine the relationship between percent conversion and degree of polymerization. One focus of synthesis reactions is to build molecular weight, and molecular weight is built by pushing the reaction to as high a conversion as possible without gelation, which would correspond to a high degree of polymerization. This work is focused on the transesterification of dimethyl terephthalate with glycerol. Glycerol has a functionality of 3 and dimethyl terephthalate has a functionality of 2. Calculating the average functionality as givien in equation 21, Carothers' equation (equation 24) can be used to estimate degree of polymerization as a function of percent conversion.

Figure 30 shows the results of Carothers' equation for a 1:1 and 2:3 ratio of glycerol to DMT. It would seem natural to take two moles of glycerol and react it with three moles of DMT since glycerol has three hydroxyl groups and

DMT has two methyl ester groups for reaction. However, for a two to three molar ratio of glycerol to DMT, gelation occurs at a conversion of about 85% and the maximum degree of polymerization is about 60. On the other hand, 1:1 ratio of glycerol to DMT would have the potential to get to higher degrees of

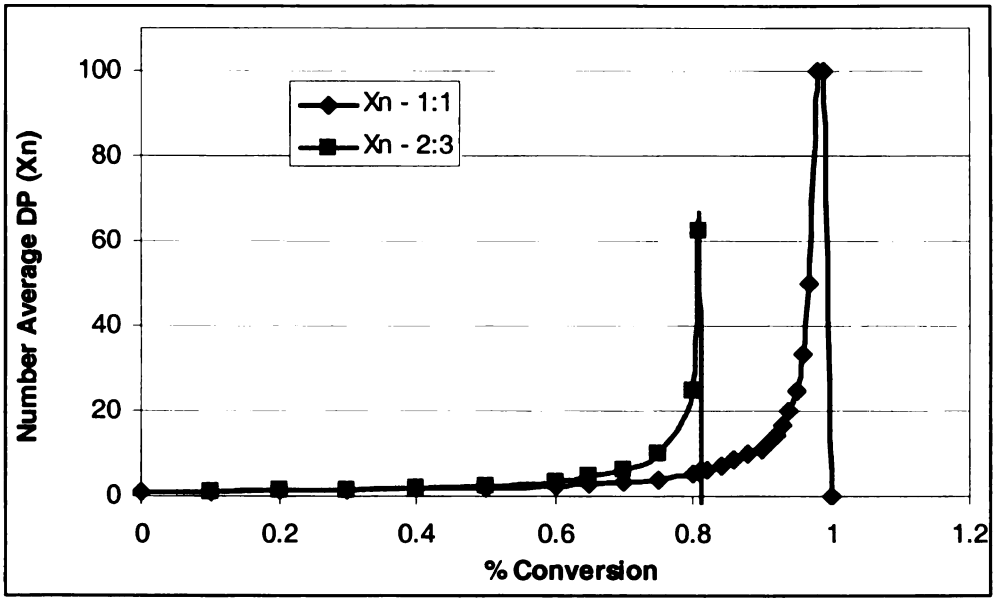

Figure 30. Degree of polymerization and gel point for a 1:1 and 2:3 mixture of glycerol:dimethyl Terephthalate

polymerization (~upwards of 95) and gelation would only occur at extremely high conversions. It is important to note that Carothers' theory is simply an estimate and in practice gelation is known to occur before the theoretical value. In this study, a 1:1 ratio of glycerol to DMT is used as the basis for forming new biobased polyesters. Overall, this study focuses on the development of a new biobased, biodegradable polyester starting with a multifunctional alcohol and reports on the molecular weight, hydroxyl values, and thermal properties associated with the new pre-polymer.

5.2 Materials and Methods

The monomers used in this synthesis were anhydrous glycerol and dimethyl terephthalate (DMT). Two catalysts, dibutyltin(IV) oxide and sodium carbonate, were used. Other chemicals used for characterization techniques include pyridine, acetic anhydride, n-butanol, tetrahydrofuran, and inhibitor-free tetrahydrofuran.

The synthesis procedure used in this study is described in the materials and methodology chapter. The characterization experiments include methanol collection, hydroxyl value, and gel permeation chromatography, along with thermal analysis of the reaction products.

5.3 Results and Discussion

In the transesterification reaction to produce glycerol-based biopolyesters, various catalyst concentrations were run to determine catalyst performance and identify an optimal catalyst and catalyst concentration. Specific reaction conditions were described earlier in this chapter, but are summarized and shown with the reaction matrix in Figure 31. All reactions were run under the same conditions using a 1:1 molar ratio, varying only the catalyst type and the catalyst amount. Sodium carbonate, denoted as NC, and dibutyltin (IV) oxide (DBTO) were used in concentrations of 0.1, 0.2 and 0.3 wt. % of dimethyl terephthalate (DMT). The reaction start time was defined as when the reaction vessel reached a temperature of 200 °C. Methanol collection was recorded over the four-hour reaction period and was expected to be about 202 mL based on stoichiometry.

The methanol data was used to estimate percent conversion (P) and the number-average degree of polymerization (X_n).

a.

Molar Ratio	1:1
Glycerol (grams)	276.28
Dimethyl terephthalate (grams)	588.38
Temperature, Time (°C,hrs.)	100,.25;200,4
Expected Methanol (ml)	202.5

b.

	Sodium Carbonate (NC)	Dibutyltin oxide (DBTO)
NC01 (wt% DMT)	0.1	----
NC02 (wt% DMT)	0.2	----
NC03 (wt% DMT)	0.3	----
DBTO01 (wt% DMT)	----	0.1
DBTO02 (wt% DMT)	----	0.2
DBTO03 (wt% DMT)	----	0.3

Figure 31. a. Reaction conditions b. Reaction Matrix

Effect of Catalyst Type and Concentration on Conversion

The synthesis of glycerol-based pre-polymers (GDMT) led to an understanding of the reaction of glycerol with the methyl ester, dimethyl terephthalate, and its behavior with two types of catalyst. Sodium carbonate and dibutyltin oxide were the catalysts of choice. This study focused on the development of pre-polymers for further development of glycerol-based materials. Using the reaction conditions shown in Figure 31, the conversion over time and the degree of polymerization as a function of conversion are shown in Figures 32 and 33.

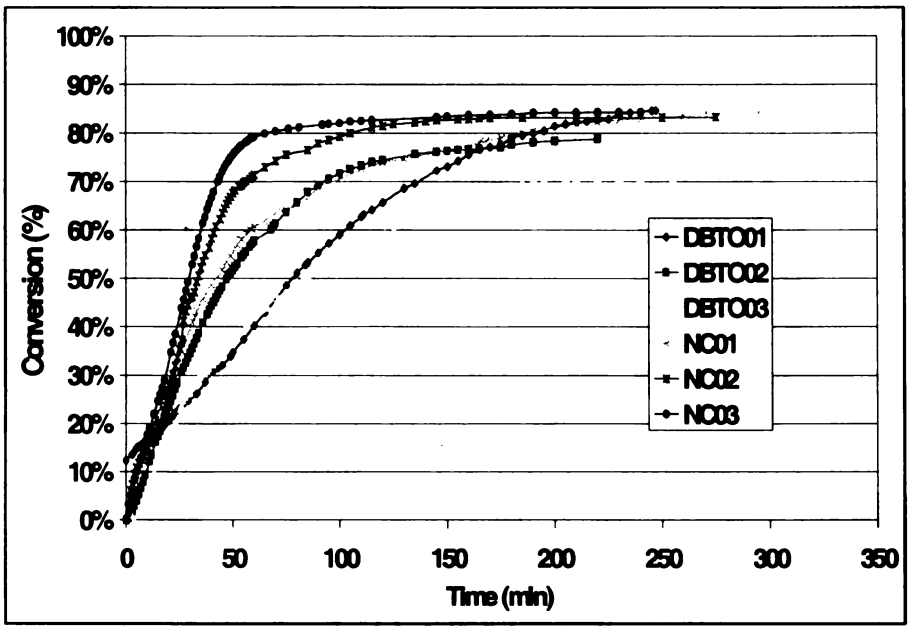

Figure 32. Conversion over time based on recorded methanol collection

The percent conversion was calculated based on recorded methanol collection. A theoretical value of 202.54 ml of methanol based on stoichiometry was expected to form upon full conversion of the reactants to products. Thus, methanol collection provided a crude estimate of the conversion of reactants that could be gathered quickly and easily. Literature shows that 50% conversion is seen within the first hour of the reaction [51, 52]. In this study, 50% conversion was seen within the first hour and a half of the reaction. Figure 33 shows the theoretical behavior of X_n as percent conversion increases with respect to all the reactions in the study as a comparison to see how far along the reactions have proceeded from a degree of conversion perspective.

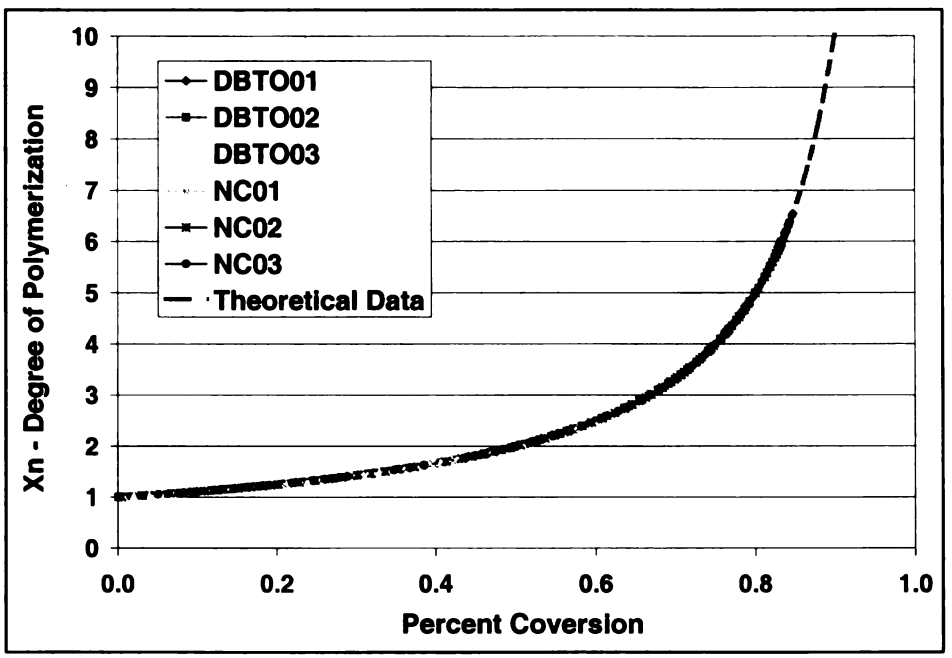

Figure 33. Degree of polymerization as calculated by Carothers' Theory for the theoretical curve and by experimental data for all other curves

It is important to note that methanol formation began at lower temperatures (150 °C) with sodium carbonate and at higher temperatures (170 °C) when DBTO was used. After four hours, DBTO02 and DBTO03 reactions seemed to lag behind reactions DBTO01 and all the NC catalyst reactions. Amongst the reactions, conversions ranged from about 70 to 80% and the degree of polymerization, from about 3 to 6. In order to get a high degree of polymerization for high molecular weight in step-growth reactions, conversions approaching 100% should be attained as shown in Figure 33 as X_n approaches infinity. The final conversion and degree of polymerization values calculated from methanol formation are tabulated in Table 14.

As a more reliable estimation of the extent of reaction, hydroxyl tests were performed for all the reactions completed and the results are also shown in Table 14. The acid and hydroxyl value yielded conversions ranging from roughly 75-77% and degrees of polymerization averaging about 4. Reactions NC02 and DBTO01 showed the highest conversion and degree of polymerization values within their respective catalyst group, relative to the results based on other reactions.

Prepolymer	Acid Value (AV)	Hydroxyl Value (HV)	% Conversion (OH #)	% Conversion (MEOH)	Xn* (OH #)	Xn* (MEOH)
NC01	0.8	310	76.78	84.04	4.3	6.3
NC02	0.4	300	77.54	83.10	4.5	6.0
NC03	0.4	336	74.88	84.14	4.0	6.4
DBTO-01	6.1	297	77.77	83.74	4.5	6.5
DBTO-02	2.1	299	77.59	78.62	4.5	4.7
DBTO-03	5.0	305	77.19	70.54	4.4	3.4

*Xn is the degree of polymerization

Table 14. Comparison of percent conversion and Xn based on hydroxyl values versus methanol formation

In the later stages of the reaction the viscosity increased significantly, possibly trapping some volatile materials (mostly methanol). The amount of methanol mixed in with the reaction product could potentially influence the hydroxyl values significantly. To account for the possibly trapped methanol in the samples, TGA was used to estimate the amount of volatiles from room temperature up to 200°C (the run temperature of the reaction).

Figures 34 and 35 show the degradation curves for the NC and DBTO catalysts sets. It was assumed that the majority of the volatile material

represented trapped methanol. For the sodium carbonate catalyst results shown in Figure 34, reaction NC02 showed the least amount of trapped methanol, suggesting that this catalyst composition was the either the furthest along in terms of conversion or highly branched. For the dibutyltin oxide catalyst, the reaction DBTO01 showed the least amount of trapped methanol while the other reactions in this catalyst group showed around 2.5% weight loss up to 200°C (Figure 34). Comparing the results of the two catalysts suggests that the sodium carbonate catalyst, when compared by weight %, did show lower amounts of trapped methanol possibly indicating being slight further along, in terms of conversion, than the reactions using dibutyltin oxide.

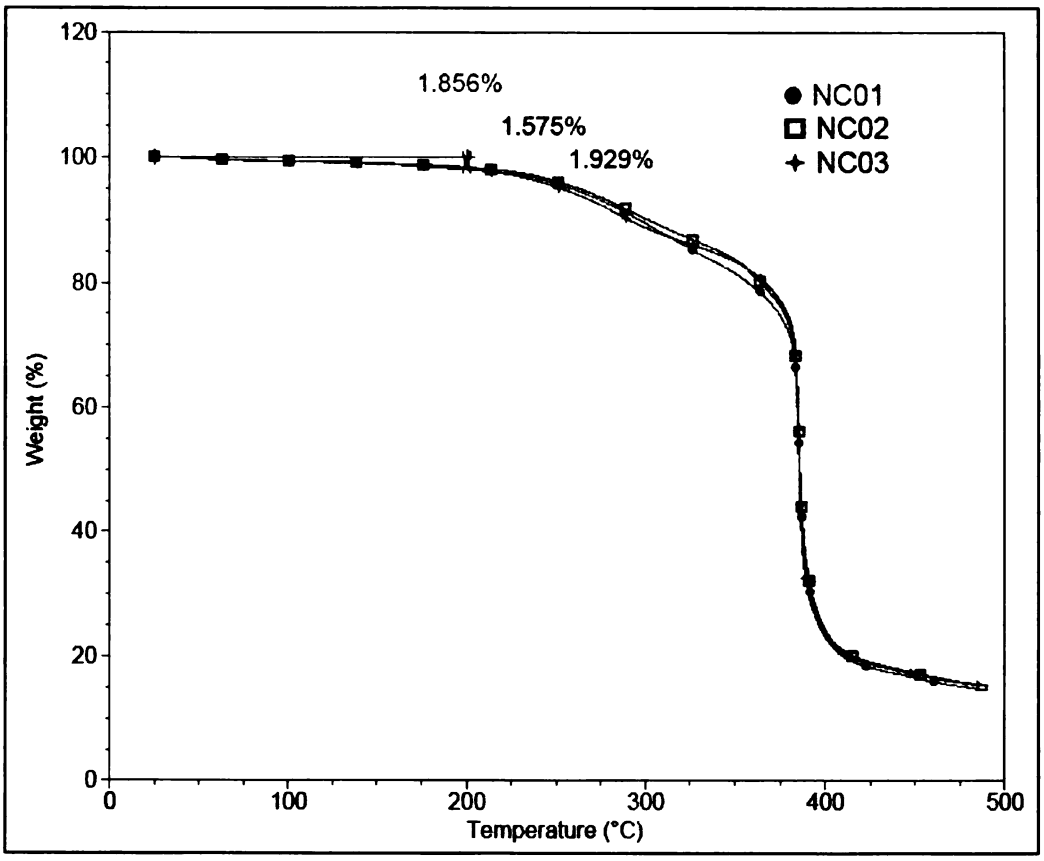

Figure 34. TGA derivative weight loss curve for NC samples showing % trapped methanol in the samples

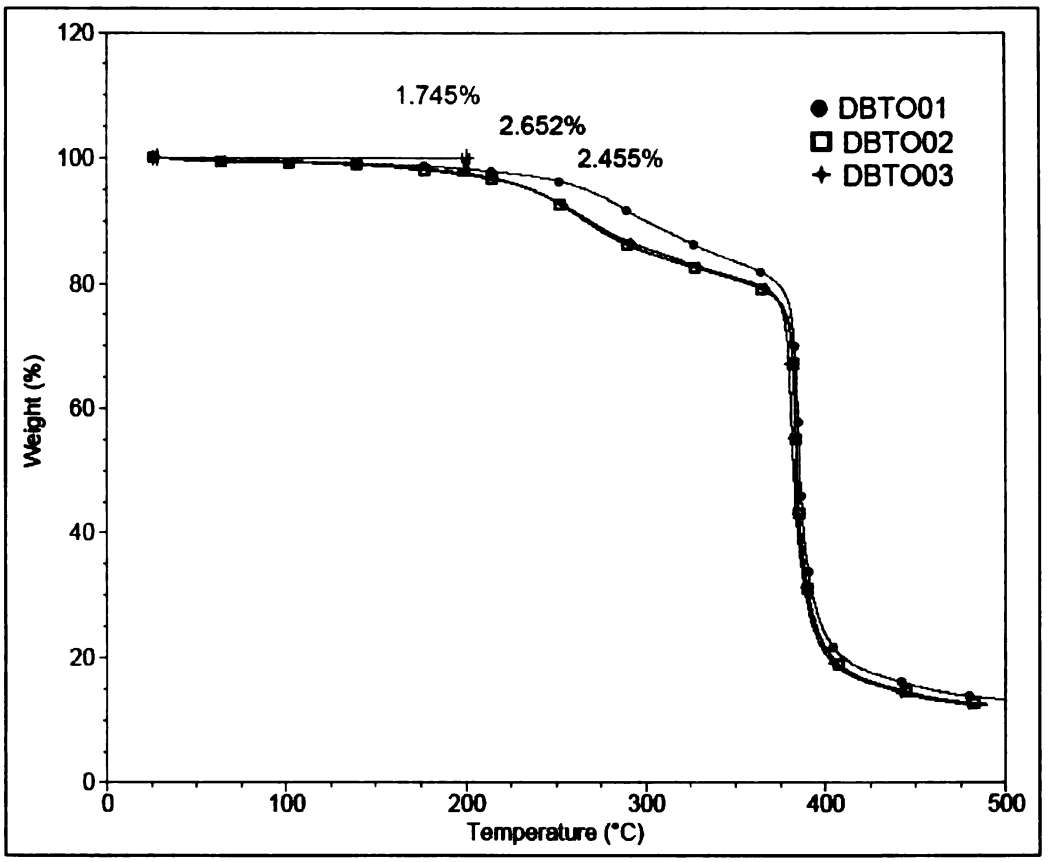

Figure 35. TGA derivative weight loss curve for DBTO samples showing % trapped methanol in the samples

The results of the amount of methanol trapped are then used to recalculate the hydroxyl values as shown in Table 15. By subtracting the weight of methanol in the sample from the weight of the sample for the hydroxyl value test the hydroxyl values could be adjusted. While reaction conversions are close, and may not be statistically different, the samples NC02 and DBTO01 exhibit the highest conversions based on hydroxyl value relative to the other samples.

Prepolymer	Acid Value (AV)	Hydroxyl Value (HV)	% Conversion (OH #)	% Conversion (MEOH)	Xn* (OH #)	Xn* (MEOH)
NC01	0.8	316	76.36	84.04	4.2	6.3
NC02	0.4	305	77.20	83.10	4.4	6.0
NC03	0.4	342	74.41	84.14	3.9	6.4
DBTO-01	6.1	310	76.80	83.74	4.3	6.5
DBTO-02	2.1	330	75.29	78.62	4.0	4.7
DBTO-03	5.0	312	76.62	70.54	4.3	3.4

*Xn is the degree of polymerization

Table 15. Comparison of percent conversion and X_n based on hydroxyl values versus methanol formation after adjustments for trapped methanol

Conversion based on methanol displays maximums both within the NC and DBTO catalyst group (Figures 36 and 37). Conversion based on OH passes through a maximum at 0.2 wt. % NC, while in the DBTO catalyst group conversion shows a decreasing trend with 0.1 wt. % DBTO as the optimal catalyst amount for that group. Hydroxyl value tests were only performed on

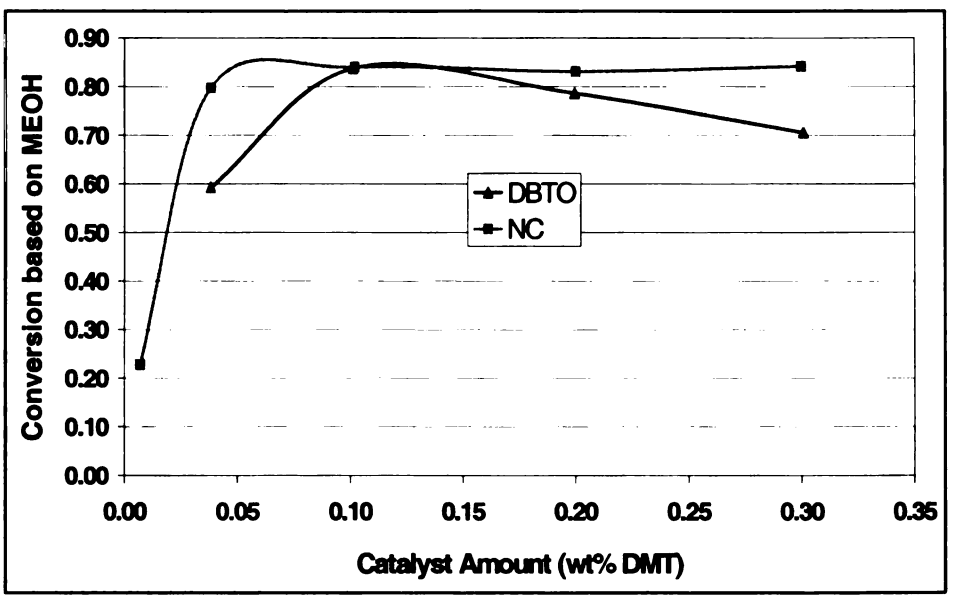

Figure 36. Catalyst perfomance based on MEOH for different types of catalysts at different concentrations

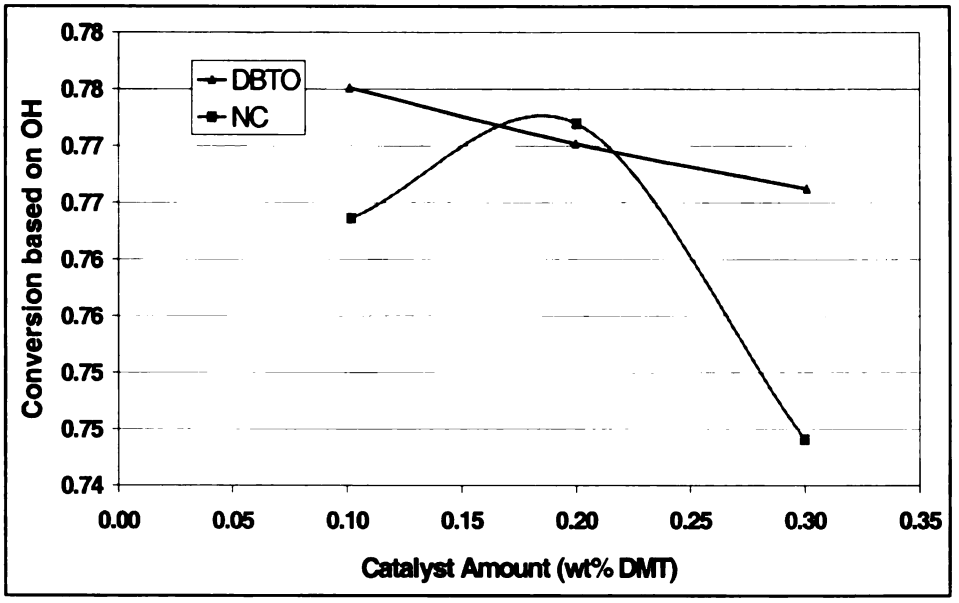

Figure 37. Catalyst perfomance based on hydroxyl # for different types of catalysts at different concentrations

samples with a high enough conversion to yield a transparent solid mass. This resulted in the methanol-based catalyst performance curves having more points than the hydroxyl-based catalyst performance curves.

Effect of Catalyst Type and Concentration on Molecular Weight

Although the conversion results only ranged from 74 – 77% conversion, the trends seen from hydroxyl values agreed closely with the weight-average molecular weights derived from GPC. The curves associated with the products of these reactions were very broad (Figure 38) indicating high polydispersity indices as shown in Table 16. It is worthwhile to note the high M_w associated with NC02 and DBTO01 reactions. These results suggest the high conversion of the glycerol hydroxyls and, possibly, the formation of a highly branched structure.

From a catalyst standpoint, sodium carbonate yielded higher M_n and M_w values overall when compared to DBTO. However the reaction DBTO01 had comparable results to the sodium catalyst group.

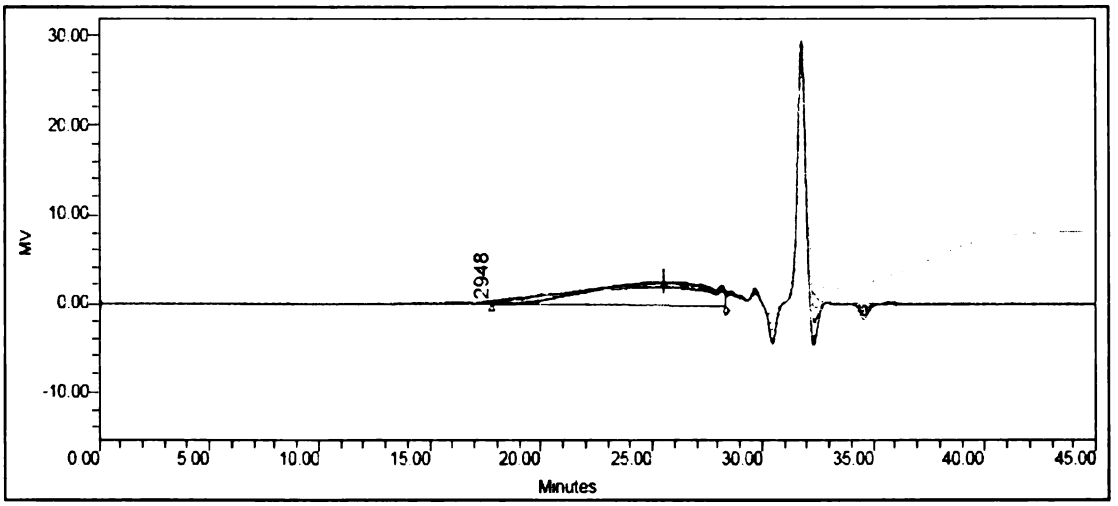

Figure 38. Chromatogram for all reactions with different catalysts and different catalyst amounts

Prepolymer	Mn (Daltons)	Mw (Daltons)	PDI
NC01	2455	7880	3.20
NC02	2750	10767	3.92
NC03	2487	7778	3.13
DBTO-01	2666	12542	4.70
DBTO-02	2233	4846	2.21
DBTO-03	2209	6257	2.83

Table 16. GPC Molecular weights and polydispersity index for all reactions

Effect of Catalyst Type and Concentration on Thermal Properties

The thermal results follow the trends of the results discussed previously. Table 17 summarizes the degradation temperatures for the polymer systems with different catalysts and varying amounts of catalyst. The Figures 39 and 40 show the degradation curves for the NC and DBTO catalysts groups, respectively. Each sample exhibits a small weight loss at around 290 °C and 385 °C. The

Sample	T_D (°C)	T_{DGDMT} (°C)
NC01	293.58	386.23
NC02	**285.59**	**386.41**
NC03	282.65	385.79
DBTO01	**287.17**	**386.04**
DBTO02	267.47	384.41
DBTO03	265.87	382.80

Table 17. TGA degradation temperature values for both catalyst sets

lower degradation temperatures are attributed to glycerol–based oligomers while the higher degradation temperatures are associated with the glycerol-based pre-polymers. For each catalyst set, the optimal concentration based on degradation is highlighted. All samples show an overall increase in thermal stability as compared to glycerol or DMT alone.

The degradation temperatures for the systems containing sodium carbonate are at about 385°C, agreeing strongly with chemical results showing reaction NC02 with the highest degradation temperature relative to the varying amounts of the sodium carbonate catalyst. On the other hand, degradation

temperatures range from 381 to 385 °C for the DBTO catalyst group. There is a slight difference between the DBTO01 reaction and the other DBTO reactions as illustrated in Figure 6. For DBTO01 a weight loss of about 9% can be seen at 294°C while this same weight loss is at 263°C for the other DBTO catalyst amounts. This supports the idea of a highly branched system possibly forming a network.

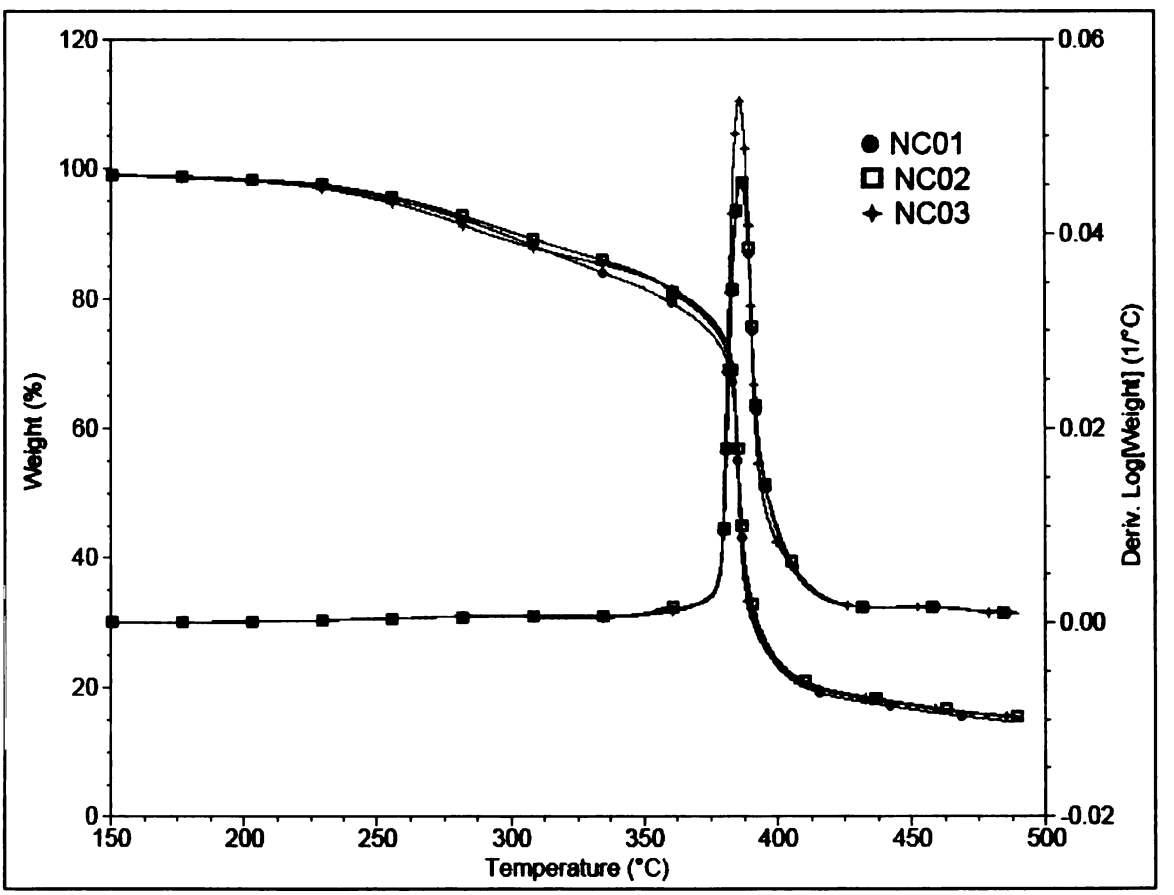

Figure 39. Sodium Carbonate percent and derivative weight loss curves based on different catalyst amounts

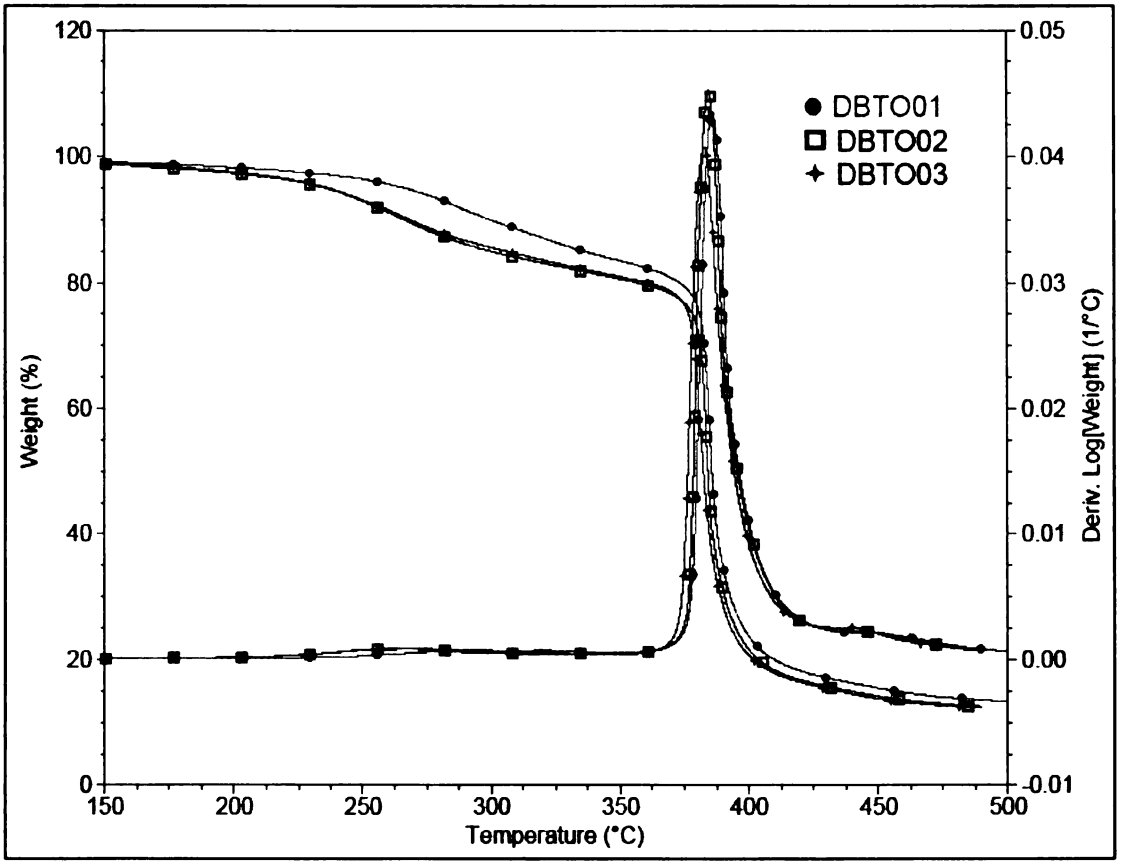

Figure 40. Dibutyltin oxide percent and derivative weight loss curves based on different catalyst amounts

The only transitions identified from DSC were glass transitions; this, and the absence of melting properies (temperature and endotherm) indicates the formation of an amorphous polymer typical of alkyd resins. Figure 41 shows the glass transition behavior for all reaction products of the study. Glass transition temperatures ranged from 26 to 33 °C for NC reactions, and 23 to 31 °C for DBTO reactions, as shown in Table 18. The highest glass transition temperatures corresponded to DBTO01, as expected from earlier results. Within

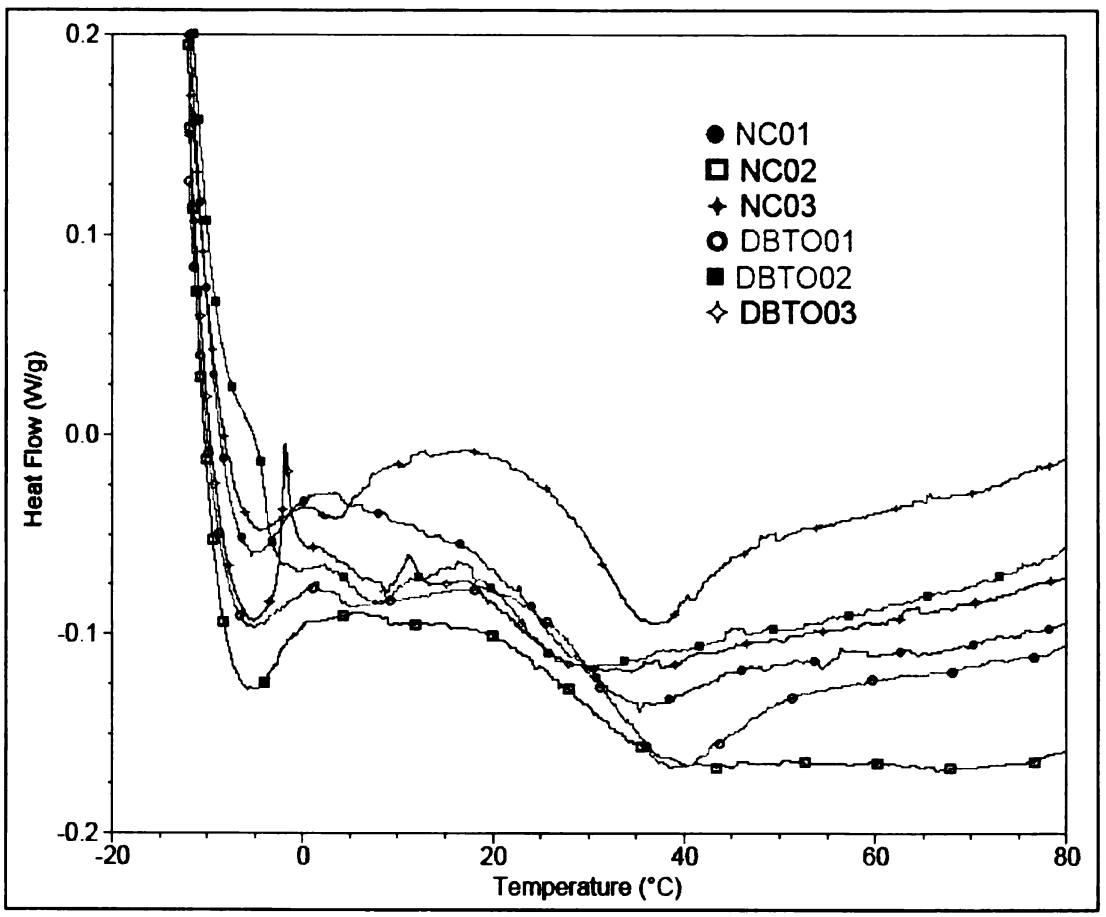

Figure 41. DSC glass transition temperature results for reaction products with varying amounts of a. Sodium Carbonate and b. Dibutyltin oxide

Sample	T_{gGDMT} *(°C)
NC01	26.09
NC02	26.21
NC03	**32.94**
DBTO01	**31.01**
DBTO02	23.26
DBTO03	19.14

Table 18. DSC glass transition temperatures of all reaction samples

the NC reactions, however, NCO3 yielded the highest glass transition temperature followed by NC02. The reaction NC03 also displayed the most volatiles, suggesting it was the least along in terms of of conversion. This result may be attributed to branching of the NC02 reaction. Branched structures help to lower T_g values. Thus sample NC02, although believed to have reacted further than sample NC03, exhibits a lower T_g value than NC03.

5.4 Summary

Homogenous, pre-polymeric glyceryl materials were synthesized from glycerol and dimethyl terephthalate yielding an amorphous highly branched or network polymer. Conversions varied slightly depending on the catalyst system and amount of catalyst used, but all conversions ranged from about 74 – 77% based on hydroxyl values and 78 – 84% based on methanol formation. Values for X_n ranged from 4 to 6.5 depending on the basis of the calculations.

Molecular weight data revealed broad curves indicative of highly branched structures. The highest number average molecular weight was 2750 Daltons with PDI's as high as 4.7. Thermal results displayed behavior suggesting trapped volatile materials in the reaction product but showed increase in thermal stability as compared to glycerol or dimethyl terephthalate alone.

Based on the overall results, dibutyltin oxide proved to be the optimal catalyst at 0.1 wt. % DMT. Although sodium carbonate at 0.2 wt. % showed comparable results, less dibutyltin oxide on a weight basis is necessary for the similar results. On a molar basis, even less dibutyltin oxide is necessary to

produce the results as compared to sodium carbonate. Successful preparation of glyceryl pre-polymers shows future potential for the development of network polymers based on glycerol.

Chapter 6

PBAT-Biopolyester Preliminary Blends

6.1 Overview

The exciting part of developing a new polyester is the really the prospect of all the potential blends that could be formed with new properties. This is exciting because it helps to increase the understanding of the behavior of the polymers interacting. What is even more intriguing is the fact that this new biopolyester incorporates at least 50% glycerol and the blending of this biopolyester to any polymer would add biobased content and, likely, biodegradation properties to the blend.

In this study PBAT is being used as the preliminary polymer for blending with the pre-polymer developed in this work (GDMT). PBAT was chosen over cellulose acetate because of the greater potential of PBAT to be affected by the addition of this pre-polymer and the ease with which it could be processed. Benefits and properties of both PBAT and GDMT were discussed in previous chapters. The objective of this work was to begin to explore the effects of GDMT blending with other polymers by studying the thermal and dynamic mechanical properties of the blend

6.2 Materials & Methods

The materials used in this study include PBAT and GDMT. The methods for processing included a reactive extrusion system and the DSM for preparation

of test specimens. The characterization techniques employed included differential scanning calorimetry, thermal gravimetric analysis and dynamic mechanical analysis.

6.2.1 Specific Processing Methodology

The PBAT was used as received from BASF. The GDMT was crushed as uniformly as possible by using a flathead hammer against small blocks of the material wrapped in a thick cloth. Reactive extrusion of PBAT and GDMT occurred using the following temperature profile from feed to die: 25/95/155/180/180/180/180/180/180/170 (°C). The melt temperature was around 175 °C and the motor speed was set at 100 RPM. The PBAT, as received from BASF, as well as the blends of 60 and 40 wt. % of PBAT and GDMT, respectively, were prepared using the twin-screw extruder system under the given conditions.

6.2.1 Specific Characterization Methods

For DSC, the sample temperature equilibrated at -50 °C and was then held isothermally at that temperature for two minutes. The temperature was then increased to 200 °C at a rate of 10 °C/min and held isothermally for two minutes. Finally the temperature was returned to 0 °C at a rate of 10 °C/min. Thermal data was gathered from this scan.

The TGA and DMA methods used are as described earlier in the general characterization section.

6.3 Results and Discussion

6.3.1 Summary of Runs

Three different GDMT samples were used in this experiment to explore catalytic effects at different concentrations. All sample compositions were 40 wt. % GDMT and 60 wt. % PBAT. Table 19 shows the compositional details for the three samples in this study.

Sample	PBAT (wt.%)	GDMT (wt. %)	Catalyst Type in GDMT	Catalyst Amt. in GDMT (wt.%DMT)
PGDNC01	60	40	NC	0.1
PGDNC02	60	40	NC	0.2
PGDDB01	60	40	DBTO	0.1

Table 19. Summary of Runs for GDMT-PBAT blends

Effect of Residual Catalyst Type and Concentration on Thermal Properties

Incorporating the low molecular weight prepolymer developed in this work, under reactive extrusion conditions, resulted in two degradation temperatures with the lower degradation temperature being associated with a small weight % loss of possibly transesterified material due to the residual transesterification catalyst in the blend. The lower degradation temperature (T_{DESTER}) is attributed to either small segments of the PBAT polymer chains or glycerol residues degrading as a result of transesterification reactions with GDMT. The GDMT-PBAT degradation temperatures, regardless of the sample, remained around the

degradation tempearature of PBAT. Table 20 summarizes the degradation temperatures associated with the samples in this study. The bulk of the weight loss for all samples occurred closer to the PBAT degradation temperatures.

Sample	T_{DESTER} (°C)	T_{DPBAT} (°C)
PBAT	---	373.68
NPBAT		375.24
PGDNC01	326.66	374.54
PGDNC02	329.39	373.88
PGDDB01	341.85	376.42

Table 20. TGA degradation temperature for GDMT-PBAT samples

Figure 42 shows the TGA weight loss curve for the samples. All blends showed a slight decrease in thermal stability as compared to NPBAT (again, referring to PBAT extruded once) as the oligoesters are degrading. The sample with 0.1 wt. % dibutyltin oxide (PGDDB01) dislayed the greatest decrease in weight loss with increasing temperature towards GDMT-PBAT, GDMT and PBAT degradation temperatures, compared to the other samples. This could be due to highly branched GDMT reacting with PBAT and forming slightly greater network structures, than lower branched GDMT reacting with PBAT (PGDNC01).

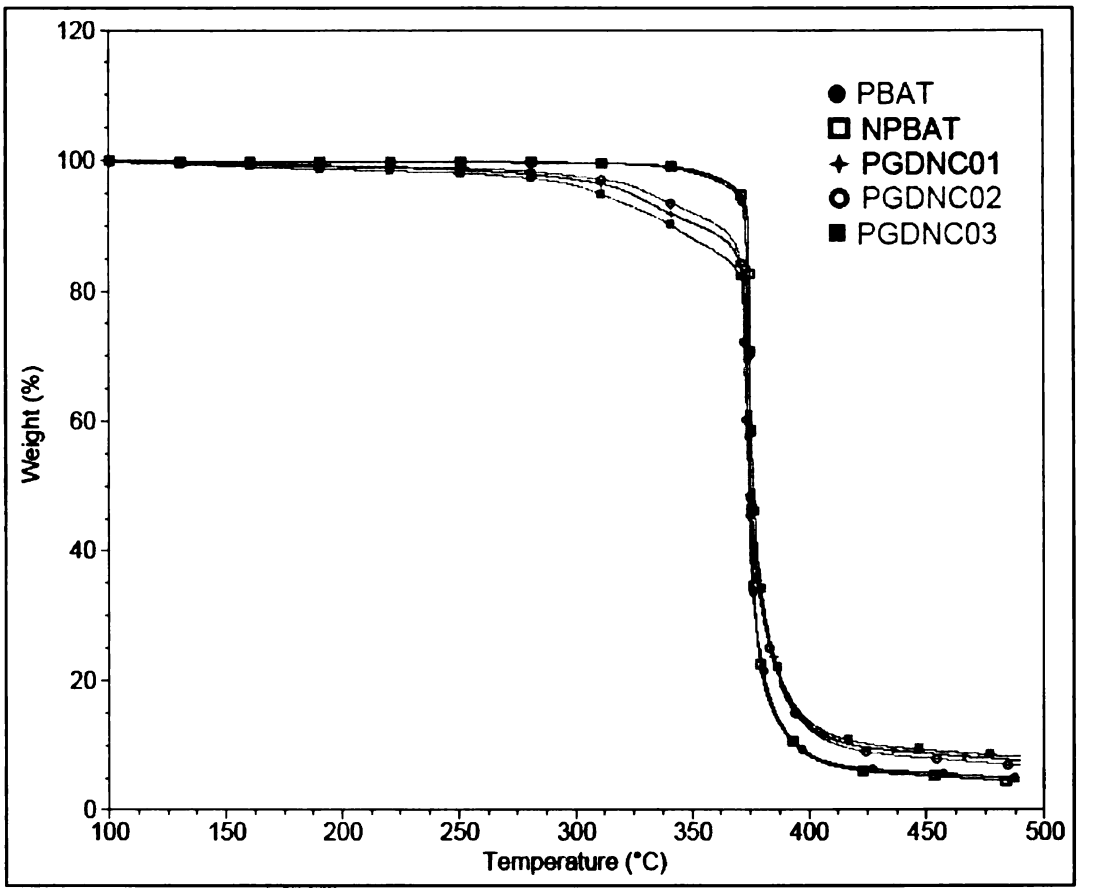

Figure 42. TGA weight loss curve for GDMT-PBAT samples

The DSC results support the idea of further reaction of GDMT with PBAT for all samples. Table 21 summarizes the thermal data for the samples. For glass transitions below zero the table shows values obtained from DMA. For glass transition temperatures above zero, DMA and DSC results are shown for comparison.

Sample	T_{gPBAT} *(°C)	T_{gGDMT} (°C)	T_{gGDMT} *(°C)	T_m (°C)	H_m (J/g)	T_{cPBAT} (°C)	H_{cPBAT} (J/g)
PBAT	-26.26	---		115.27	18.49	25.88	13.99
NPBAT	-27.90	---		123.31	13.33	76.55	17.09
PGDNC01	-22.01	38.01	38.56	105.96	10.25	63.59	7.88
PGDNC02	---	33.42	---	101.20	13.20	58.42	12.28
PGDDB01	-23.77	37.22	38.58	108.73	12.22	65.34	10.48

Table 21. DSC thermal transitions for blends of GDMT-PBAT; * indicates values obtained from DMA

Addition of GDMT to PBAT resulted in an increase in the glass transition temperatures of both GDMT and PBAT components of the blend as revealed by DSC and DMA results. This increase in the T_g suggests a decrease in chain flexibility possibly caused by the reaction of several chains of PBAT to various OH groups of GDMT. Glass transition temperatures from DSC above 0 °C show about the same values as those from DMA, as expected.

The decrease in chain flexibility of all the blends causes a slight decrease in the melting temperature and the melting endotherm as compared to NPBAT because stiffer, amorphous chains are not allowing the chains of PBAT to order as quickly to form more crystalline material. Thus the lower amount of chains that have ordered and crystallized melt at about 7 to 14 °C lower than PBAT. Less flexibility of the amorphous segments of PBAT also hinder crystallization to a small extent. In addition, branching could be playing a role in the extent of crystallization as seen in the relative comparison of samples that are thought to have higher branching (PGDNC02 and PGDDB01) than others (PGDNC01). Lower branched GDMT material would affect longer chain segments of PBAT,

whereas higher branched GDMT material would be limited to shorter PBAT chain segments.

The decrease in crystallization endotherms show a similar effect that could be explained by the branching explanation given earlier. Figure 43 depicts the slight shifts in crystallization temperatures for the samples. Comparing residual catalysts, the sample PGDDB01 had higher melting and crystallization properties as compared to PGDNC01. Increase in residual catalyst resulted in the slight lowering of melting and crystallization temperatures, while increasing the extent of crystallization. The higher branching at 0.2 wt. % sodium carbonate (PGDNC02) is, again, potentially responsible for this behavior by interfering with less of the PBAT chain segments.

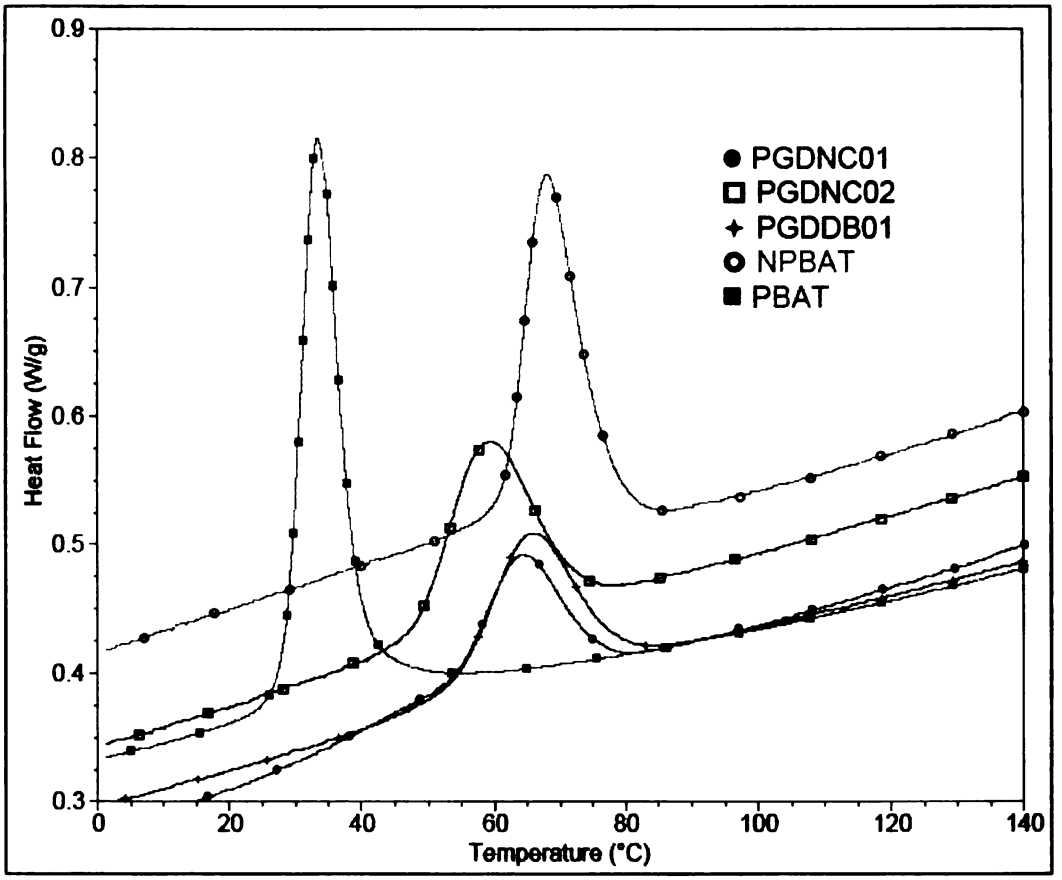

Figure 43. DSC crystallization transition for blends of GDMT-PBAT

Effect of Residual Catalyst Type and Concentration on Dynamic Mechanical Properties

The possible formation of network-like structures with the reaction of GDMT and PBAT is the reason for the increased storage modulus seen for the sample with 0.1 wt. % dibutyltin oxide (PGDDB01) shown in Figure 44. The storage moduli comparing blends with residual catalysts are shown in Figure 44 with PBAT and NPBAT. While the sodium catalyst carbonate blend shows only a slight increase in storage modulus at low temperatures as compared to NPBAT,

the blend containing residual dibutyltin oxide showed a greater increase at lower temperatures as compared to NPBAT.

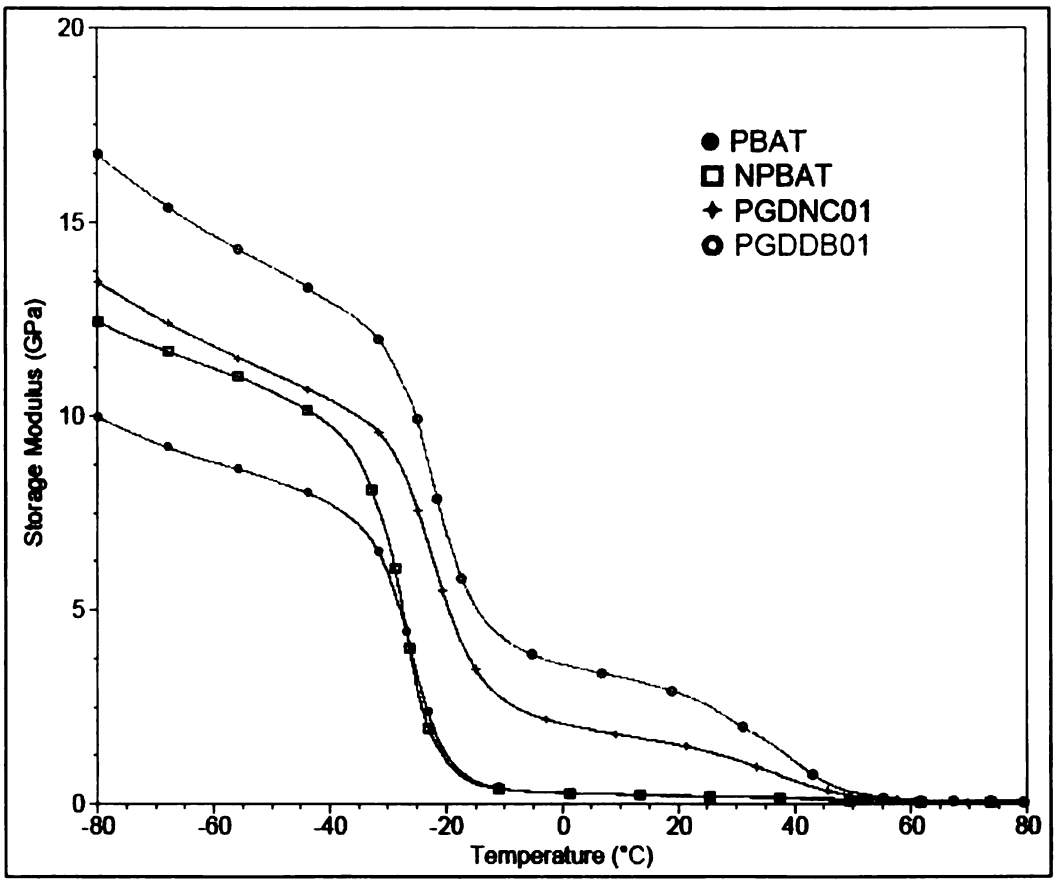

Figure 44. Storage modulus of GDMT-PBAT blends

The damping curves shown in Figure 45 support the idea that transesterification is taking place. The ratio of the height of the two peaks per sample shown in Figure 45 is reported to approximate the amount of each material in the mixture [77]. In this case, the tan delta representing the PBAT-based component of the mixture is lower for the PGDDB01 because more reactions have taken place in this mixture decreasing the amount of the pure

PBAT in the mixture. As the temperature increases, there is a shift in the GDMT-based tan delta curve and the sample PGDDB01 is now higher than the PGDNC01 curve indicating a higher concentration of PBAT-GDMT materials in the PGDDB01 mixture.

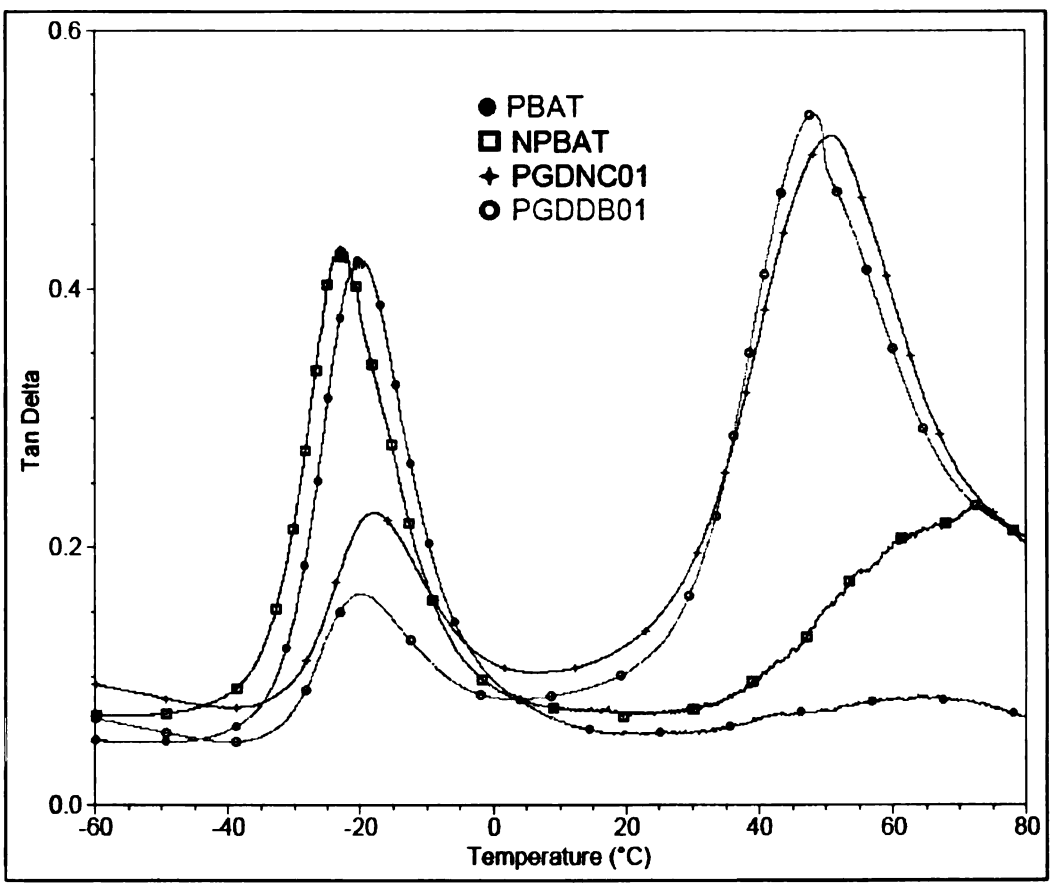

Figure 45. DMA tan delta curve for GDMT-PBAT blends

6.4 Summary

Based on the results of the thermal and dynamic mechanical data, reaction of GDMT with PBAT is believed to have caused the formation of some network-like structures. These structures only cause slight decreases in the melting and crystallization properties (temperatures and endotherms) of pure PBAT. In addition, the amorphous chains of both PBAT and GDMT components increase slightly resulting in a stiffer amorphous segment. In this study, while transesterification did result in the degradation of some oligomers at lower temperatures as compared to PBAT, transesterification also resulted in stronger networks between PBAT and GDMT components. The stronger network allows for an the addition of biobased materials to PBAT without dramatically affecting the thermal properties of PBAT. More transeterification occurred with the dibutyltin oxide catalyst at 0.1 wt%, and increasing the concentration of the catalyst (at least in the case of sodium carbonate) seemed to promote more crystallization as compared to sodium carbonate at 0.1 wt% (most likely due to the branching effects of the sample containing 0.2 wt. % residual sodium carbonate).

Chapter 7

Conclusions and Recommendations for Future Work

7.1 Conclusions

The goal of this research was to increase the biobased content of synthetic materials by the addition of the biobased materials glycerol and cellulose acetate. To accomplish this goal, three main objectives were met:

- The effects of composition, plasticizer and catalyst on blends of CA and PBAT were studied
- Catalyst performance on the glycerol-based biopolyester were determined
- The effects of catalyst type and catalyst amount on blends of GDMT with PBAT were studied

The reactive extrusion route to incorporating biocontent into PBAT showed promising results. Results showed that when PBAT and CA were physically blended with no additives, PBAT acted as a plasticizer, reducing the glass transition temperature of CA with increasing PBAT content. While the addition of CA reduced the extent of crystallinity and slightly increased the T_g of the PBAT component in the blend, the overall blends exhibited a higher M_n as compared to PBAT alone due to acidic end groups of PBAT reacting with hydroxyl groups of CA. Results of plasticized CA blends versus unplasticized CA blends showed that plasticized blends allowed for more interaction of CA with PBAT, thereby increasing reactions between the two resulting in increased molecular weights as compared to the unplasticized blends. All of the plasticized blends decreased

the extent of PBAT crystallinity further than the unplasticized blend. Catalysis results showed that the properties of the uncatalyzed blends were superior to those of the catalyzed blends, for reasons mostly associated with the interference of triacetin in the esterification reactions as triacetin is of low molecular weight and does have ester groups.

Overall, blends of CA and PBAT did show interactions between the CA and PBAT, which suggests that although the blend was not miscible, blends were compatibilized via the reactive extrusion of the two polymers. In addition, the plasticized CA sample at 70% loading of PBAT showed some of the best properties as compared to the other blends. However, the unmodified blend of CA with 70% PBAT loading was more promising given the goals of this study. This is because of the larger amount of CA actually within the blend. (30 versus 21 wt. % for unplasticized (CP37) and plasticized (CTP37) blends, respectively).

Biocontent was incorporated in the synthesis design phase of the transesterification reaction, which resulted in a transparent solid. Catalyst performance was a crucial step in obtaining a maximum degree of polymerization. For the NC catalyst, a concentration of 0.2 wt. % catalyst was determined to have the highest conversion and molecular weight values. At the same time the polydispersity increased significantly, suggesting branched pre-polymers. The sample containing the DBTO catalyst at 0.1 wt. % was found to be the optimal catalyst given the range of concentrations studied. While the M_n of the mixture was slightly lower, as compared to sodium carbonate at 0.2 wt. %, the M_w and PDI at this concentration were the highest of all the samples studied.

This is most likely a result of how much branching occurred and which end groups were added to the pre-polymer (acidic DMT or basic glycerol). Thermal studies showed that degradation temperatures associated with both catalyst groups were about the same at around 385 °C. However at 0.1 wt. % DBTO, degradation temperatures were comparable to the NC temperatures. Results from DSC showed higher glass transition temperatures overall for the samples in the NC catalyst group and lower glass transition temperatures for the samples in the DBTO catalyst group, except at 0.1 wt. % of DBTO.

Overall, while some major differences could be seen amongst the concentrations within the DBTO catalyst group, the differences within the NC catalyst group were small. However these small differences did show a specific trend. This suggests that a wider range of catalyst concentrations may have shown more of a difference in results. While on a weight-basis the samples containing catalyst DBTO01 and NCO2 exhibited similar results, on a molar basis much less DBTO was necessary to produce about the same or, in some cases, better results. Successful incorporation of glycerol at over 50% in the synthesis of GDMT resulted in a significant amount of biocontent in the developed pre-polymer.

Biocontent was, again, incorporated into PBAT via GDMT. The use of these pre-polymeric glycerol-based materials in blends seems promising. Reactive extrusion of GDMT and PBAT showed that increasing catalyst concentration decreased melting and crystallization temperatures due to the branching effects of the GDMT with 0.2 wt. % residual sodium carbonate. The

addition of GDMT also slightly decreased the extent of PBAT crystallinity, but not to the level that it was decreased in the plasticized CA blends. This could be attributed to these prepolymers only affecting small segments of the PBAT chains. Comparing the catalysts, DBTO promoted more reactions as compared to NC. This resulted in slightly higher DSC transition results for DBTO versus NC at equal wt. %. Although incorporation of biocontent to PBAT was the overarching goal of this work, the objective of this study was to study residual catalyst performance in promoting reactions with PBAT. Based on this study the residual dibutyltin oxide at 0.1 wt. % did the best job (on wt. and molar basis) in maintaining overall PBAT properties while adding biocontent.

Addition of biocontent through PBAT and DMT with the use of CA and glycerol proved to be a viable route to the advancement of biobased polymers. Out of this work a novel bio pre-polymer that is solid and transparent was produced, and has a high potential for being a biopolyester in the near future. This work also resulted in biobased, biodegradable blends of CA and PBAT.

7.2 Recommendations for Future Work

Completion of this work has led to ideas for more work in this area of increasing biocontent. Some areas for future work are listed below.

- Transesterification of physical blends of CA and PBAT
- Maleation of PBAT for use in blends with CA
- Compatibilization studies on CA and PBAT with maleated PBAT and the determination of optimal compositions

- Further development and characterization of glycerol-based polyesters to higher degrees of polymerization
- Blending of developed glycerol-based polyesters for applications coatings as well as injection molded plastics
- Re-blending of developed glycerol-based polyesters with PBAT

References

[1] Narayan, Ramani. Drivers for biodegradable/compostable plastics & role of composting in waste management & sustainable agriculture. Bioprocessing of Solid Waste & Sludge 1(1) 2001.

[2] Johnson, Jeff. Ethanol-Is it Worth It?. Chemical & Engineering 85(1), 19-21, January 2007.

[3] National Research Council. Biobased Insdustrial Products: Priorities for Research and Commercialization. The National Academy Press, Washington, DC 2000.

[4] Nabar, Y, Narayan, R, Schindler M. Twin-screw extrusion production and characterization of starch foam products for use in cushioning and insulation applications. Polymer Engineering and Science, 46 (4), 438-451 April 2006.

[5] Biobased Plastic Flexes Its Muscle. ScienceDaily. http://www.sciencedaily.com/releases/2005/12/051216185231.htm. 2005

[6] Summary of the Kyoto Protocol. Energy Information Administration. http://www.eia.doe.gov/oiaf/kyoto/kyotobrf.html. 2002.

[7] Duncan, Marvin. U.S. Federal Initiatives to Support Biomass Research and Development. The Journal of Industrial Ecology, 7 (3-4) 2004.

[8] Narayan, Ramani. Rationale and Design of Environmentally Degradable Plastics. Standardization News, 17 (11), 40 (1989).

[9] Brookes, Chisa K. *A comparative life cycle assessment: polyethylene and starch foams.* M.S. Thesis. Michigan State University, East Lansing, MI 2004.

[10] Cellulose. Wikipedia: The Free Encyclopedia. http://en.wikipedia.org/wiki/Cellulose 2007.

[11] Encyclopedia of Polymer Science and Technology: Casting to Cohesive Energy. John Wiley & Sons, Inc. Volume 3 New York 1965.

[12] Fibrous Cellulose Acetate in Engineered Structures. Eastman Chemical Company. May 1999.

[13] Brydson, J. A. Plastic Materials. Newnes-Butterworths. London, (1975).

[14] Technical Glossary of Common Audiovisual Terms: Diacetate. National Film and Sound Archive, ©Commonwealth of Australia. http://screensound.gov.au/glossary.nsf/Pages/Diacetate?OpenDocument 2002.

[15] Edgar, K.J., Buchanan, C.M. et al. Advances in cellulose ester performance and application. Progress in Polymer Science 26 (2001).

[16] Schauber, T., De Vos, S., et al. Phase behavior and mechanical properties of blends of cellulose propionate and an alternating propene-carbon monoxide copolymer. Macromolecular Chemistry and Physics 200(3) 1999.

[17] Light R. R., Dombroski J.R., Hawkins J.M. Cellulose ester/copolyacrylate composition. US Patent 4,263,183 (1981).

[18] Nabar, Y, Gupta, A, Narayan, Ramani. Isothermal Crystallization Kinetics of Poly(Ethylene Terephthalate)—Cellulose Acetate Blends. Polymer Bulletin, 53, 117-125 (2005).

[19] Ghiya, V. P., Dave, V. et al. Plasticization and Biodegradation of Cellulose Acetate. SPE ANTEC 3726-3727 (1995).

[20] Mohanty, A. K.; Wibowo, A.; Misra, M.; Drzal, L. T. Development of renewable resource-based cellulose acetate bioplastic: Effect of process engineering on the performance of cellulosic plastics. Polymer Engineering and Science 43(5), 1151-1161 (2003).

[21] Wibowo, A., Misra, M., et. al. Biodegradable nanocomposites from cellulose acetate: Mechanical, morphological, and thermal properties. Composites: Part A 37, 1428-1433 (2006).

[22] Park, H., Mohanty, A. K., et al. Effect of Sequential Mixing and Compounding Conditions on Cellulose Acetate/Layered Silicate Nanocomposites. Journal of Polymers and the Environment, 14 (1), 27-35 January 2006.

[23] Rosa, D. S., Guedes, C. G. F., Casarin, F., et al. The effect of the M-w of PEG in PCL/CA blends. Polymer Testing 24 (5), 542-548 August 2005.

[24] Nie, L., Narayan, R. Grafting Cellulose Acetate with Styrene Maleic Anhydride Random Copolymers for Improved Dimensional Stability of Cellulose Acetate. Journal of Applied Polymer Science 54 (5), 601-617 October 1994.

[25] Lee SH, Yoshioka M, Shiraishi N. Polymer blend of cellulose acetate butyrate and aliphatic polyestercarbonate. Journal of Applied Polymer Science 77 (13) September 2000.

[26] Maheras, J.C., Hopkins Jr., J.B., Tatzlaff, H. Polymer blend composed of cellulose acetate and starch acetate and starch used to form fibers, films and plastic materials and a process to prepare said blend. US Patent 5,446,140 (1995).

[27] Buchanan C.M., Pearcy B.G., White A.W., Wood M.D., et. Al. The relationship between blend miscibility and biodegradation of cellulose acetate and poly(ethylene succinate) blends. Journal of Environmental Polymer Degradation 5(4), 209-223 October 1997.

[28] Guruprasad, K. H., Shashidhara, G. M. Grafting, blending, and biodegradability of cellulose acetate. Journal of Applied Polymer Science 91 (3), 1716-1723 February 2004.

[29] Teramoto, Y., Nishio, Y. Biodegradable cellulose diacetate-graft-poly(L-lactide)s: Thermal treatment effect on the development of supramolecular structures. Biomacromolecules 5 (2), 397-406 March-April 2004.

[30] Teramoto, Y., Nishio, Y. Biodegradable cellulose diacetate-graft-poly(L-lactide)s: Enzymatic hydrolysis behavior and surface morphological characterization. Biomacromolecules 5 (2), 407-414 March-April 2004.

[31] Teramoto, Y., Nishio, Y. Cellulose diacetate-graft-poly(lactic acid)s: synthesis of wide-ranging compositions and their thermal and mechanical properties. Polymer 44 (9), 2701-2709 April 2003

[32] Braganca, F. C., Rosa, D. S. Thermal, mechanical and morphological analysis of poly(epsilon-caprolactone), cellulose acetate and their blends. Polymers for Advanced Technologies 14 (10), 669-675 October 2003.

[33] Yoshioka, M., Hagiwara, N., Shiraishi, N. Thermoplasticization of cellulose acetates by grafting of cyclic esters. Cellulose 6 (3), 193-212 September 1999.

[34] Yoshioka, M., Okajima, K., Miyazaki, T., et al. Plasticization of cellulose derivatives by reactive plasticizers II: characterization of plasticized cellulose acetates and their biodegradability. Journal of Wood Science 46 (1), 22-31 (2000).

[35] Teramoto, Y., Yoshioka, M., Shiraishi, N., et al. Plasticization of cellulose diacetate by graft copolymerization of epsilon-caprolactone and lactic acid. Journal of Applied Polymer Science 84 (14), 2621-2628 June 2002.

[36] Lee, S. H., Shiraishi, N. Plasticization of cellulose diacetate by reaction with maleic anhydride, glycerol, and citrate esters during melt processing. Journal of Applied Polymer Science 81 (1), 243-250 July 2001.

[37] Suvorova, A. I. and Demchik, L. Y. Chemical structure of plasticizers, compatibility of components and phase equilibrium in plasticized cellulose diacetate. Die Makromolekulare Chemie, Volume 195 (5) 1315-1321 (2003).

[38] Someya, y., Sugahara, Y. and Shibata, M. Nanocomposites Based on Poly(butylene adipate-co-terephthalate) and Montmorillonite. Journal of Applied Polymer Science, Volume 95, 386-392 9 (2005).

[39] Nabar, Yogaraj U., Draybuck D. and Narayan, R. Physicomechanical and Hydrophobic Properties of Starch Foams Extruded with Different Biodegradable Polymers. Journal of Applied Polymer Science, Volume 102, 58-68 (2006).

[40] Nabar, Y., Raquez, J. M., Dubois, P., et al. Production of starch foams by twin-screw extrusion: Effect of maleated poly(butylene adipate-co-terephthalate) as a compatibilizer. Biomacromolecules 6 (2), 807-817 March-April 2005.

[41] Jiang, L., Wolcott, M. P., Zhang, J. Study of Biodegradable Polylactide/Poly(butylenes adipate-co-terephthalate) Blends. Biomacromolecules 7, 199-207 (2006).

[42] Paul, D. R., Newman, S. Polymer Blends: Volume 1. Academic Press Inc. New York 1978.

[43] Rudin, Alfred. The Elements of Polymer Science and Engineering, 2nd Edition. Academic Press, San Diego, CA 1999.

[44] Young R.J., Lovell, P.A. Introduction to Polymers, 2nd Edition. Chapman and Hall, Cambridge 1991.

[45] Baber, T, M. *A Novel Application of Ozone Chemistry for Biodiesel Improvement: Product Development and Characterization.* Doctoral Dissertation. Michigan State University, East Lansing, MI 2005.

[46] Rodriguez, Ferdinand. Principles of Polymer Systems, 4th Edition. Taylor and Francis, Washington, DC 1996.

[47] Kienzle, S. Y. Polymer Blends and Alloys: Guidebook to Commercial Products. Technomic Publishing pp. 1-6 (1988).

[48] Schlumberger oilfield glossary. Schlumberger, Ltd. http://www.glossary.oilfield.slb.com/search.cfm 2007.

[49] Scheirs, J. and Long, T. Modern Polyesters. John, Wiley and Sons, Ltd., West Sussex, England 2003.

[50] Kienle, R. H.. Alkyd resins, development of and contributions to polymer theory. Journal of Industrial and Engineering Chemistry (Washington, D.C.), 41, 726-729 (1949).

[51] Kienle, R. H.; Hovey, A. G. Polyhydric; alcohol-polybasic acid reaction, I. Glycerol-phthalic anhydride. Journal of the American Chemical Society, 51, 509-519 (1929).

[52] Kienle, R. H.; Hovey, A. G. Polyhydric alcohol-polybasic acid reaction. II. Ethylene glycol-phthalic anhydride. Journal of the American Chemical Society, 52, 3636-3645 (1930).

[53] Kienle, R. H.; Van der Meulen, P. A.; Petke, F. E. Polyhydric alcohol-polybasic acid reaction. III. Further studies of the glycerol-phthalic anhydride reaction. Journal of the American Chemical Society, 61, 2258-2268 (1939).

[54] Kienle, R. H.; Van der Meulen, P. A.; Petke, F. E. Polyhydric alcohol-polybasic acid reaction. IV. Glyceryl phthalate from phthalic acid. Journal of the American Chemical Society, 61, 2268-2271 (1939).

[55] Kienle, R. H.; Petke, F. E. Polyhydric alcohol-polybasic acid reaction. VI. The glyceryl adipate and glyceryl sebacate polyesters. Journal of the American Chemical Society, 63, 481-484 (1941).

[56] Kienle, R. H.; Petke, F. E. Polyhydric alcohol-polybasic acid reaction. V. The glyceryl succinate and glyceryl maleate polyesters. Journal of the American Chemical Society, 62, 1053-1056 (1940).

[57] Odian, George. Principles of Polymerization, 4th Edition. John, Wiley and Sons, Inc., Hoboken, NJ 2004.

[58] Otton, Jean; Ratton, Serge. Investigation of the formation of poly(ethylene terephthalate) with model molecules: kinetics and mechanism of the catalytic esterification and alcoholysis reactions. I. Carboxylic acid catalysis (monofunctional reactants). Journal of Polymer Science, Part A: Polymer Chemistry, 26(8), 2183-2197 (1988).

[59] Otton, Jean; Ratton, Serge; Vasnev, V. A.; Markova, G. D.; Nametov, K. M.; Bakhmutov, V. I.; Komarova, L. I.; Vinogradova, S. V.; Korshak, V. V. Investigation of the formation of poly(ethylene terephthalate) with model molecules: kinetics and mechanisms of the catalytic esterification and alcoholysis reactions. II. Catalysis by metallic derivatives (monofunctional reactants). Journal of Polymer Science, Part A: Polymer Chemistry, 26(8), 2199-2224 (1988).

[60] Otton, Jean; Ratton, Serge; Markova, G. D.; Nametov, K. M.; Bakhmutov, V. I.; Vinogradova, S. V.; Korshak, V. V. Investigation of the formation of poly(ethylene terephthalate) with model molecules. III. Metal-catalyzed esterification and alcoholysis reactions: influence of the structure of the reactants and of the nature of the reaction medium. Journal of Polymer Science, Part A: Polymer Chemistry, 27(11), 3535-3550 (1989).

[61] Otton, Jean; Ratton, Serge. Investigation of the formation of poly(ethylene terephthalate) with model molecules. IV. Catalysis of the esterification of ethylene glycol with benzoic acid and of the condensation of ethylene glycol monobenzoate. Journal of Polymer Science, Part A: Polymer Chemistry, 29(3), 377-391 (1991).

[62] Tsutsumi, Naoto; Chen, Ying Hsien; Kiyotsukuri, Tsuyoshi. Novel regular network polyester films from aromatic tetracarboxylic acids and ethylene glycol. Journal of Polymer Science, Part A: Polymer Chemistry, 29(13), 1963-1970 (1991).

[63] Kiyotsukuri, Tsuyoshi; Tsutsumi, Naoto; Chen, Ying Hsien. Novel regular network polyester films from benzenetricarboxylic acids and glycols. Journal of Polymer Science, Part A: Polymer Chemistry, 28(5), 1197-1208 (1990).

[64] Kiyotsukuri, Tsuyoshi; Tsutsumi, Naoto; Sugimoto, Mariko; Saito, Naomi. Novel regular network polyamide films from trimesic acid and aliphatic diamines. Polymer Communications, 31(2), 56-67 (1990).

[65] Kiyotsukuri, Tsuyoshi; Kanaboshi, Masato; Tsutsumi, Naoto. Network polyester films from glycerol and dicarboxylic acids. Polymer International, 33(1), 1-8 (1994).

[66] Nagata, M., Machida, T., Wataru, S. and Tsutsumi, N. Synthesis, Characterization and Enzymatic Degradation of Network Aliphatic Copolyesters. Journal of Polymer Science: Part A: Polymer Chemistry, Volume 37, 2005-2011 (1999).

[67] Pramanick, D., Pramanick, R., and Betal, G. Copolyester of Trimellitic Acid, Glycerol, and Poly(ethylene glycol): Synthesis and Characterization. Journal of Applied Polymer Science, volume 91, 343-346 (2004).

[68] Shenoy, M., Parikh, P. Aromatic Polyesters Based on Bisphenol-A for Liquid Insulating Systems: A Synthetic Approach. Journal of Applied Polymer Science, Volume 95, 606-614 (2005).

[69] Jikei, Mitsutoshi; Kakimoto, Masa-Aki. Hyperbranched aromatic polyamides prepared by direct polycondensation. High Performance Polymers, 13(2), S33-S43 (2001).

[70] Hao, Jianjun; Jikei, Mitsutoshi; Kakimoto, Masaaki. Preparation of Hyperbranched Aromatic Polyimides via A2 + B3 Approach. Macromolecules, 35(14), 5372-5381 (2002).

[71] Lin, Qin; Long, Timothy E.. Polymerization of A2 with B3 monomers: A facile approach to hyperbranched poly(aryl ester)s. Macromolecules, 36(26), 9809-9816 (2003).

[72] Unal, Serkan; Long, Timothy E. Highly Branched Poly(ether ester)s via Cyclization-Free Melt Condensation of A2 Oligomers and B3 Monomers. Macromolecules, 39(8), 2788-2793 (2006).

[73] Stumbe, Jean-Francois; Bruchmann, Bernd. Hyperbranched polyesters based on adipic acid and glycerol. Macromolecular Rapid Communications, 25(9), 921-924 (2004).

[74] Wyatt, Victor T.; Nunez, Alberto; Foglia, Thomas A.; Marmer, William N. Synthesis of hyperbranched poly(glycerol-diacid) oligomers. Journal of the American Oil Chemists' Society, 83(12), 1033-1039 (2006).

[75] ASTM D1980. Standard Test Method for Acid Value of Fatty Acids and Polymerized Fatty Acids. Annual Book of ASTM Standards, Volume 11.01, 397-398 (1998).

[76] ASTM D1980. Standard Test Method for Hydroxyl Value of Fatty Oils and Acids. Annual Book of ASTM Standards, Volume 11.01, 375-376 (2001).

[77] Nielson, Lawrence E. Mechanical Properties of Polymers. Reinhold Publishing Corporation, New York 1962.

MICHIGAN STATE UNIVERSITY LIBRARIES
3 1293 02956 4345